Donia Daghighi BSc

Permeability of layered soils

MASTER'S THESIS

to achieve the university degree of

Master of Science

Master's degree programme: Earth Sciences

submitted to

Graz University of Technology

Supervisor

Dr.techn. Roman Marte
Institute of Soil Mechanics and Foundation Engineering

Dr.rer.nat Qian Liu
Institute of Applied Geosciences

Graz, march 2016

AFFIDAVIT

I declare that I have authored this thesis independently, that I have not used other than the declared sources/resources, and that I have explicitly indicated all material which has been quoted either literally or by content from the sources used. The text document uploaded to TUGRAZonline is identical to the present master's thesis dissertation.

Date

Signature

Eidesstattliche Erklärung

Ich erkläre an Eides statt, dass ich die vorliegende Arbeit selbstständig verfasst, andere als die angegebenen Quellen/Hilfsmittel nicht benutzt, und die den benutzten Quellen wörtlich und inhaltlich entnommenen Stellen als solche kenntlich gemacht habe.

Graz, am …… ……

(Unterschrift)

Statutory declaration

I declare that I have authored this thesis independently, that I have not used other than the declared sources / resources, and that I have explicitly marked all material which has been quoted either literally or by content from the used sources.

Graz, …… ……

(signature)

Preface of the author

This Master's thesis is the independent work of the author, D. Daghighi, and was submitted at Graz University of Technology in February 2016. The project was realized in cooperation of the Institute of Soil Mechanics and Foundation Engineering and the Institute of Applied Geosciences of the Graz University of Technology. The working progress was supervised and guided by Dr.techn. Roman Marte, Dr.rer.nat Qian Liu and DI Georg Ausweger.

The thesis deals mainly with the comparison of different laboratory methods for permeability determination. Additionally, the author aimed to point out the geotechnical significance of testing permeability in layered soils in the laboratory.

A special thanks applies to DI. Odalys Morales-Calderon, who was helpful in the evaluation of laboratory tests and who facilitated the usage of laboratory devices at the FH Joanneum – University of Applied Sciences in Graz. Particular thanks are also due to the entire team of the Soil Mechanics Laboratory of the Graz University of Technology, who supported and helped in several situations.

Kurzfassung

Diese Arbeit umfasst eine Beschreibung der Durchführung und Auswertung von Durchlässigkeitsversuchen in homogenen und geschichteten Bodenproben. Die Diskussion von Hangstabilität und Bodentragfähigkeit in Abhängigkeit von der Durchlässigkeit unterstreicht die geotechnische Bedeutung von Durchlässigkeitsversuchen. Die Wichtigkeit von Laborversuchen ist weiters anhand der Komplexität und Heterogenität von natürlichen geschichteten Formationen wie beispielsweise den Sedimenten des Bodensees oder des Achenseedamms, Österreich, erläutert. Die Anwendungsgrenzen und die Genauigkeit von verschiedenen Laborversuchen und theoretischen Methoden zur Durchlässigkeitsbestimmung werden für ungeschichtete und geschichtete Böden diskutiert. Versuchsanordnungen mit fallender Druckhöhe wurden in Ödometerzellen durchgeführt. Als Versuchsanordnungen mit konstanter Druckhöhe wurden triaxiale Durchlässigkeitsgeräte und Durchlässigkeitszylinder verwendet. Die graphischen Methoden zur C_v-Bestimmung nach Casagrande und Fadum (1940) und Taylor (1942) wurden zur Bestimmung des Durchlässigkeitsbeiwerts von Schluff genutzt und mit direkt gemessenen Werten verglichen. Die hydraulische Leitfähigkeit von geschichteten Proben wurde zudem anhand von direkt gemessenen Durchlässigkeitswerten von Schluff und Sand berechnet. Die in Versuchen mit fallender Druckhöhe direkt gemessenen Durchlässigkeitswerte von geschichteten Proben wurden mit den berechneten Werten verglichen.

Abstract

This thesis comprises a description of the implementation and evaluation of permeability tests in laboratory and a comparison of the different methods of permeability determination in homogeneous and layered soil samples. The discussion of slope stability and soil bearing capacity in dependence of permeability underlines the geotechnical significance of permeability testing. From another viewpoint, the importance of laboratory tests is illustrated through the discussion of the complexity and heterogeneity of natural layered formations such as the sediments of Lake Constance and the dam of Lake Achen, Austria. Further, the application limits and the accuracy of diverse laboratory tests and theoretical methods of permeability determination are discussed both for homogeneous and layered soil samples. Falling-head tests in oedometer cells and constant-head tests in permeability cylinders and triaxial permeability cells were conducted and evaluated. The graphical methods of C_v-determination introduced by Casagrande and Fadum (1940) and Taylor (1942) were used to determine the coefficient of permeability of silt and were compared with directly measured values. Additionally, the hydraulic conductivity of layered samples was calculated using the permeability of the homogeneous soil samples of silt and sand, determined in oedometer falling-head tests. The directly measured results from falling-head tests in layered samples were compared with the calculated values.

Table of contents

List of figures

List of tables

List of symbols and abbreviations

Capital letters

A	[cm²]	cross-sectional area of specimen
$A50$	[ ]	interval ratio
C_{uB}	[ ]	uniformity coefficient of the base material
C_{uF}	[ ]	uniformity coefficient of the filter material
C_v	[m^2/s]	coefficient of consolidation
D	[mm]	grain size of the filter material
L	[mm]	length
Q	[cm^3]	amount of water passing through the sample in a permeability test
T	[°C]	temperature
T_v	[ ]	Time factor used in graphic curve fitting methods

Small letters

a	[mm^2]	cross-sectional area of manometer tube
d	[m]	thickness of a soil layer
d	[mm]	grain size of the base material
d_n	[m]	thickness of a number of n soil layers
g	[ms^{-2}]	acceleration due to gravity
h_0	[cm]	overflow level of oedometer cell (height above y_0)
h_1, y_1	[cm]	upper mark in a falling-head test (height above h_0, y_0)
h_2, y_2	[cm]	lower mark in a falling-head test (height above h_0, y_0)
h_3, y_3	[cm]	intermediate mark in a falling-head test (height above h_0, y_0)
k	[ms^{-1}]	hydraulic conductivity
k_n	[ms^{-1}]	hydraulic conductivity in a layered soil with n layers
kT	[ms^{-1}]	hydraulic conductivity at the temperature T
k_{10}	[ms^{-1}]	hydraulic conductivity at a temperature of 10°C
l	[cm]	length
t	[s]	time
s_0	[µm]	settlement at 0% consolidation
s_{50}	[µm]	settlement at 50% consolidation
s_{100}	[µm]	settlement at 100% consolidation
y_0	[cm]	reference level in a falling-head test
Δh	[cm]	height difference between two water levels (pressure head)

Δh_M	[cm]	height difference between water levels in two manometer tubes

Greek letters

ρ_d	[g/cm³]	dry soil density
ρ_f	[g/cm³]	wet soil density
ρ_w	[kg/m³]	density of water

1 Introduction

In this work various laboratory tests and theoretical approaches for determining the permeability of layered soils are compared. Furthermore the geological formation of layered soils is described. Concerning the soil mechanics part of the work, special focus is given to the question whether same results are yielded using different theoretical and practical approaches for the permeability determination. Laboratory results are compared with theoretically determined results from graphical methods and calculations. Direct measurements were conducted in triaxial permeability cells and permeability cylinders as constant-head tests and in oedometer cells using a falling-head test. For indirect permeability determination two graphical methods after Casagrande and Taylor (cmp. Head, 1982) were used, which allow the determination of C_v from time-settlement curves and a further calculation of k from the C_v-value.

A total of two different soil types were tested in the laboratory. The permeability of clayey silt and medium sand was measured both in constant-head and falling-head tests. Clayey silt permeability was additionally determined through the C_v-value derived from time-settlement curves. Artificial samples made up of layers of clayey silt and medium sand were tested in oedometer cells using a falling-head test. The layered samples should represent natural lacustrine layered sediments consisting mainly of silt, clay and sand, with the sand fraction occurring as a layer between clayey silt layers. The conclusions, based on the testing of artificial samples, should give an instruction on how to conduct permeability tests on layered samples in an optimal way.

Formation of layered soils is explained on the basis of the geological setting of a postglacial basin. Glacially formed basins and valleys are one of the main settings that involve the deposition of layered fine sediments and are widely found in the Alpine region. Examples of alpine basins and valleys with their typical glacial and postglacial sedimentation and consolidation features are discussed.

For the permeability determination based on the consolidation behavior, 22 samples were tested in the oedometer using the “Pero Scher/KD” device in the soil mechanics laboratory of the Graz University of Technology and the corresponding software “Pero/Scher/KD/Triax”. Direct permeability measurements were carried out on 13 of them. Triaxial permeability tests were performed on 3 samples in the same laboratory. Another 3 samples were tested in permeability cylinders in the soil mechanics laboratories of the Graz University of Technology and the FH Joanneum – University of Applied Sciences in Graz.

2 Geology

2.1 (Post-) glacial sedimentation in valleys and basins of the alpine region

The Würm glaciation is defined as the last large-scale glacial event in the alpine region, during which wide parts of this area have been covered with ice. In southern Germany, the beginning of the Würm glaciation is dated to about 115.000 years ago with the advance of the Rhine Glacier over today's Lake Constance to the foreland. The glacial period ended 11.700 years ago (Hoffmann, 2015).

Fine clastic lacustrine laminites depict only one out of a broad range of sedimentary facies occurring in glacially formed valleys and basins. Fluviatile sedimentation (terrace formation), alluvial sedimentation (delta sediments), turbidite events, rockfall events, ice-rafting (glacial erratic blocks) and moraines (glacial debris) are examples for sources of different sedimentary bodies occurring in a (post-) glacial deposit.

Late- and post-glacial fine clastic lacustrine sediments are the product of siltation of glacial lakes. Such lacustrine deposits consist mainly of sand, silt and clay. The sand fraction often appears as layers in silt or clay. Varved clay, consisting of rhythmically layered silt and clay, is also formed in this sedimentary environment (Berner, 2015). Investigations of New Liskeard, Canada, varved soil have shown, that transitional layers with intermediate moisture content can occur between the fine, moist layers and the coarse, less moist fraction (Chan & Kenney, 1973, cmp. Das, 2002).

The dam of Lake Achen, Tyrol, and the sediments in and around Lake Constance are examples of Würm-glacial and post-glacial sedimentary deposits including lacustrine layered sediments. Different depositional and geologic mechanisms can act in a glacial setting and can cause complex sedimentary sequences. The spatial and genetic complexity of (post-) glacial deposits shows the necessity of combining field and laboratory work. Spatial relationships can only be studied in the field while laboratory tests can give detailed information about soil parameters.

2.1.1 Proglacial layered deposits described at the dam of Lake Achen

The example of the dam of Lake Achen describes the formation of lacustrine terrace sediments in the estuary area of an alpine side valley (Achen valley) during a glacial period. The dam can be interpreted as a proglacial sedimentary accumulation of the

Zillertal Glacier with a paleo-lake forming towards its south-east side (Poscher, 1994). Due to accumulation of proglacial and marginal glacial sediments the paleo-lake silted up and the present-day Lake Achen formed on the reverse side of the dam (north-west). Poscher (1994) mentioned two types of layered lacustrine sediments occurring in the dam of Lake Achen. On the one hand, lacustrine laminites are found as varved clays of the paleo-lake Achen, consisting of mm-thick silt-layers that are coarsening-up to cm-thick silt and sand layers (Fig. 4). On the other hand laminites are found as marginal accumulations of the Zillertal glacier. The varved clays show a distinct fraction of fine sand, while the marginal accumulated facies consists of >95% of silt and clay (Poscher, 1994).

Different mechanisms of accumulation occur in a proglacial environment and caused the high complexity of the sedimentary bodies in the dam of Lake Achen. The facies built in e.g. alluvial, fluviatile or lacustrine environments interfinger vertically and they are laterally not persistent. Fig. 2 shows a geologic map by Poscher (1994) of the dashed area in Fig. 1, which illustrates the lateral extent within which the sedimentary units of the dam of Lake Achen were mapped. A profile by Poscher (1994), mapped from a drilling within the sand facies (red mark in Fig. 2), is shown in Fig. 3. The profile shows the high heterogeneity and complexity of the stratigraphic sequences within one facies, which underlines the necessity of studying heterogeneous layered soils in laboratory tests.

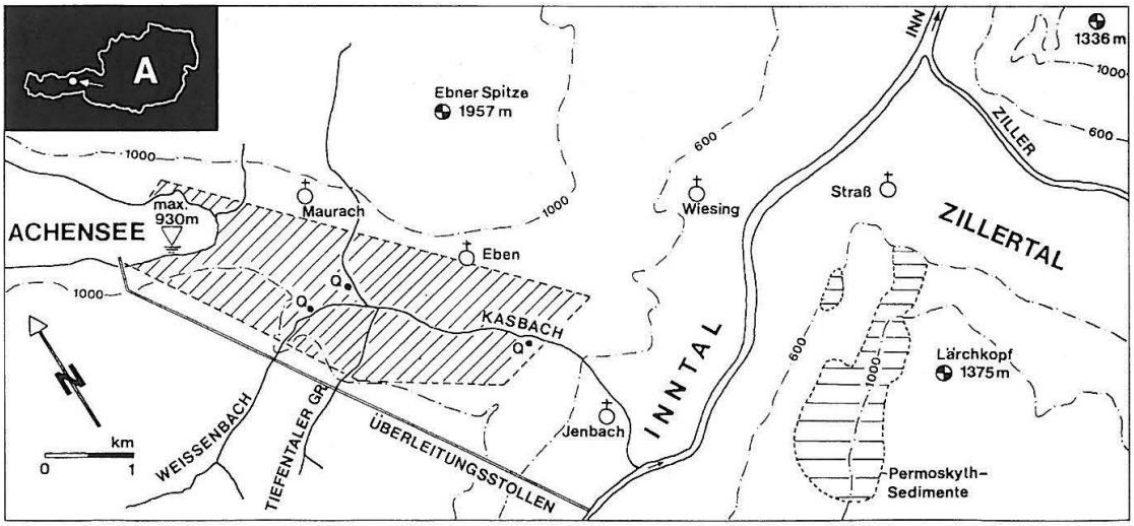

Fig. 1 Mapping area of the sedimentary units of Lake Achen (Poscher, 1994)

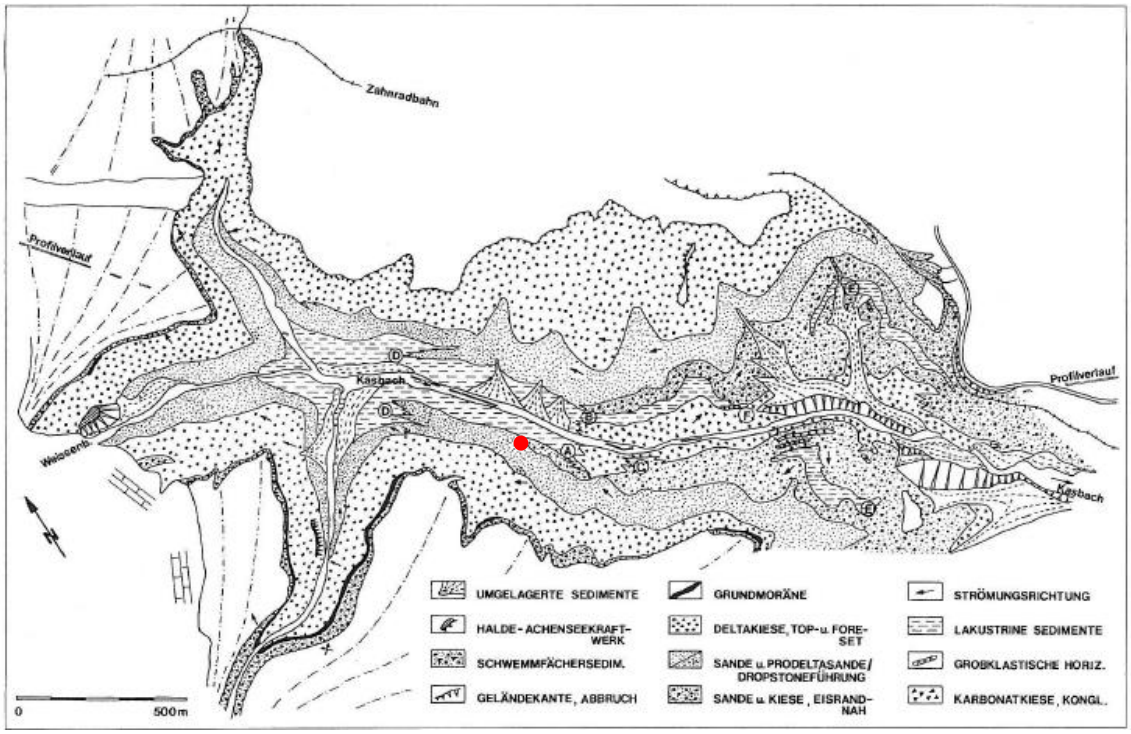

Fig. 2 Geologic map of the area between Kasbach and the south-east end of Lake Achen (Poscher, 1994)

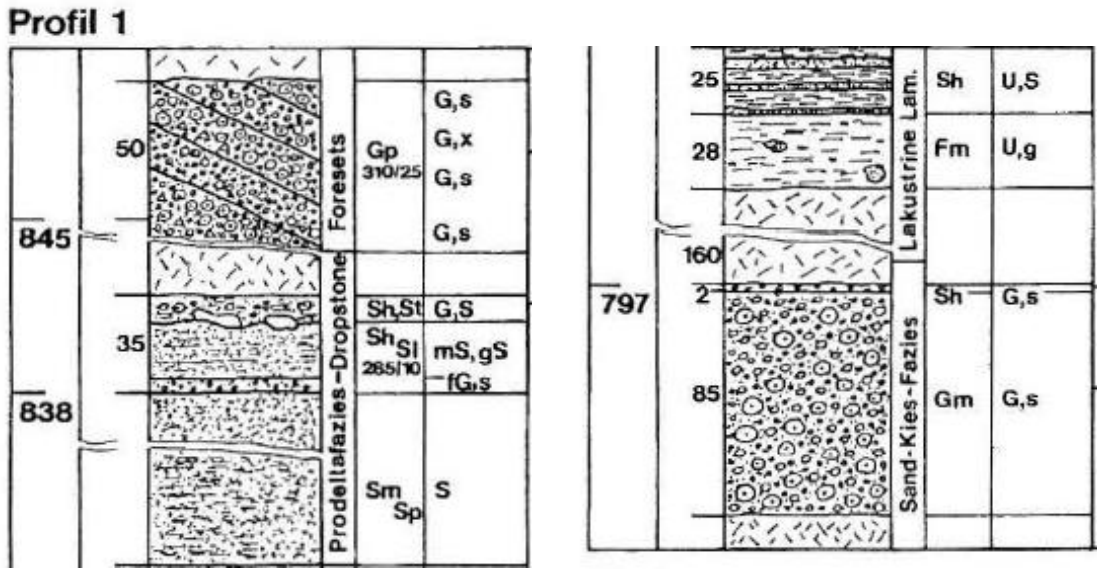

Continues in the right column

Fig. 3 Profile mapped within the sand facies (red mark in Fig. 2) by Poscher (1994)

In order to summarize the stratigraphic order of all sedimentary bodies, that were deposited during the glacier recession between the south-east end of Lake Achen and Kasbach, a vertical idealized profile was drawn (Fig. 4). In the sketch correct spatial

relationships are disregarded and the persistency of all units is presumed. The sea levels at which the sedimentary units occur in drillings in the mapping area differ from north to south. In Fig. 4, the minimum heights above sea level, that Poscher (1994) mentions for each sedimentary unit, were used.

According to Poscher (1994), the deepest unit occurring in the dam is built of alluvial fan conglomerates (1). The conglomerates are overlain by proglacial fluviatile sands and gravels, that interfinger with the conglomerates (2). Silt/clay laminites (3), which are believed to have been formed at the former glacier margin, are found between facies 2 and 4. Layered lacustrine sediments (4) with a coarsening upward trend occur to the north of facies 1 and 2 and are interpreted as varved clay of the paleo-lake Achen. Facies 4 interfingers with the overlying cross-bedded sandy sediments of a prograding delta (5). Delta gravel (6) from the fore-set occurs at a height of at least 850m above sea level. The delta top-set (7) consists of coarse clastic material. A few meters of ground moraine (8) as well as recent alluvial sediments are deposited on top of facies 7. The sea level of Lake Achen is marked in Fig. 4 at 929m above sea level.

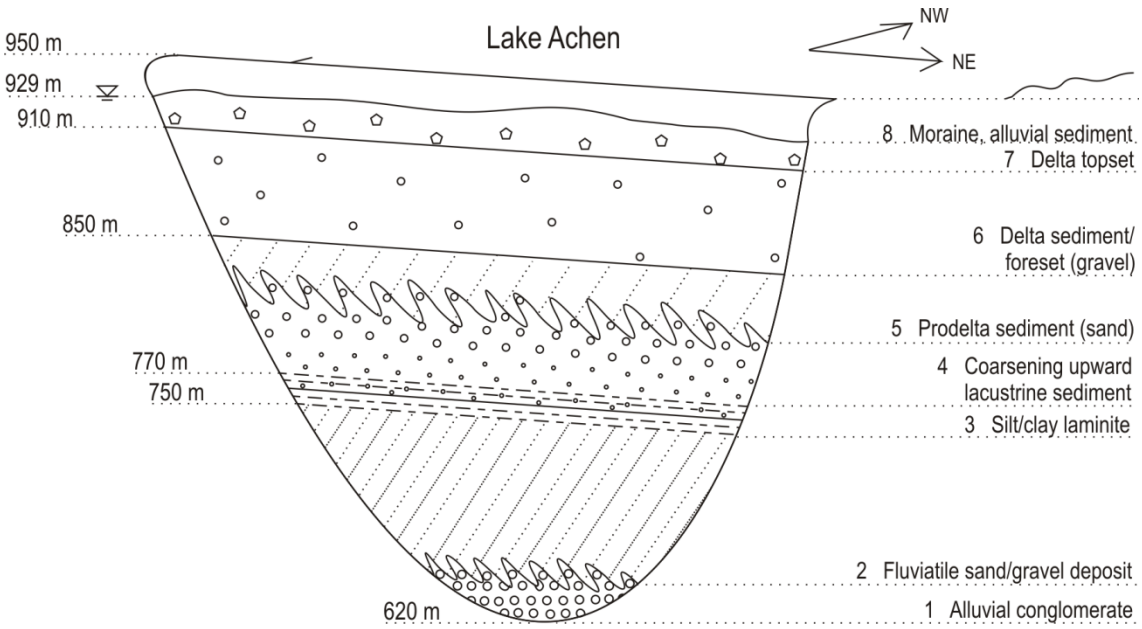

Fig. 4 Idealized concept of sedimentary units of the dam of Lake Achen

2.1.2 Post-glacial layered deposits described at Lake Constance

The recent sedimentation in Lake Constance is an example of the formation of a post-glacial lacustrine deposit. At the end of the Würm glaciation, when the Rhine Glacier

started to recede (approximately 18.000 years ago), proglacial lakes started to form between the end moraine and the new glacier margin. The tongue basin of the recent Lake Constance was formed both by tectonic forces and the erosive effect of the Rhine Glacier recession (Mueller, 1966).

The sedimentation in Lake Constance is governed by the flow regime of the lake. In general, the grain size of proximal sediments is higher than the grain size of distal sediments, as the flow energy is less in the central deep area of the lake. Effects on the flow conditions are mainly due to changes in the water level of the tributaries, that occur seasonally, annually and also per decade. These changes result in the formation of layered deposits. High or low water events in the Alpine Rhine affect the amount and type of sediment transported to Lake Constance. High water in the Alpine Rhine causes the deposit of coarser sediment than during low water periods. Seasonal changes in the water level of the tributaries are recorded in the sediment as a series of fine, some µm thick layers (Mueller, 1966). The sedimentation rate in the central region of the lake amounts to approximately 1 mm per annum (Mueller, 1966).

15.000 years ago, Lake Constance covered an area of more than double the size of the recent lake (Mueller, 1966). Bore profiles indicate a thickness of lacustrine layers of at least 25m in the surroundings of Lake Constance (Gebreselassie & Kempfert, 2004). In the present about 3 million m^3 of sediment are brought into Lake Constance per year by the river Rhine.

2.2 Consolidation and glacial overdeepening

According to Poscher (1993), the overdeepening of valleys or basins through glacio-erosive effects hardly exceeds 500 meters in the areas to the north of the main chain of the alps. The overdeepening of valleys and basins in eastern alpine regions amounts to 180 to 340 meters, while in southern alpine regions overdeepening is significantly higher (Poscher, 1993).

In case of the Inn Valley, Tyrol, two cycles of glacial overdeepening can be reconstructed by observing the degree of consolidation of the valley fillings. The stratigraphic order of sedimentary bodies in the Upper Inn Valley was described by Poscher (1993) and is sketched in Fig. 5. The valley fillings are built up of a series of glacial, postglacial and eventually also preglacial deposits and can be classified into four main horizons. The two uppermost horizons consist of late-glacial and post-glacial

sediments. Drillings and seismic velocities indicate that the youngest horizon is built up by clayey lacustrine sediments or water-saturated fluviatile or alluvial gravels (Poscher, 1993). The second horizon consists of late würm-glacial lacustrine sediments, delta gravels and basal till (Poscher, 1993). The base of the second horizon is believed to correspond to the basal level of the last glacial overdeepening of the valley, since it is the border between the overconsolidated third horizon and the normally consolidated sediments above. The third horizon has been deposited on top of a sedimentary body, suspected to consist of preglacial sediment (Poscher, 1993). Surmising that the basal deposit is of preglacial age, the border between the third and the fourth horizon represents the base of the maximum depth of glacial erosion taken place in the Upper Inn Valley.

As mentioned above, consolidation of the sediments in glacial settings depends on the time relationship between deposition, glacier advance and glacier recession. Layered lacustrine sediments in late-glacial or postglacial settings are normally or lowly consolidated, since they have been deposited during or after glacier recession. Sediments deposited before glacier advance are left overconsolidated after the glacier recession (cmp. Upper Inn Valley). Soft soils of late- and postglacial ages in regions to the north of the alps are mainly normally consolidated (Bjerrum, 1973, cmp. Soumaya, 2005). Lowly consolidated laminated lacustrine clays, locally known as “Salzbuger Seeton”, are found in the Salzburg Basin. Lacustrine clays in the area and surroundings of Lake Constance are mostly normally consolidated and locally lowly consolidated (Berner, 2015).

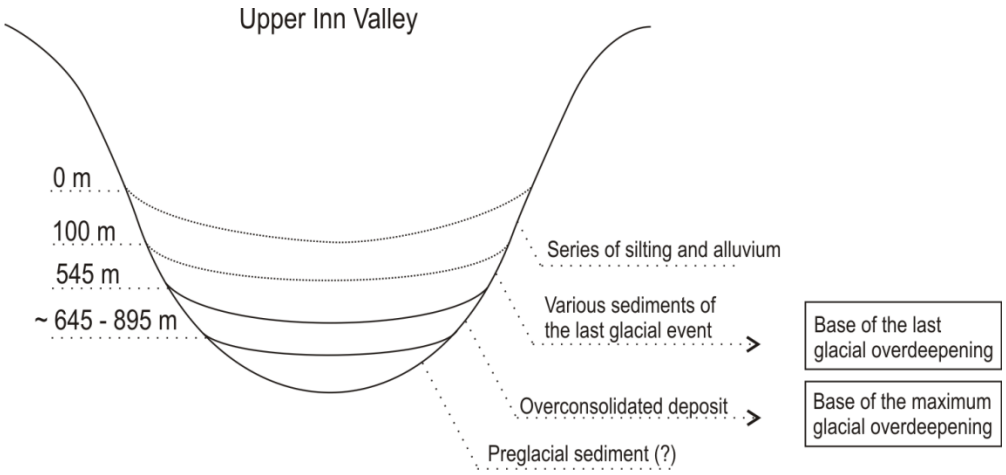

Fig. 5 Profile sketch showing the four main horizons of the Upper Inn Valley fillings

2.3 Geotechnical significance of permeability in layered soils

2.3.1 Permeability governing the formation and triggering of landslides

Permeability is a key parameter in the generation of landslides. The below mentioned triggering mechanisms describe how the exposure to natural events can set a mass movement in motion. Landslides are either triggered by the rapid increase of stresses on the land mass or by reduction of the strength of the material (Turner & Schuster, 1996). Particularly superficial mass movements (1-2m) are often triggered by events of heavy, continuous rainfall. Infiltrating water causes temporary saturation, resulting in reduced soil strength that triggers the landslide (Van Asch & Sukmantalya, 1993, cmp. Van Asch et al., 1999). The effect of increasing stresses may occur in the case of a rapid drawdown against a slope and is illustrated in Fig. 6. If the water level is dropped fast after a period of high tide, the slope is left with excess pore-water pressures. The resulting higher shear stresses can lead to a mass movement on the hillside (Terzaghi,1943, Lambe & Withman,1969, cmp. Turner & Schuster, 1996). Particularly mass movements in low permeable soils (e.g. clays, silts), that build up lake or river banks, are often generated this way (Turner & Schuster, 1996). According to Van Asch et al. (1999), deeper mass movements are mostly influenced by the effect of high pore-water pressures. Deeper landslides (5-20m) are rather triggered by long periods of above-average amounts of rainfall than by short events, since they need greater amounts of water to reach triggering conditions (Van Asch et al., 1999). Martelloni et al. (2011) mentions, that the pore water pressures react faster to rainfall in permeable zones than in low permeable zones. Hence, permeable terrains should tend to form

shallow landslides, while deeper landslides should rather develop in low permeable areas.

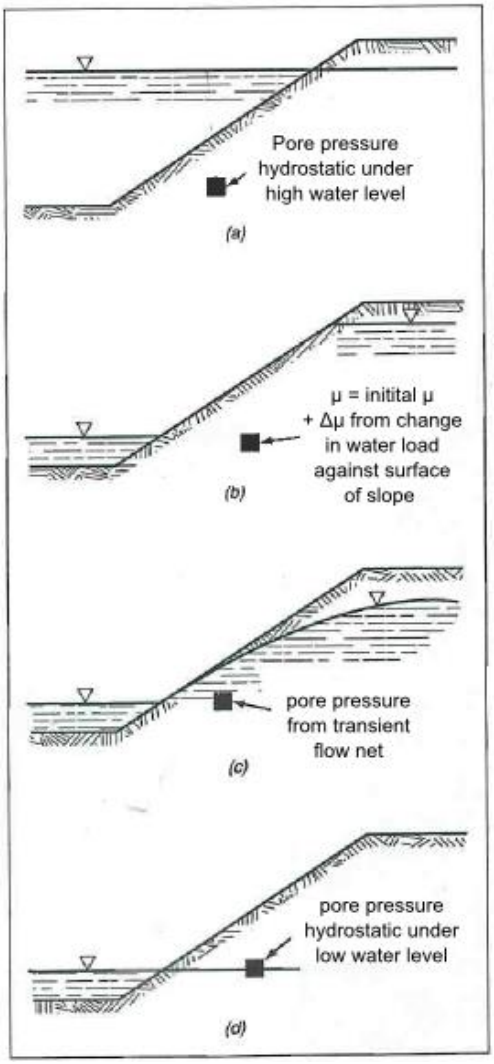

Fig. 6 Rapid drawdown against a slope: a) initial equilibrium condition b) after drawdown c) after consolidation adjustment d) final equilibrium condition (Lambe and Whitman, 1969, cmp. Turner & Schuster, 1996)

The actual cause of a landslide needs to be distinguished from its triggers. Causes of landslides in earth materials are geologic conditions, that result in the formation of a potential sliding plane. According to Turner & Schuster (1996), slides of soil material are divided into earth slides and debris slides. In the context of landslides, the soil is defined as earth if at least 80% of the grains are smaller than 2mm (Bates & Jackson, 1987, cmp. Turner & Schuster, 1996). The two main types of movement, that are possible in earth materials, are earth slides and earth flows. The typical deformations observed on earth slides are a basal rupture surface and deformations (e.g. riedel-

shears) on the sides of the displaced mass (Turner & Schuster, 1996). According to Turner & Schuster (1996), an earth flow occurs along a broader zone of distributed shear and rather shows high internal deformation. The mode of sliding depends on the water content and cohesion of the moving material. If a sliding mass absorbs water and loses cohesion while propagating downslope, it can start moving like a viscous fluid and turn to a flow (Turner & Schuster, 1996). Often, landslides in earth masses show characteristics of both a slide and a flow. According to Turner & Schuster (1996), the displaced mass should in this case be called a composite earth flow – earth slide.

2.3.2 Landslides in bedded sediments

Layering plays a major role in the formation of landslides. The sliding plane of landslides in large-scale layered deposits develops in dependence of the layering. Rotational earth slides can form easily in these materials, since the surface of rupture generally follows natural discontinuities within the sediment (Varnes, 1978, cmp. Turner & Schuster, 1996). The failure can occur as a base failure in a horizontally bedded deposit or as a slope failure. A sliding plane will develop, following the dip of the weaker layer (Turner & Schuster, 1996). Weak layers might be e.g. soft clay bedded with firm shale (Fig. 7). Differences in permeability and water content of the layers have reactivated the Gschliefgraben landslide in Upper Austria during the winter of 2007 – 2008, where a less permeable layer slid on a thinner, higher permeable layer (Poisel et al., 2012) (Fig. 8). The mass movement could only be decelerated by disrupting the natural permeability conditions (e.g. pumping out of water, reducing pore water pressures, preventing water from soaking into the soil) (Poisel et al., 2012). Van Asch et al. (1999) described a case in the French Alps where the soil permeability controls the landslide motion. A low permeable layer of varved clays underlying a higher permeable colluvial deposit is believed to stand in contact with a sliding plane. The amount of water stored in the upper permeable layer governs the stability of the landslide (Van Asch et al., 1999).

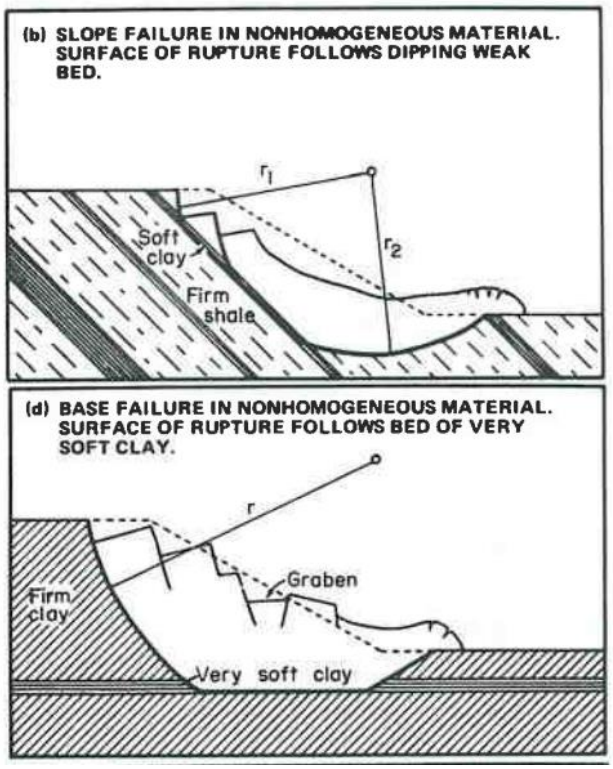

Fig. 7 Rotational landslides in layered sediment (Varnes, 1978, cmp. Turner & Schuster, 1996)

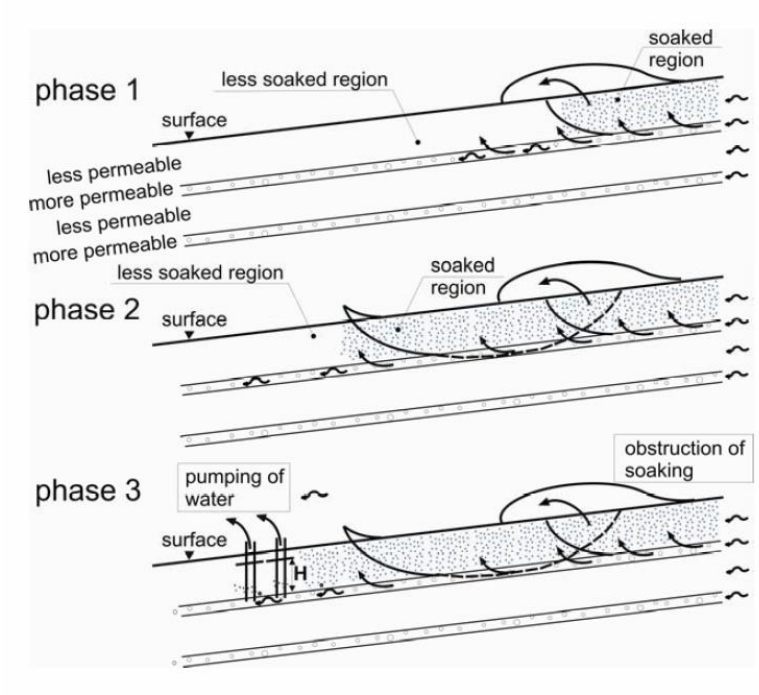

Fig. 8 Mechanism of the Gschliefgraben earth flow (Poisel et al., 2012)

2.3.3 Permeability and soil bearing capacity

Bearing capacity is a key parameter in the design of geotechnical structures, amongst others also for shallow foundations. It is governed by several mechanical and geological factors (e.g. strength parameters, soil stratification, position of the groundwater table) and by the size, weight and type of structure, that is built.

The soil bearing capacity expresses the amount of load, that can be applied by a foundation on the subsoil, without causing a failure in the supporting soil. Overstressing a soil mass results in large settlements and shear failure (Das, 2002). Fig. 9 shows the mechanism of general and local shear failure of soil under the load of a foundation. In the case of general shear failure, large settlement of the footing occurs, pushing downwards a wedge-shaped elastic zone (I) of soil (Das, 2002). The surrounding soil masses are displaced along radial shear zones (II) and Rankine passive zones (III) (Das, 2002). The soil will rise in the respective areas around the foundation and build bulges on the ground surface. In the case of a local shear failure, the radial shear surfaces end somewhere in the underground. Zone III does not occur, but bulges on the surface are possible.

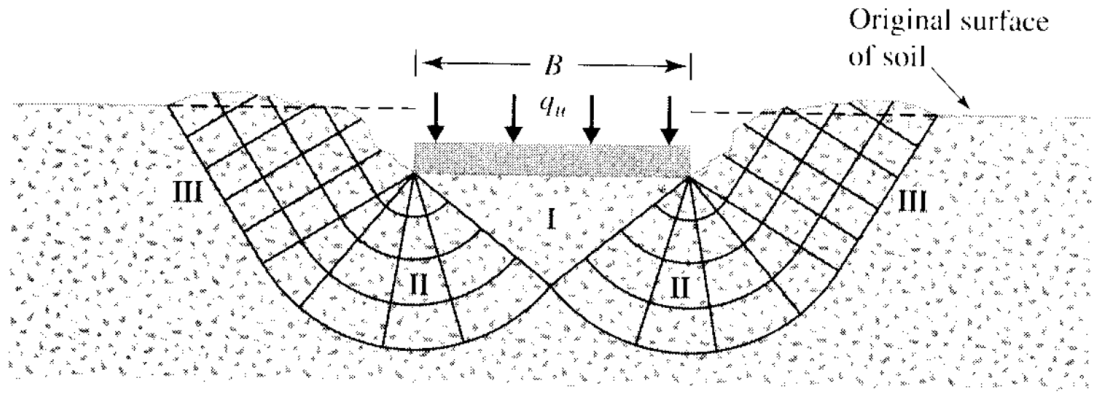

Fig. 9 General and local shear failure of soil (Das, 2002)

According to Das (2002), the occurrence of general or local failure depends on the soil type: Bearing capacity failure in stiff soils is likely to occur as a general shear failure. Loose or medium dense sand rather undergoes local shear failure. The failure in layered soils is more complex and depends on the layer thickness.

Groundwater fluctuations and heavy rainfalls might also lead to a bearing capacity failure in the subsoil. According to Shahriar et al. (2013), rises in the ground water table can cause additional settlements and failure below shallow foundations as the strength

and the stiffness of the soil are reduced. How fast the position of the groundwater table changes is essentially influenced by the permeability of the soil.

Furthermore, the ratio between loading speed and permeability of the soil governs whether a soil mass behaves drained or undrained. In an undrained state, the loading leads to excess pore pressures which can significantly reduce the bearing capacity of the soil. This is especially true for layered soils with different permeability of the single layers, as excess pore pressures occur in the higher permeable layers.

As the bearing capacity of foundations is not within the scope of this work, these facts are only mentioned for the sake of completeness and to show the huge influence of soil permeability in the field of soil mechanics.

3 Testing Procedures

3.1 Introduction

Different laboratory tests were carried out in order to determine the permeability of pure and layered soil samples and to compare the results of different laboratory methods. Constant-head and falling-head direct measurement arrangements were used both for clayey silt and medium sand. According to ÖNORM B 4422-1, lowly permeable soils are generally tested in a falling-head test set-up while highly permeable soils should be tested in a constant-head system. For the purpose of research, both types of tests were performed regardless of soil permeability.

For tests on silt samples the usually for low to medium permeable soils performed constant-head triaxial permeability test and the oedometer falling-head test were chosen. Additionally, graphic curve-fitting methods for cohesive soils were used for calculation of hydraulic conductivity using the time-settlement curves from oedoemter tests.

Sand was tested in a constant-head system (permeability cylinder), which is generally used for medium to highly permeable soils, as well as in oedometer falling-head tests.

In a next step, artificial samples were produced made up of layers of the two tested materials. The permeability of these artificial samples was determined in a falling-head test in the oedometer. In general, falling-head tests can be performed additionally to any oedometer test by connecting a manometer tube to the oedometer cell. Thus, this test is not compulsory bound to a certain permeability range but to the possibility of conducting an oedometer test on the sample.

3.2 Triaxial permeability test

The triaxial permeability test is a procedure applicable for materials with coefficients of permeability ranging from 10^{-8} to 10^{-5} m/s (OENORM B4422-1, DIN ISO/TS 17892-11). It basically consists of a bottom plate and a top plate between which a hard plastic cylinder is fixed using metal screws. The specimens are produced using the proctor compaction. They are cylindrically shaped with a height of approximately 12 cm and a diameter of 10 cm. The specimen is coated with a rubber plastic which prevents lateral entrance of water. Once the specimen is mounted, the cell is filled with water up to a chosen mark. The water level is checked regularly on this mark in order to detect

possible leakage. The top and bottom of the sample are covered by porous ceramic filter stones and connected to a water supply. By application of air pressure on the water surface inside the cell a constant confining pressure on the specimen is created while water enters the specimen through a bottom inlet. A tube, connecting the upper filter stone and the bottom plate of the cell, leads the incoming water out of the cell into a beaker. The amount of water passing through the specimen over a certain span of time is weighed. The coefficient of permeability is calculated using the formula

$$\mathrm{k} = \frac{\mathrm{Q} \times \mathrm{l}}{\mathrm{A} \times \Delta\mathrm{h} \times \mathrm{t} \times 100} \quad [m/s] \qquad \text{Equ. 1}$$

Q	[cm³]	amount of water passing through sample
l	[cm]	length of specimen
A	[cm²]	cross-sectional area of specimen
⊿h	[cm]	pressure head
t	[s]	time

Both DIN ISO/TS 17892-11 and OENORM B 4422-1 do not give particular standard values for air pressure or *⊿h*. It is important though to create a cell pressure high enough to maintain the specimen fracture-proof during the test. Since the specimen is simply coated with a thin and not supportive plastic, the test is restricted to use on cohesive soils only.

Fig. 10 shows a triaxial permeability cell in the soil mechanics laboratory of the Graz University of Technology, where the test is generally run with a pressure head of $\Delta h = 360$ cm and a sample height of 12 cm (therefore *i* = 30). The applied air pressure amounts to approximately 5 bar.

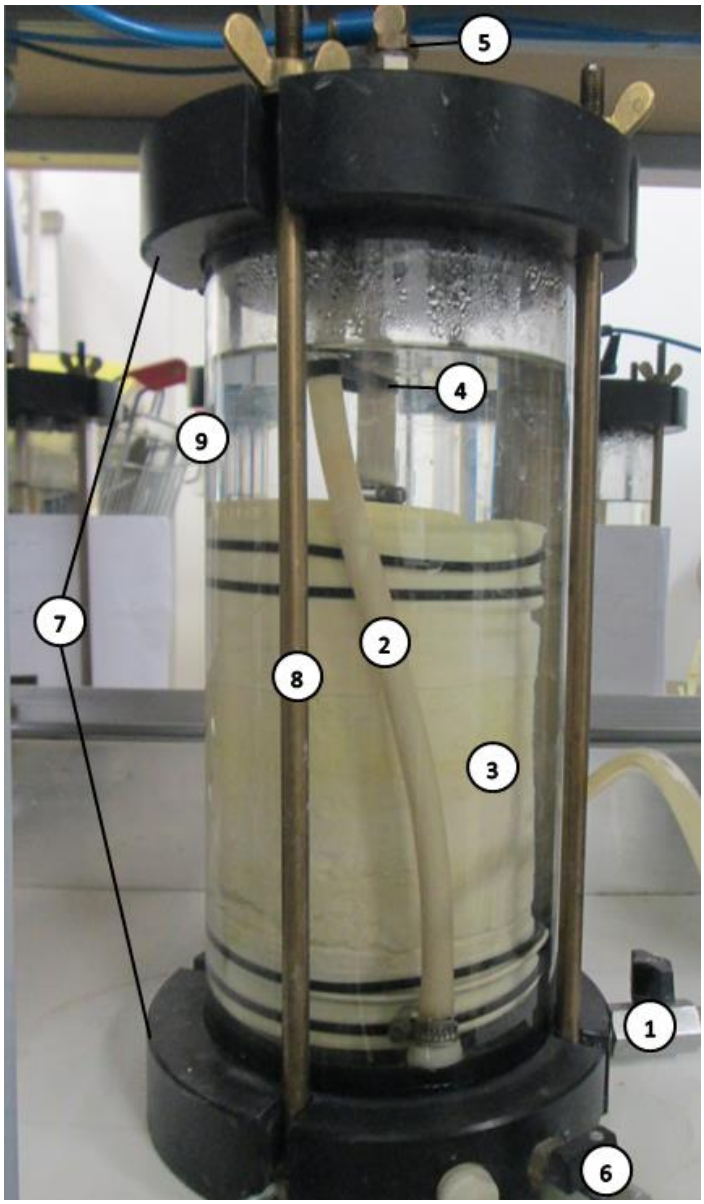

Fig. 10 Triaxial permeability cell. 1: bottom inlet, 2: connecting tube between upper filter stone and bottom outlet, 3: specimen inside rubber plastic, 4: control mark for water level, 5: inlet for air pressure, 6: bottom outlet, 7: bottom and top plate, 8: metal screw, 9: hard plastic cylinder

3.3 Permeability cylinder

The permeability cylinder is a laboratory device for determining the permeability of coarse grained soils like sand, gravel or a mixture of both within a constant-head arrangement (DIN 18 130 Part 1). These soil types are expected to have a hydraulic conductivity of more than 10^{-4} m/s. The permeability cylinder mainly consists of a massive metal ring that is clamped between a bottom and a top plate by metal screws. The cylinder is 12 cm high with a diameter of 10 cm. Inside the bottom and top plates ceramic filter stones are fixed. Small holes with attached linking pieces are on the side

of the bottom plate and on the top of the top plate. The inlet and the outlet beaker are connected with the cylinder by plastic tubes at the linking pieces. The inlet beaker is connected to a tab and constantly recharged with distilled water. In order to keep the head difference between the beakers constant, excess water in the outlet beaker is led to a weighing beaker. By changing the height difference between the beakers the amount of water passing through the sample is controlled. Additionally, two apertures in the metal ring with a distance *a* of at least 3 cm to the top and the bottom plate are linked with manometer tubes. The hydraulic gradient is determined from the height difference Δh_M between the water levels in the manometer tubes over the length *l* between the apertures (Equ. 2). Fig. 11 gives a schematic view of the complete test arrangement.

$$i = \frac{\Delta h_M}{l} \qquad \text{Equ. 2}$$

(DIN 18 130 Part 1)

In each test run the amount of water *Q* passing through the sample per second is collected in the weighing beaker and weighed. Permeability is calculated using the relationship in Equ. 3.

$$k = \frac{Q}{A \times i \times \Delta t \times 100} \qquad \text{Equ. 3}$$

Q [cm³] amount of water passing through sample

Δt [sec] time

A [cm²] cross-sectional area of specimen

i [ ] hydraulic gradient

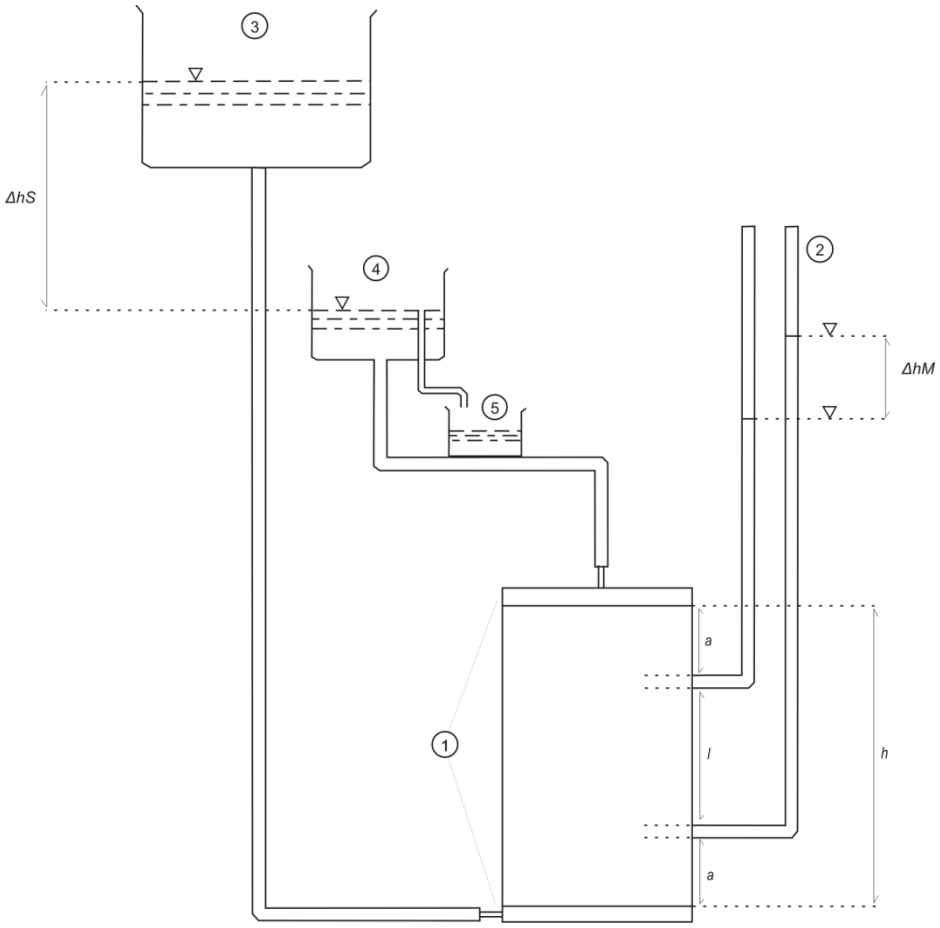

Fig. 11 Schematic view of a constant-head permeability cylinder test set-up. 1: top and bottom filter plate, 2: manometer tubes, 3: inlet beaker, 4: outlet beaker, 5: weighing beaker

3.4 Oedometertest

In the oedometer test a laterally confined soil sample fixed in a confining ring is axially loaded in several load steps. The sample should be prestressed with a load of 2 kPa in order to eliminate influences of an uneven sample surface or inadequate installation of the sample. As the sample is confined, there is no lateral strain. According to ÖNORM B4420 the load in every subsequent load step should be increased to the double of the previous step until the sample is unloaded. After the unloading stage, the sample has to be reloaded in the same manner as before.

The vertical deformation under each load is observed over a time span depending on the soil type. Highly permeable soils require a much shorter time to reach a consolidated state than lowly permeable soils. As soon as the sample shows a constant value of settlement, the next load increment can be applied. According to OENORM B 4420, constant settlement is reached as soon as the compression of the

sample per hour is less than 0.05 ‰ of the initial height of the sample. The adequate duration of the load steps can thus be calculated from the evaluation of the time-settlement-curve of the first load step. In general, durations ranging from less than 24 hours for highly permeable soils to a few days for lowly permeable soils are appropriate.

The height of the specimen should be approximately 0.2 – 0.4 times of its diameter (OENORM B4420). On both sides, the specimen is covered by porous metal filters which enable the in- and outflow of water into the sample. For the purpose of permeability measurement, the sample has to be put under distilled water at the beginning of the test. During the test the specimen has to be saturated.

Within the scope of this work the consolidation behaviour of a total of 22 samples was measured using the “Pero Scher/KD” device in the soil mechanics laboratory of the Graz University of Technology. Direct permeability measurements in the oedometer cell were carried out on 13 of them. Silt samples were prepared with a water content of 13.4%, 14.7% or 15.4% and wet densities between 1.99 and 2.35 g/cm³ (Tab. 1). All sand samples were mounted to the oedometer with a water content of 5%. Layered samples are produced out of silt layers with 15.4% and sand layers with 5% water content. After preparing the oedometer samples, they were mounted into cells and connected to the “Pero Scher/KD” device. The general test procedure was set in the control program to include a loading stage with load steps ranging from 10 to 320 kPa, an unloading stage with load steps ranging from 20 to 80 kPa and a reloading stage with load steps ranging from 40 to 640 kPa. According to ÖNORM B 4420, every sample has been prestressed with 2 kPa. The duration of each load step in one test was kept the same, ranging from 12 hours for sand to 48 hours for silt and layered samples. The general test program is shown in Tab. 2.

Tab. 1 Water content and density of silt samples before oedometer test

SILT			
Sample №	water content [%]	ρf [g/cm³]	ρd [g/cm³]
19146-1	15.4	2.19	1.82
19146-2	15.4	2.21	1.82
19146-3	15.4	2.21	1.82
19146-42	14.7	2.13	1.82
19146-43	14.7	2.35	1.82
19146-5	15.4	2.12	1.82
19146-7	13.4	1.99	1.82
19146-8	13.4	2.10	1.82

Tab. 2 General oedometer test program

1. Loading	
2	kPa
10	kPa
20	kPa
40	kPa
80	kPa
160	kPa
320	kPa
2. Unloading	
80	kPa
20	kPa
3. Reloading	
40	kPa
80	kPa
160	kPa
320	kPa
4. Loading	
640	kPa

3.4.1 Indirect permeability determination

Since the primary consolidation of a soil sample is governed by its permeability, graphic methods of fitting the primary part of the curve can be used to determine C_v and further k. Equ. 4 is used for permeability calculation from consolidation parameters.

$$k = \frac{C_v \times \rho_w \times g}{E_{oed}}$$ Equ. 4

(DIN 180135)

C_v [m^2/s] coefficient of consolidation

ρ_w [kg/m^3] density of water

g [m/s^2] gravitational acceleration

E_s [kPa] E-modulus during the respective load step in the oedometer test

Time-settlement curves from oedometer tests are usually fitted using the logarithm-of-time curve-fitting method (Casagrande and Fadum, 1940, cmp. Head, 1982) or the square-root-of-time curve-fitting method (Taylor, 1942, cmp. Head, 1982). According to Head (1982), the procedures are valid for various cohesive soil types. Clay soils provide the standard curves. Clayey silts and silts provide non-standard curves due to their higher permeability (Head, 1982). Deviations from the standard curve can restrict the application of graphic methods.

Fig. 13 shows the logarithm-of-time curve-fitting method, where the settlement is plotted on a natural scale against a logarithmic time scale. Two points A and B are chosen within the top curved part of the graph with the corresponding time values of t_A and t_B for which the relationship $t_B = 4t_A$ is valid (steps 1 and 2). A point C is marked above A and B with a vertical distance CA = AB (step 3). The value of settlement at the point C corresponds to theoretical 0% consolidation. In order to determine the settlement at 100% consolidation, two tangents are fitted to the curve (step 4). The first tangent is parallel to the linear part of the section of primary consolidation. The second tangent is set as the prolongation of the straight portion of secondary compression. The intersection point of the tangents provides the values of time and settlement corresponding to 100% consolidation.

The settlement at 50% consolidation is determined using the relationship in Equ. 5 (step 5).

$$s_{50} = \frac{s_0 + s_{100}}{2}$$ Equ. 5

s_0 [µm] settlement at 0% consolidation

s_{50} [µm] settlement at 50% consolidation

s_{100} [µm] settlement at 100% consolidation

The theoretical time value T_v, corresponding to a degree of consolidation of 50%, is 0.196 (DIN 18135). t_{50} (step 6) is used to calculate the coefficient of consolidation C_v [cm^2/s] by the formula

$$C_v = \frac{0.196 \times {H_{50}}^2}{t_{50}} \qquad \text{Equ. 6}$$

(DIN 18135).

H_{50} [cm] average specimen height during one load step

t_{50} [s] time taken for the soil specimen to reach 50% consolidation

The theoretical log-time curve, which is fitted by the described method after Casagrande, is shown in Fig. 12. Since laboratory curves (cmp. Fig. 13) usually deviate from the theoretical graph, the prolongation of the straight part at the end of the graph can involve difficulties. Curves from laboratory tests often show more than one straight part after the inflexion point of the graph. In deciding from where to prolong the latter part of the curve one should bear in mind that the intersection of the tangents should plot in a realistic area. In a log-time plot the inflexion point of the graph occurs at approximately 75% consolidation, from which it is possible to roughly estimate the point of 100% consolidation (Head, 1982).

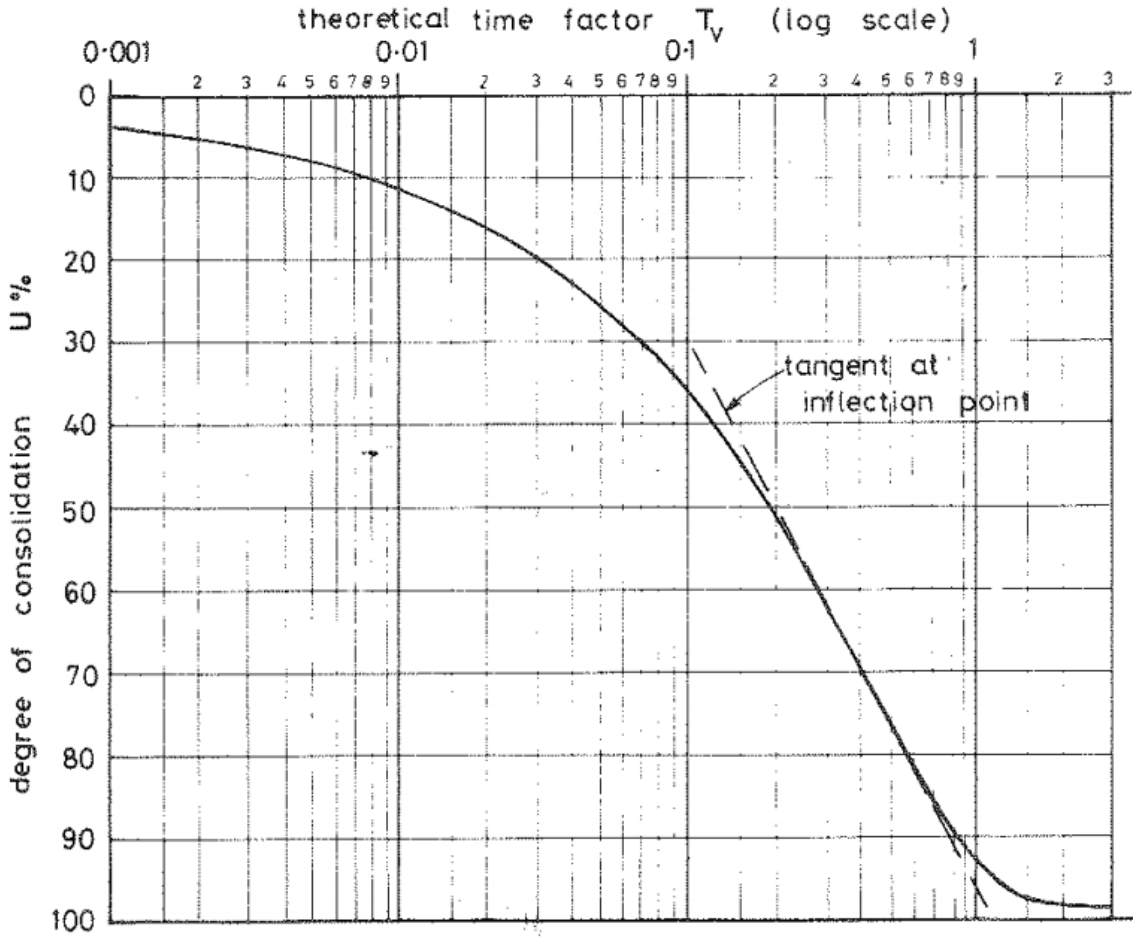

Fig. 12 Theoretical log-time curve: “Time factor T_v related to degree of consolidation *U%*“ (Head, 1982).

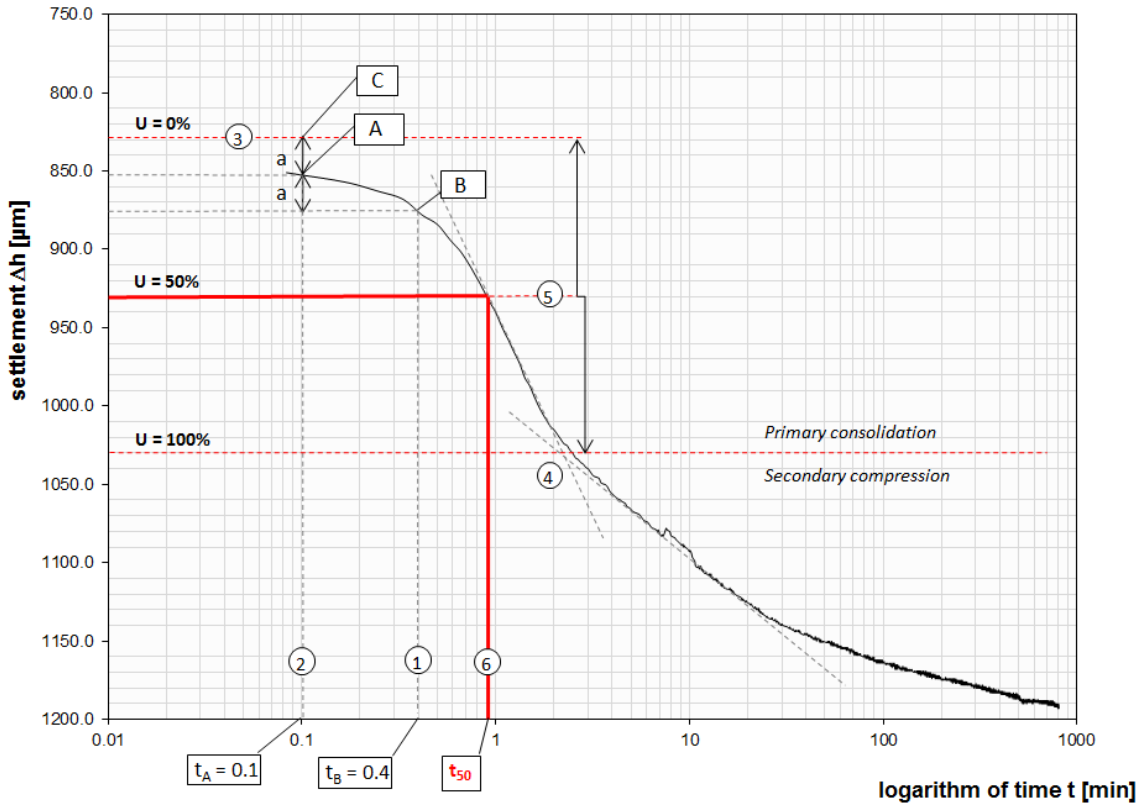

Fig. 13 Casagrande method of C_v-determination illustrated on a time-settlement curve of sample 19146-8

Fig. 15 depicts the square-root of time curve-fitting method: The settlement is plotted on a natural scale against the $\sqrt{\text{time}}$. A line is fitted parallel to the linear part of initial consolidation (step 1). The upper end of the line corresponds to theoretical 0% consolidation during the current load step (point *A*). In step 2, a point *B* is chosen on the tangent with a distance *x* from the vertical axis. A horizontal line is drawn through *B*. On this horizontal line, a third point *C* with a distance of 1.15*x* from the vertical axis is set (step 3). In step 4 the line *AC* is drawn. The intersection of the line *AC* with the time-settlement curve provides the time value t_{90} on the x-axis (step 5) and the value of settlement at 90% consolidation of the sample during the current load step (step 6). The C_v-value is calculated using the relationship shown in Equ. 7 (DIN 18135).

.

$$C_v = \frac{0.848 \times H_{50}{}^2}{t_{90}} \qquad \text{Equ. 7}$$

t_{90} [s] time taken for the soil specimen to reach 90% consolidation

Olson (1986) mentions, that laboratory curves often deviate from the theoretical standard-curves in either the initial, the end or even the middle section of the graph. Probably due to their higher permeability, compared with the standard material (clay), the laboratory data of the tested silts deviates in the initial part of the curve. In a standard curve, the point of 0% consolidation is supposed to plot below the initial reading. For the tested silts, this is not given and the point of 0% consolidation is a pure theoretical value. Fig. 14 shows the theoretical square-root of time curve on which Taylor's curve-fitting method is based.

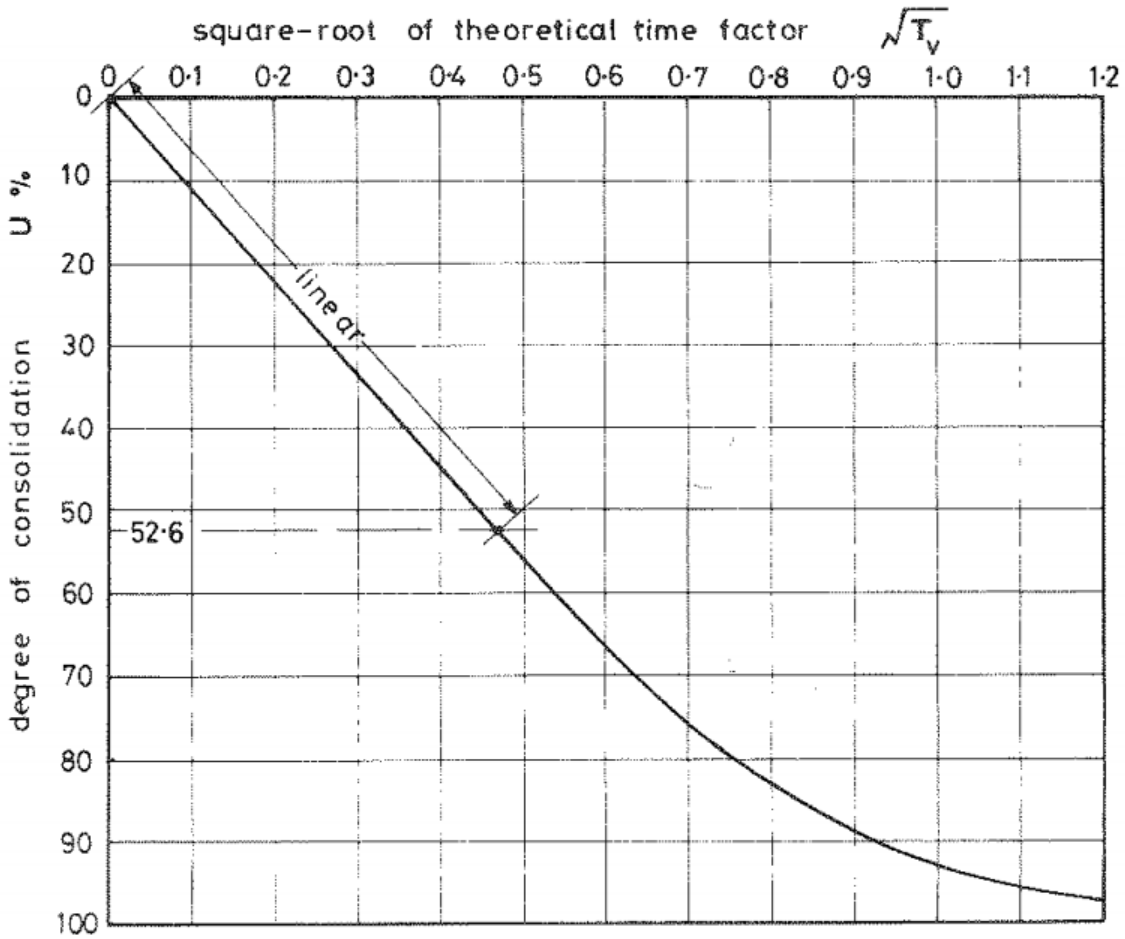

Fig. 14 Theoretical √time curve: "Square-root of time factor , √T_v, related to degree of consolidation *U%*" (Head, 1982).

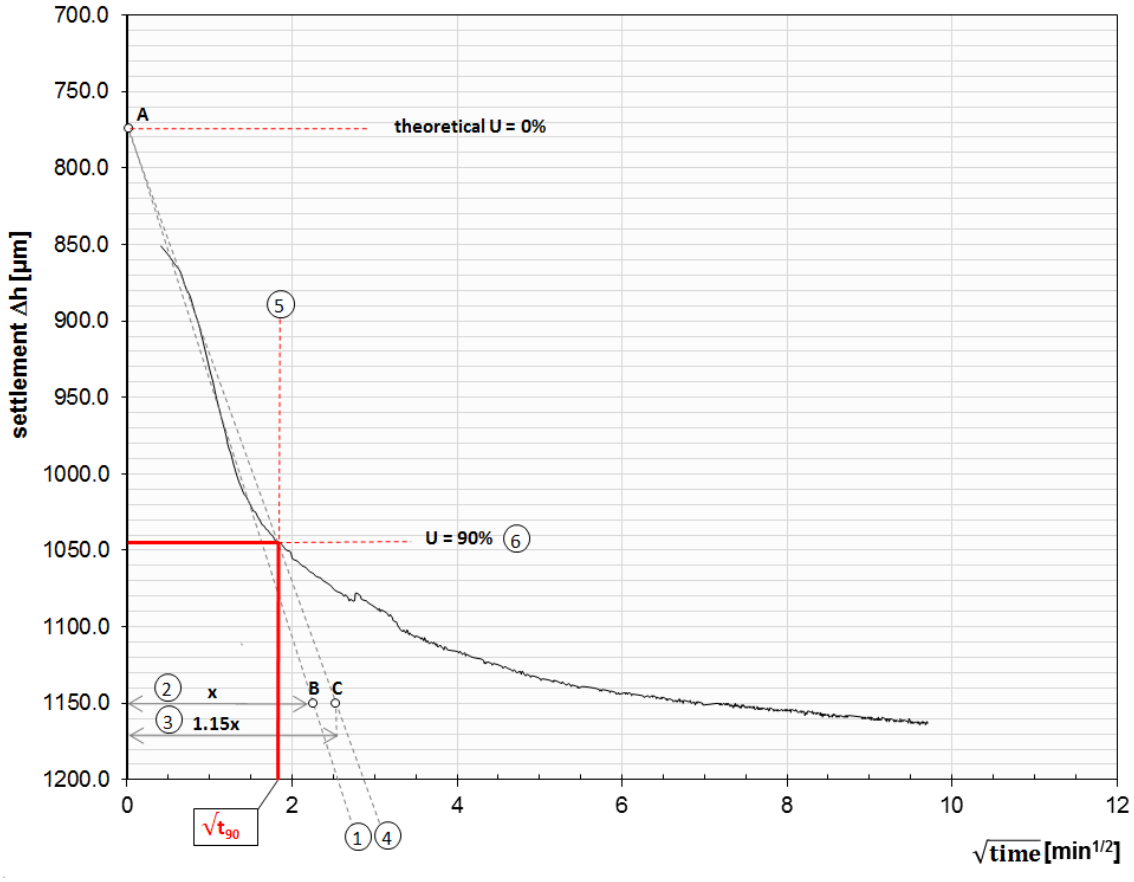

Fig. 15 Taylor method of C_v-determination showed on a time-settlement curve of sample 19146-8

According to Olson (1986, cmp. Yong & Townsend 1986), for the determination of the point of 0% consolidation, Taylors approach generally is to be preferred to the plot over a logarithmic scale. Since the oedometer tests performed on the silt samples provided non-standard curves, difficulties in the determination of the value of settlement at 0% consolidation occurred. Furthermore, C_v-values determined from the $\sqrt{time}$-method almost always exceed values determined from the logarithmic method (Olson, 1986, cmp. Yong & Townsend, 1986). Tewatia & Venkatachalam (1997) concluded, that due to the effects of initial and secondary compression, C_v is higher if the curve is fitted in its initial part (cmp. Taylor's method) and lower if fitted close to the latter part (cmp. Casagrande's method). The improvement of the $\sqrt{time}$-method proposed by Tewatia & Venkatachalam (1997) uses T_{70} (=0.405) and gives higher values of C_v than both Taylor's and Casagrande's method. The coefficient of consolidation determined in the

field always exceeds the values determined in laboratories (Leroueil, 1988, cmp. Tewatia & Venkatachalam, 1997). Using $C_{v(70)}$ results in the highest *k*-values, which should be closest to real field values (Tewatia & Venkatachalam, 1997).

Head (1982) and Olson (1986, cmp. Yong & Townsend, 1986 p.35) mentioned, that secondary compression affects the primary consolidation path in the following load step. According to Head (1982), the effect is problematic if one load step is repeated or maintained for particularly long time, as secondary compression will be prolonged compared to other load steps. Using the discussed indirect methods for permeability determination by curve fitting, possible restrictions in their application due to the laboratory situation (e.g. prolongation of load steps) have to be considered.

While for cohesive soil samples, graphic methods are applied, permeability in layered samples can be derived mathematically using the *k*-values of the single layers. Vertical permeability in horizontally layered samples is calculated according to Equ. 8 (Von Soos & Engel, 2008).

$$k_v = \frac{d}{\frac{d_1}{k_1} + \frac{d_2}{k_2} + \cdots + \frac{d_n}{k_n}} \qquad \text{Equ. 8}$$

d [m] total vertical thickness of all soil layers ($d = d_1 + d_2 + \ldots + d_n$)

d_n [m] vertical thickness of soil layer n

k_n [m/s] permeability of soil layer n

3.4.2 Direct permeability determination

For direct permeability measurements a falling head test is conducted while the specimen is kept under constant load. Through the bottom inlet the specimen is connected to a manometer tube. As soon as load and settlement are constant under a certain load step, the standpipe is filled with distilled water. The standpipe needs to be free from any air bubbles. Three marks h_1, h_2 and h_3 are made on the manometer tube. 50mm below the top of the tube the h_1-mark is set which corresponds to the height y_1 above the reference level y_0 minus the height of the overflow level h_0 of the oedometer cell. The h_2-mark is placed at a random point but at a height y_2 of at least 200mm

above h_0. h_3 is calculated using the formula $h_3 = \sqrt{(h_1 \times h_2)}$. The corresponding mark on the manometer tube is set at the height $y_3 = h_3 + h_0$ above the reference level. Fig. 16 shows the correct setting and determination of the marks h_1 to h_3 and y_1 to y_3 respectively.

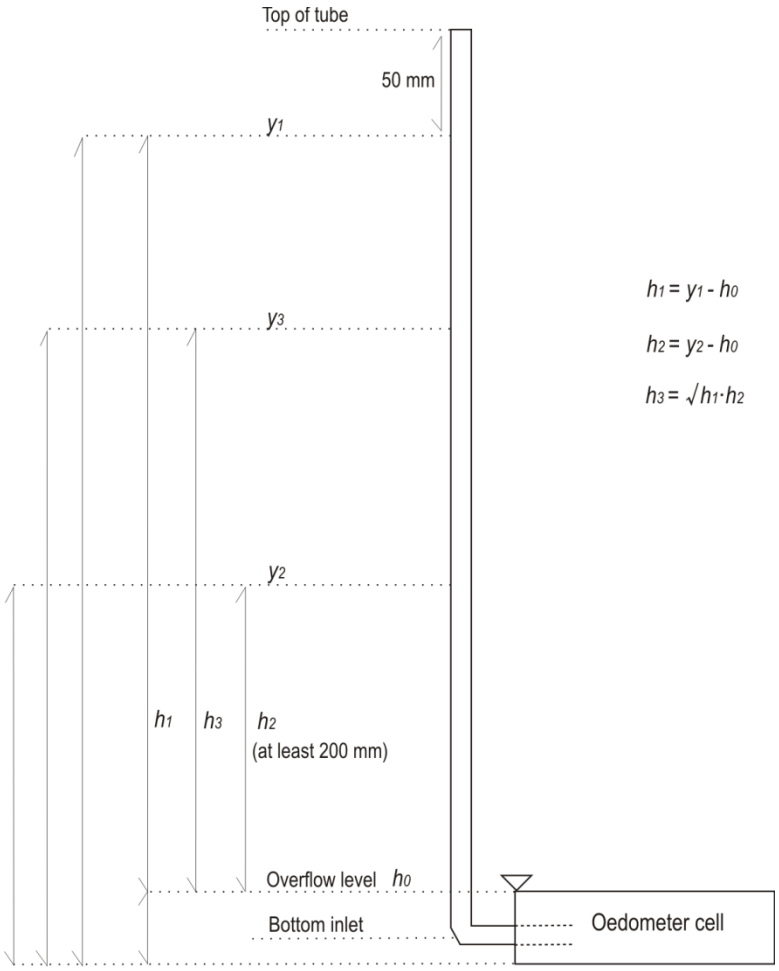

Fig. 16 Schematic view of oedometer cell with connected manometer tube

The time taken for the water level in the tube to fall from h_1 to h_3 should be the same as for the distance between h_3 and h_2 (Head, 1982). If the error between these two measurements is higher than 10%, the test has to be repeated. In order to receive a statistically reliable result the test is repeated at least 2-3 times. For the calculation of permeability at the temperature T the relationship in Equ. 9 is used (Head, 1982).

.

$$k_T = \frac{2.303 \times aL}{1000 \times A \times t} \log_{10} \frac{h_1}{h_2}$$ Equ. 9

a [mm²] cross-sectional area of manometer tube

L [mm] length of cell body

A [mm²] cross-sectional area of specimen

t [s] average time for each test run

T [°C] temperature of water

As the permeability of a soil sample depends on the viscosity of the water passing through it, the value k_{10}, corresponding to the permeability at 10°C, is used in order to allow comparison of results. The temperature correction according to Equ. 10 was done for all direct measurements.

$$k_{10} = \frac{1.359}{(1 + 0{,}0337 \times T + 0{,}00022 \times T^2)} \times k_T$$ Equ. 10

(OENORM B 4422-1)

Fig. 17 shows an oedometer cell in the soil mechanics laboratory of the Graz University of Technology.

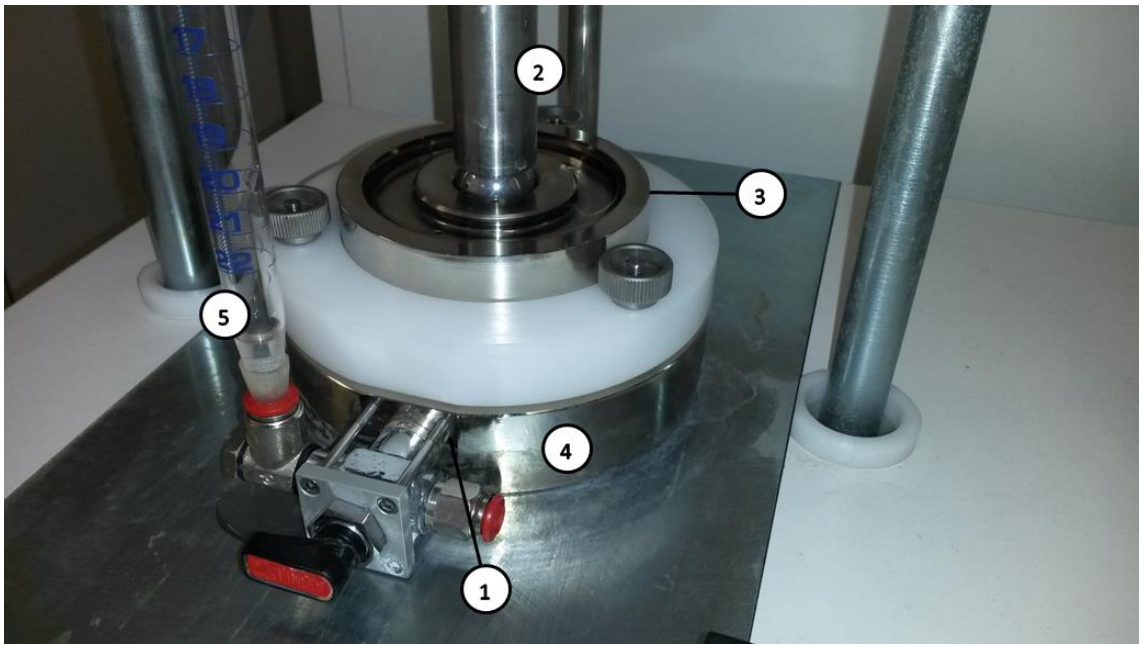

Fig. 17 Oedometer cell. 1: bottom inlet, 2: load applicator, 3: confining ring and overflow level, 4: cell body, 5: manometer tube

For the implementation of a series of test runs in lowly permeable soil samples the respective load step had to be repeated. As already mentioned in chapter 3.4.1, prolonged secondary compression affects the primary path of the following load step (Head, 1982). Due to this effect, it was impossible to apply graphic methods of C_v-determination on the time-settlement curves of the concerned load steps.

To enable direct permeability measurement in soil samples of low permeability it is necessary to use manometers of particularly small diameter. A total of 7 different manometers were used in oedometer falling-head tests, depending on the soil type (Tab. 3).

Tab. 3 Cross-sectional areas of manomters used in falling head tests

Manometer №	1	2	3	4	5	6	7
cross-sectional area [mm²]	5.26	150	14.7	100	50	420	5

For silt samples three different manometers were used:

- Manometer 1
- Manometer 4

- Manometer 5

Experiments have shown that from the used manometer tubes manometer 1 offers the optimum cross-sectional area for measuring silt permeability. The average test time amounts to 6.93 hours for a complete test run on a silt sample. In order to reduce the test time manometers with a tinier cross-sectional area than 5.26 mm² were used. The filling of these manometers without any introduction of air bubbles turned out to be difficult and more time consuming than using a manometer of bigger diameter.

For sand samples two different manometers were used:

- Manometer 4
- Manometer 6

Manometer 6 is considered to offer the optimum cross-sectional area for measuring permeability of medium sand. The average test time amounts to 19.35 seconds for a complete test run on a sand sample.

For layered samples four different manometers were used:

- Manometer 1
- Manometer 2
- Manometer 3
- Manometer 7

Concerning layered samples, the key parameters in the testing are the hydraulic gradient *i* and the orientation of the flow. The hydraulic gradient governs filter stability between two layers with different hydraulic conductivity (Saucke, 2006).

The hydraulic gradient acting on a soil sample was calculated by the relationship

$$i = \frac{h_3}{L} \qquad \text{Equ. 11}$$

h_3 [mm] intermediate water level used in falling-head tests

L [mm] specimen height during the respective load step

All filter criteria which have been considered work with the grain sizes *D* of the filter material and the grain sizes *d* of the base material. The values for the tested soils were determined by grain size distributions and are listed in chapter 4, Tab. 4.

The geometric criterion for filter stability developed by Terzaghi and Peck (1948) (cmp. Saucke, 2004) treats the mechanic possibility of particle movement from the fine base material into the coarser filter material. The geometric criterion by Terzaghi and Peck (1948) is applicable to soils with continuous grading only (Saucke, 2004). The criterion requires uniformity coefficients for the base and filter material of $C_{U_B},\ C_{U_F} \leq 2$. If the requirement in Equ. 12 is fulfilled, the soils are filter stable.

$$\frac{D15}{d85} \leq 4 \qquad \text{Equ. 12}$$

The geometric criterion by Cistin and Ziems (1969) is applicable for soils with bigger uniformity coefficients ($C_{U_B}, C_{U_F} > 2$) and involves the interval ratio (Saucke, 2004).

The interval ratio is defined as

$$A50 = \frac{D50}{d50} \qquad \text{Equ. 13}$$

If the interval ratio *A50* does not exceed the allowed value determined from Fig. 18, the soils are filter stable (Equ. 14)

$$A50_{given} \ \leq \ A50_{allowed} \qquad \text{Equ. 14}$$

Geometric requirements of the Cistin and Ziems geometric criterion are

- $0.1\ mm\ \leq d50\ \leq 30\ mm$
- $4\ mm \leq D50\ \leq 100\ mm$
- $C_U \leq 20$ for both soils

(Striegler and Werner, 1969)

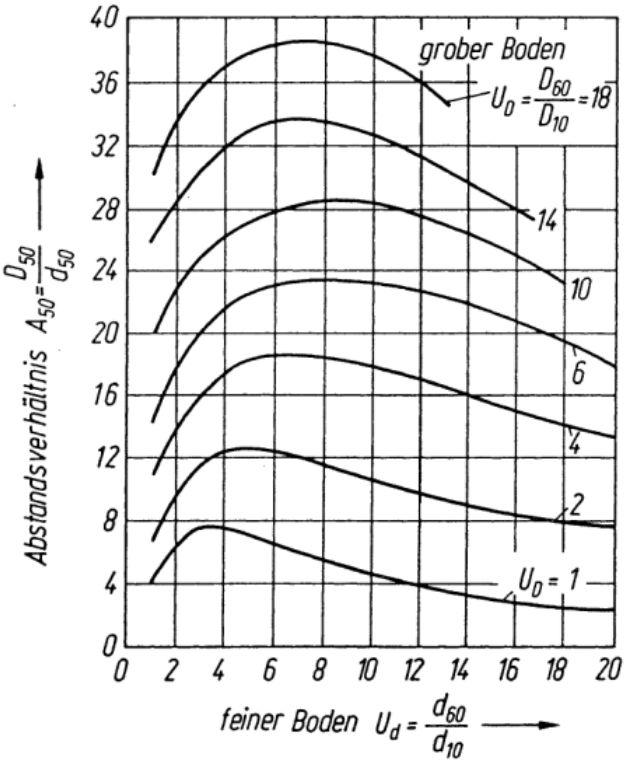

Fig. 18 Hydraulic filter criterion by Cistin/Ziems (cmp. Adam et al., 2012)

Hydraulic criteria developed by several authors treat filter stability in dependence of the hydraulic gradient. In a horizontally layered sample, contact erosion between two layers of different hydraulic conductivity occurs as soon as the hydraulic gradient of an upright flow through the specimen reaches the critical value i_{krit}. This type of inner erosion can occur exclusively in the contact zone with flow direction from the less permeable (fine grained) to the more permeable (coarse grained) layer (Saucke, 2006). Ziems (1969) and Zweck (1956) described adequate criteria for this scenario.

The hydraulic criterion by Ziems (1969, cmp. Saucke, 2004) is applicable for an upright flow in horizontally layered samples with $C_{U_B} \leq 5$. If the requirements are fulfilled, the critical gradient in the fine base material can be calculated using Equ. 15.

$$i_{krit_B} = 0.66 + \frac{6}{d10^2 \times A50^2} \qquad \text{Equ. 15}$$

The hydraulic criterion by Zweck (1956) gives a graphic solution for filter stability. Filter stability in a base material with a minimum value for *d50* of 0.06 mm and a maximum hydraulic gradient of 14 acting on the specimen can be determined using Fig. 19.

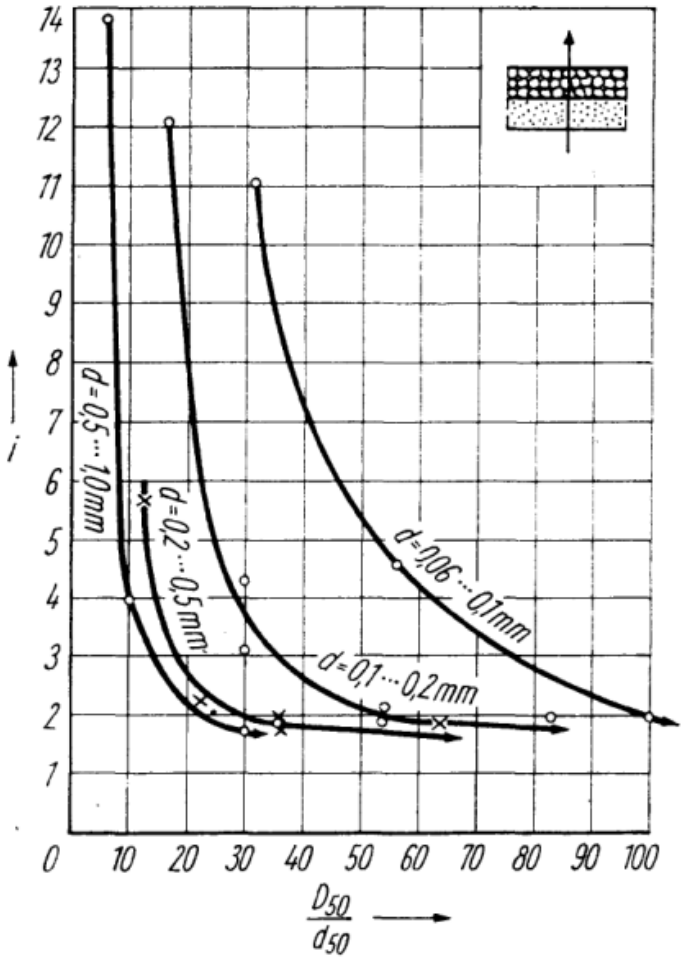

Fig. 19 Hydraulic filter criterion by Zweck (1956) (cmp. Striegler and Werner, 1969) for horizontal filters with upright flow direction

4 Test results

In laboratory tests, silt and sand dominated soils were used. The silt dominated soil consists of 26.7% clay, 57.7% silt and 15.6% sand. The sand dominated soil contains approximately 2.2% of particles with a grain size less than 0.063mm, 24.8% fine sand, 65% medium sand, 7.8% coarse sand and 0.2% gravel. The dry density of silt and sand is ρ_d=1.82 g/cm^3 and ρ_d=1.5 g/cm^3 respectively. Fig. 20 and Fig. 21 show the grain size distributions of the used materials.

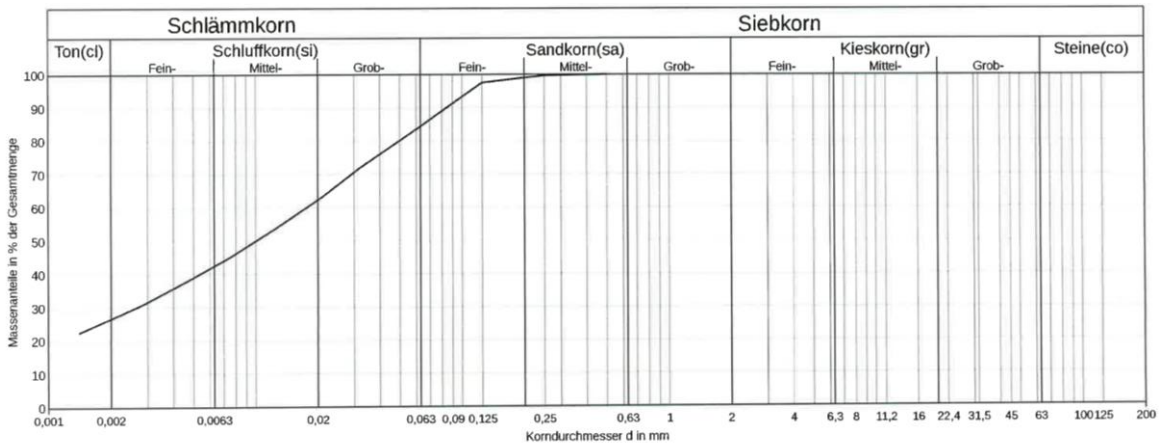

Fig. 20 Grain size distribution of clayey silt, evaluated by the soil mechanics laboratory of the Graz University of Technology.

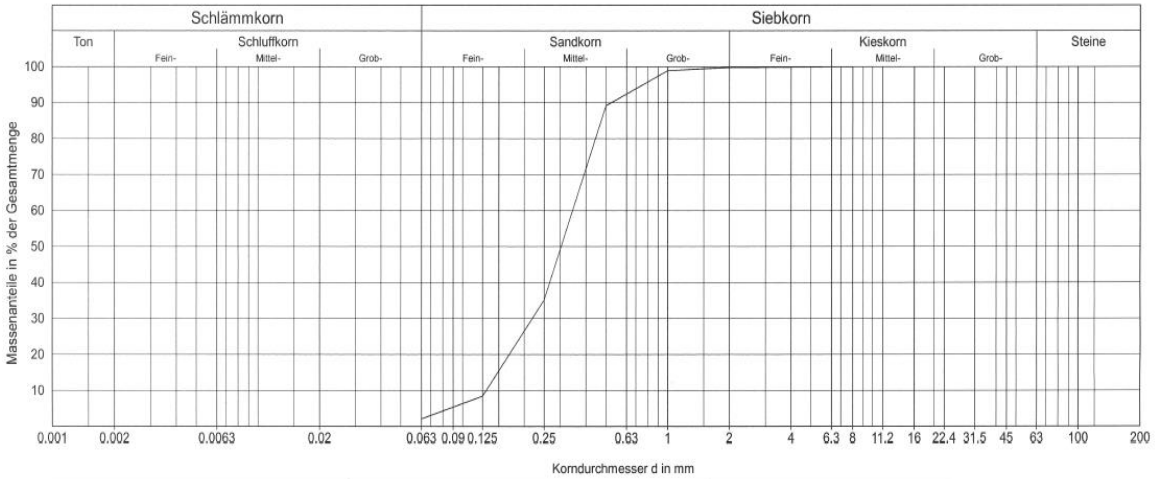

Fig. 21 Grain size distribution of medium sand, evaluated by the soil mechanics laboratory of the Graz University of Technology.

From the grain size distributions the values *d10*, *d15*, *d50*, *d60* and *d85* have been determined for both materials (Tab. 4).

Tab. 4 Particle sizes [mm] for silt and sand used in the laboratory

Silt				
d10	**d15**	**d50**	**d60**	**d85**
<0.002	<0.002	0.01	0.0176	0.063
Sand				
D10	**D15**	**D50**	**D60**	**D85**
0.13	0.15	0.30	0.33	0.49

4.1 Oedometer test

For the oedometer tests, circular shaped soil samples with a height of 2cm and differing diameters were prepared. A total of three different oedometer cells were used for the measurements. Cell 1 offers space for a circular sample with a diameter of 8 cm. Samples in cell 2 need to be shaped with a diameter of 5 cm and the diameter of cell 3 was measured to be 7.17 cm (Tab. 5).

Tab. 5 Dimensions of cells used in oedometer tests

	Cell 1	Cell 2	Cell 3
V	100.531	39.27	80.75
d	8	5	7.17
h	2	2	2
A	50.265	19.63	40.38

4.1.1 Silt samples

The samples 19146-1, -2, -3, -42, -43, -5, -7 and -8 are silt samples that were mounted into oedometer cells. Direct measurements were performed on the samples 19146-1, -43 and -8. Samples 19146-3 and -42 were evaluated graphically only. Due to technical defects, 19146-2, -5 and -7 could not be evaluated. Tab. 6 lists the dimensions of each sample and the used manometers and cell types.

In sample 19146-1 a series of falling head tests were carried out while applying a load of 320kPa (loading stage). With a hydraulic gradient of 16 an average value of permeability of 1.88E-07 m/s was determined through the direct measurements using

manometer 4 (Tab. 3). No visible water leakage at the connecting tubes between the manometer and the cell could be detected. After unmounting the sample no cracks or failure zones within the sample or at its borders could be detected. The clearly too high coefficient of permeability must be the result of, from the outside invisible, leaky zones between the confining ring and the specimen ring of the oedometer cell 1 (Tab. 5, Fig. 22). For the same reason, dissatisfying results were obtained from direct measurements in sample 19146-43. Using manometer 5 (Tab. 3) during the 160kPa and the 320kPa load step, average permeability values of k=4.48E-07 m/s and k=3.59E-07 m/s respectively were determined (i=30).

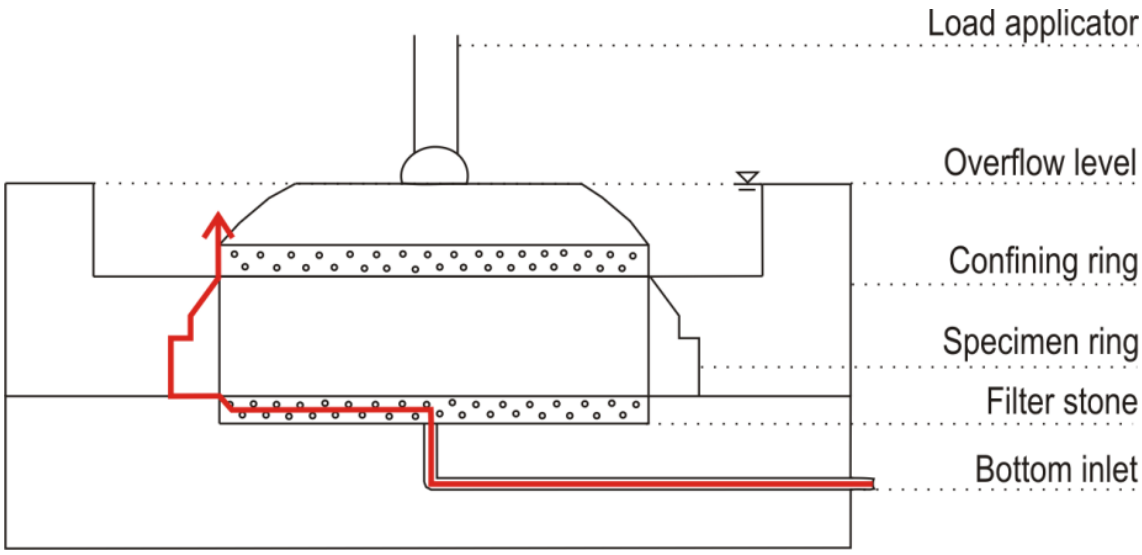

Fig. 22 Suspected path of water through the metal rings of the oedometer cell

For tests of sample 19146-8, the 160kPa and the 320kPa load step of the loading and reloading stage have been prolonged to 6 times the testing time used on other silt samples. The test was optimized by using the ideal manometer (manometer 1, Tab. 3) and an odeometer cell of type 3 (Tab. 5). Additionally, laboratory grease was applied between the metal rings of the cell, to ensure that the cell is not leaking. Several series of falling head tests were carried out during the prolonged load steps. During the 160kPa load step of the loading stage the falling-head test with a hydraulic gradient of 32 gave an average value of permeability of k=8.10E-11 m/s. For the 320kPa load step of the loading stage and a hydraulic gradient of 33 an average coefficient of permeability of 5.20E-11 m/s was computed. The values determined for the 160kPa and 320kPa steps of the reloading stage are 6.76E-11 m/s and 5.97E-11 m/s respectively (i=33).

For indirect permeability determination the time-settlement-curve of the primary consolidation paths of the samples 19146-1, -3, -42, -43 and -8 were examined. The results of direct and indirect permeability determination on silt samples are listed in Tab. 7. Diagrams showing the evaluation for each sample are attached in the appendix (chapter 8.1). The *k*-values determined through the log-time method range from 5.09E-11 m/s to 5.39E-10 m/s for the 160kPa load stage and from 1.55E-10 m/s to 5.70E-10 m/s for the 320kPa load stage. Using the square-root-of-time method, permeability values between 2.10E-10 m/s and 9.43E-10 m/s were obtained for the 160kPa load stage. The values determined for the 320kPa load stage range from 1.70E-10 m/s to 7.59E-10 m/s. In general, the square-root method gives higher *k*-values than the log-time method.

Tab. 6 Sample dimensions and used cells/manometers for silt samples

	SILT SAMPLES							
19146 -	**1**	**2**	**3**	**42**	**43**	**5**	**7**	**8**
diameter [cm]	8	8	8	8	8	5	5	7.17
height [cm]	2	2	2	2	2	2	2	2
cell type	1	1	1	1	1	2	2	3
manometer type	4	-	-	-	5	-	-	1

Tab. 7 Mean permeability values determined in silt samples by direct and indirect methods.

SILT SAMPLES				SILT SAMPLES			
	direct k [m/s]			indirect k [m/s]			
	falling-head test			log-time method		square-root method	
	160 kPa	320 kPa	i	160 kPa	320 kPa	160 kPa	320 kPa
19146-1	-	1.88E-07 (l)	16	2.00E-10	5.40E-10	3.20E-10	5.26E-10
19146-3	-	-	-	1.83E-10	1.55E-10	2.10E-10	1.70E-10
19146-42	-	-	-	6.54E-11	5.70E-10	9.43E-10	7.59E-10
19146-43	4.48E-07 (l)	3.59E-07 (l)	30	5.09E-11	5.00E-10	7.62E-10	5.01E-10
19146-8	8.10E-11 (l)	5.20E-11 (l)	32-33	5.39E-10	-	8.19E-10	
	6.76E-11 (r)	5.97E-11 (r)					

(l) loading stage
(r) reloading stage

4.1.2 Sand samples

The samples 19147-1, -2, -3, -4, -5, and -6 are sand samples that were mounted into oedometer cells. Direct measurements were performed on the samples 19147-1, -5 and -6. Tab. 8 lists the dimensions of each sample and the used manometer and cell type.

Using a hydraulic gradient of 16 the average values of k=1.01E-06 m/s and k=8.44E-07 m/s respectively were determined for the 320kPa load step of the loading and reloading stage in sample 19147-1. The clearly too low permeability obtained from the tests is due to the low permeability of the used filter stones in the oedometer cell. Thus, instead of measuring soil permeability, the k-value of the filter stones was determined. The range of permeability values determined in sample 19147-5 (Tab. 9) shows, that the same error as in the measurement of 19147-1 occurred.

Sample 19147-6 was mounted to cell type 2. The low permeable metal filter stones were replaced by higher permeable metal filter stones. Gaps between the confining ring and the specimen ring of the oedometer were greased to avoid leakage. During the 80kPa load step of the loading stage an average coefficient of permeability of 5.45E-05 m/s was determined in sample 19147-6. Measurements in the same load step of the reloading stage gave the value k=6.19E-05 m/s. For the 160kPa load step of the loading stage and the reloading stage average values for permeability of k=5.95E-05 m/s and k=6.23E-05 m/s respectively were computed. The k-values determined during the 320kPa load steps are 6.04E-05 m/s for the loading stage and 5.04E-05 m/s for the reloading stage. All measurements were performed with a hydraulic gradient of 30.

Tab. 8 Sample dimensions and used cells/manometers for sand samples

	SAND SAMPLES					
19147-	1	2	3	4	5	6
diameter [cm]	8	8	8	8	8	5
height [cm]	2	2	2	2	2	2
cell type	1	1	1	1	1	2
manometer type	4	-	-	-	6	6

Tab. 9 Mean permeability values determined in sand samples by direct methods.

SAND SAMPLES				
	direct k [m/s]			
	falling-head test			
	80 kPa	160 kPa	320 kPa	i
19147-1	-	-	1.01E-06 (l)	16
			8.44E-07 (r)	
19147-5	3.42E-06 (l)	2.49E-06 (l)	1.63E-06 (l)	33
		2.11E-06 (r)	1.24E-06 (r)	
19147-6	5.45E-05 (l)	5.95E-05 (l)	6.04E-05 (l)	30
	6.19E-05 (r)	6.23E-05 (r)	5.04E-05 (r)	

(l) loading stage
(r) reloading stage

4.1.3 Layered samples

In addition to the tests in sand and silt samples, 3 types of artificially layered samples were fabricated. All of them were shaped circularly with the dimensions demanded by the oedometer cell type 3 (Tab. 5). Sample type 1 is built up of a sand layer embedded by two silt layers. The thickness of the silt layers amounts to 0.69cm for the upper one and 0.6cm for the lower layer. The sand layer is 0.7cm thick. Sample type 2 consists of a fine sand layer with a thickness of 1cm embedded by two silt layers of 0.5cm thickness. Sample type 3 is built up of two fine sand layers of 0.75cm thickness embedding a 0.5cm thick silt layer. Fig. 23 sketches the dimensions of each sample type.

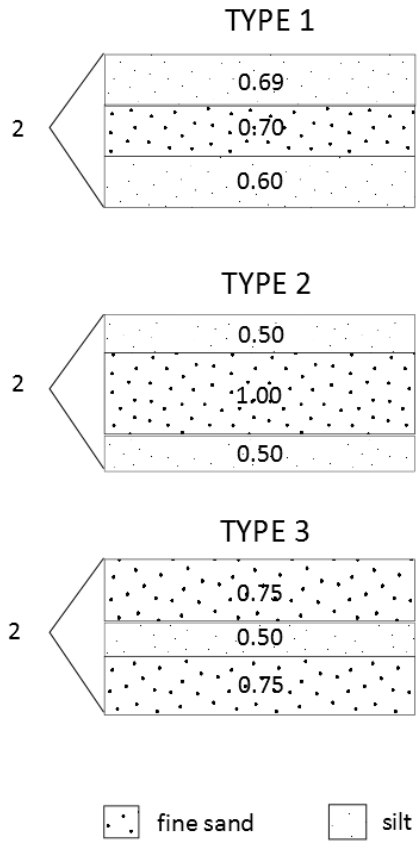

Fig. 23 Types of artificially layered samples. Dimensions in [cm].

Two geometric and two hydraulic filter criteria for horizontally layered samples with upright flow were summarized in chapter 3.4.2. In the tested layered samples, silt represents the base material and sand the filter material. Using the data from Tab. 4, the uniformity coefficients for sand and silt were calculated (Equ. 16).

$$C_{u_{Sa}} = \frac{D60}{D10} = 2.5$$

Equ. 16

$$C_{u_{Si}} = \frac{d60}{d10} \geq 8.8$$

The geometric criteria by Terzaghi/Peck (1948) and Cistin/Ziems (1969) could not be applied for the used soils. C_{uSi} and C_{uSa} exceed the critical values for the uniformity coefficient in the Terzaghi/Peck (1948) criterion and the medium grain sizes *D50* and *d50* are not within the allowed range for the Cistin/Ziems (1969) criterion. The hydraulic criterion by Ziems (1969) could not be applied, since C_{uSi} exceeds 5. The filter criterion

by Zweck (1956) was developed based on the testing of soils with a minimum value for *d50* of 0.06 mm. The highest hydraulic gradient used in the tests was 14. The criterion does not clearly exclude the used silt, but due to the boundaries of the experimental curves the critical gradient for the given *d50* cannot be determined.

For calculation of permeability in layered samples (Equ. 8), mean k-values of representative silt and sand samples determined in the 160kPa and the 320kPa load steps of the loading stage were used. From the 320kPa load step, the values 6.04E-05 m/s (sand) and 5.20E-11 m/s (silt) were used. From the 160kPa load step, the values 5.95E-05 m/s (sand) and 8.10E-11 m/s (silt) were used (Tab. 10). The respective minimum and maximum permeability determined in the same silt and sand samples were used to calculate a minimum and maximum permeability of layered samples. The results for each layered sample type are listed in Tab. 11.

Tab. 10 Mean, minimum and maximum permeability measured in sample 19146-8 (silt) and 19147-6 (sand)

	MEAN		MINIMUM		MAXIMUM	
Load step	k [m/s]					
kPa	silt	sand	silt	sand	silt	sand
160	8.10E-11	5.95E-05	7.43E-11	5.88E-05	8.69E-11	6.02E-05
320	5.20E-11	6.04E-05	4.70E-11	5.88E-05	5.45E-11	6.19E-05

Tab. 11 Calculated permeability for layered samples of type 1, 2 and 3

Calculated permeability *k* [m/s]				
	kPa	Mean	Maximum	Minimum
Type 1	160	1.26E-10	1.35E-10	1.15E-10
	320	8.06E-11	8.45E-11	7.29E-11
Type 2	160	1.62E-10	1.74E-10	1.49E-10
	320	1.04E-10	1.09E-10	9.40E-11
Type 3	160	3.24E-10	3.48E-10	2.97E-10
	320	2.08E-10	2.18E-10	1.88E-10

The permeability of the layered samples 19148-1, -2, -3, -4, -6, -7 and -8 was determined directly in oedometer falling-head tests. Because of the experiences with leakage from previous tests, the oedometer cells were closed with laboratory grease additionally to the rubber rings. The tests were performed with the manometers listed in Tab. 12.

Tab. 12 Sample type and used manometers for layered samples

	LAYERED SAMPLES							
19148-	1	2	3	4	5	6	7	8
sample type	1	2	3	2	3	3	2	3
manometer type	7	2	3	1	-	2	1	2

In order to conduct a series of measurements, the 160kPa and 320kPa load steps were kept for 4 to 6 days, while other load steps were kept for 24 hours. Except for sample 19148-6, results similar to the values expected from calculations were obtained. Sample 19148-1 was tested at 315kPa in one test run. A coefficient of permeability of 1.16E-10 m/s was obtained from the test (Tab. 13).

On sample 19148-2, several direct measurements were performed during the prolonged steps of the loading and reloading stage. During the loading stage the soil permeability was measured to be 6.08E-10 m/s for the 160kPa load step and 3.36E-10 for the 320kPa step. During the reloading stage the soil permeability was measured to be 4.37E-10 m/s for the 160kPa step and 3.54E-10 for the 320kPa step. The post-test state of sample 19148-2 shows a uniformly compressed sample without any visible cracks. One thinner zone in the upper silt layer occurs which shows the entrance of small amounts of sand from the middle layer. The upper silt layer was uniformly thinner after the test whilst the lower silt layer maintained its original thickness.

For sample 19148-3, direct measurements taken in the 160kPa step of the loading stage gave an average coefficient of permeability of 2.07E-10 m/s. At the 320kPa step of the loading stage a *k*-value of 1.46E-10 was obtained. The test was stopped at the 320kPa load step of the reloading stage in order to collect more data of the loading stage by testing further samples. The post-test state of sample 19148-3 does not show any noticeable characteristics indicating a failed permeability measurement. The layers seem to be uniformly compressed and do not show any weakness zones.

Permeability of sample 19148-4 was tested directly during the loading stage. The soil permeability during the 160kPa and 320kPa load steps was determined to be 1.59E-10 m/s and 9.18E-11 m/s respectively. The post-test state of sample 19148-4 shows plane upper and lower silt layers without any fissures or cracks. The gap between the silt and the sand layer, visible in Fig. 24, was caused when unmounting the specimen. The sample was fabricated with silt layers of laterally varying thickness. After the test a thinner area of the upper silt layer is visible. Sand from the middle layer has entered

the upper silt layer from beneath. Sand grains are visibly disturbing the upper silt layer in its thinner zone (Fig. 24). The mixture of the upper and middle layer in this area indicates, that the water flow concentrated in this area. This certain zone is located at the boundary of the sample. The permeability measured in this sample could have been increased through the occurrence of a thinner zone in the upper layer. The *k*-values determined from direct measurements indicate, that the lower silt layer had been stable enough to reduce the permeability down to the from calculations expected value for a type 2 sample.

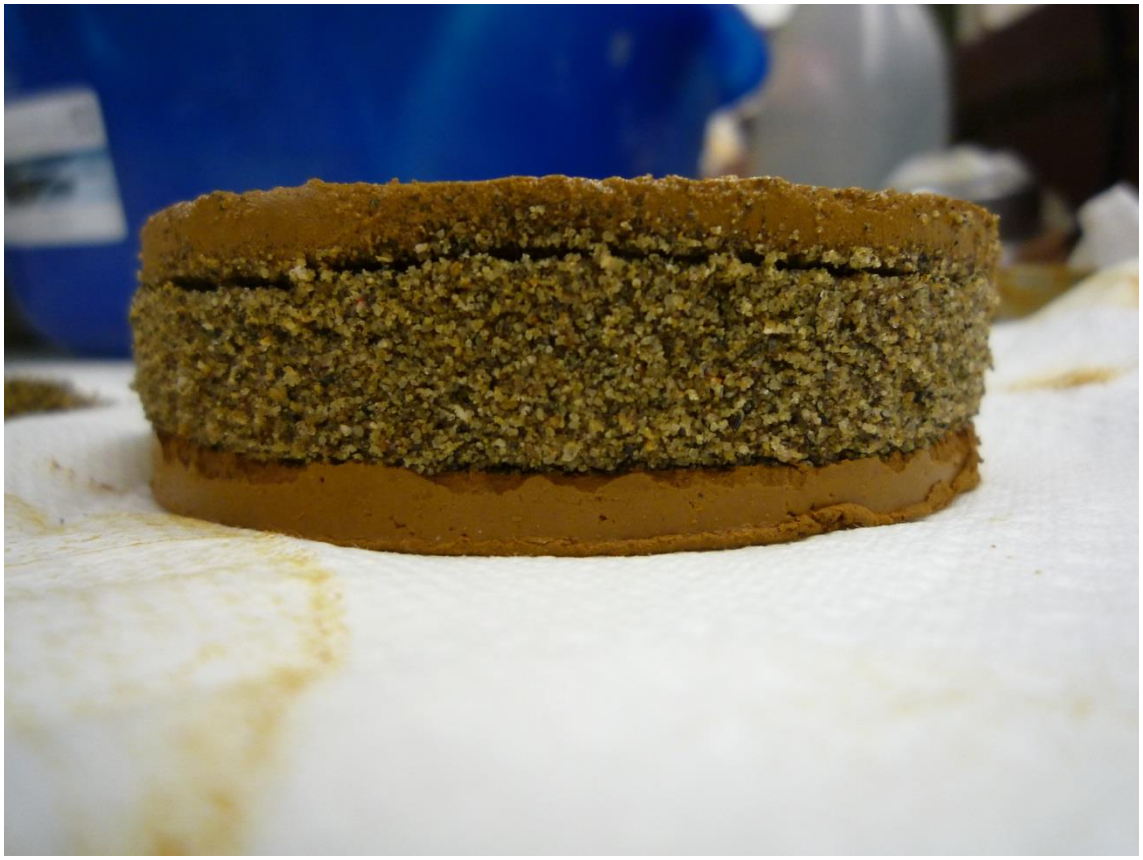

Fig. 24 Post-test state of sample 19148-4; side view.

Sample 19148-5 has been afflicted with water flow of a hydraulic gradient close to 30 before any preconsolidation or load application took place. Grains and particles were flooded out and cumulated on the top outlet of the oedometer cell. The upper side of the sample (Fig. 25) shows the upper sand layer disturbed by silt particles. Particularly on one side silt from the middle layer is jetted into the upper layer. In Fig. 26 it is visible, that just beneath the disturbed area of the upper sand layer the silt layer is broken. The breakout in the silt layer occurred very abrupt immediately after the

application of the high water gradient. Due to failure of the sample no direct measurements were carried out.

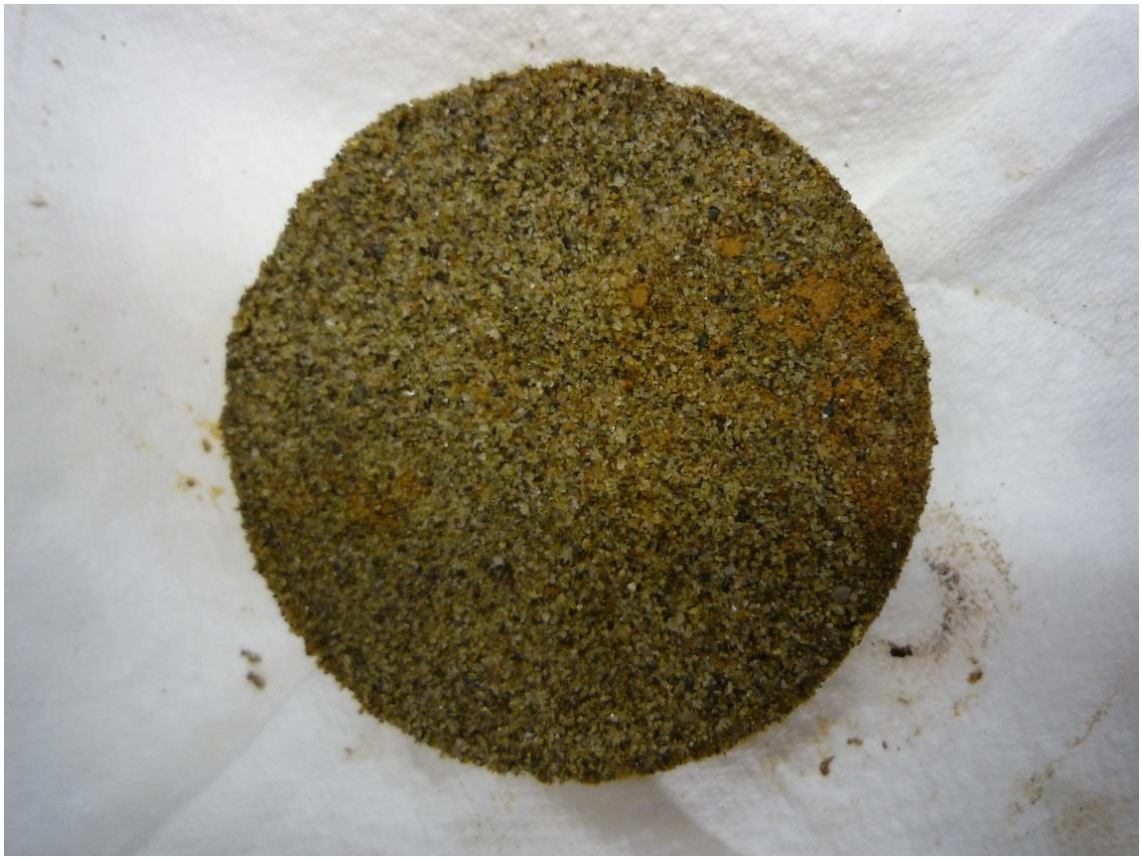

Fig. 25 Post-test state of sample 19148-5; view from above.

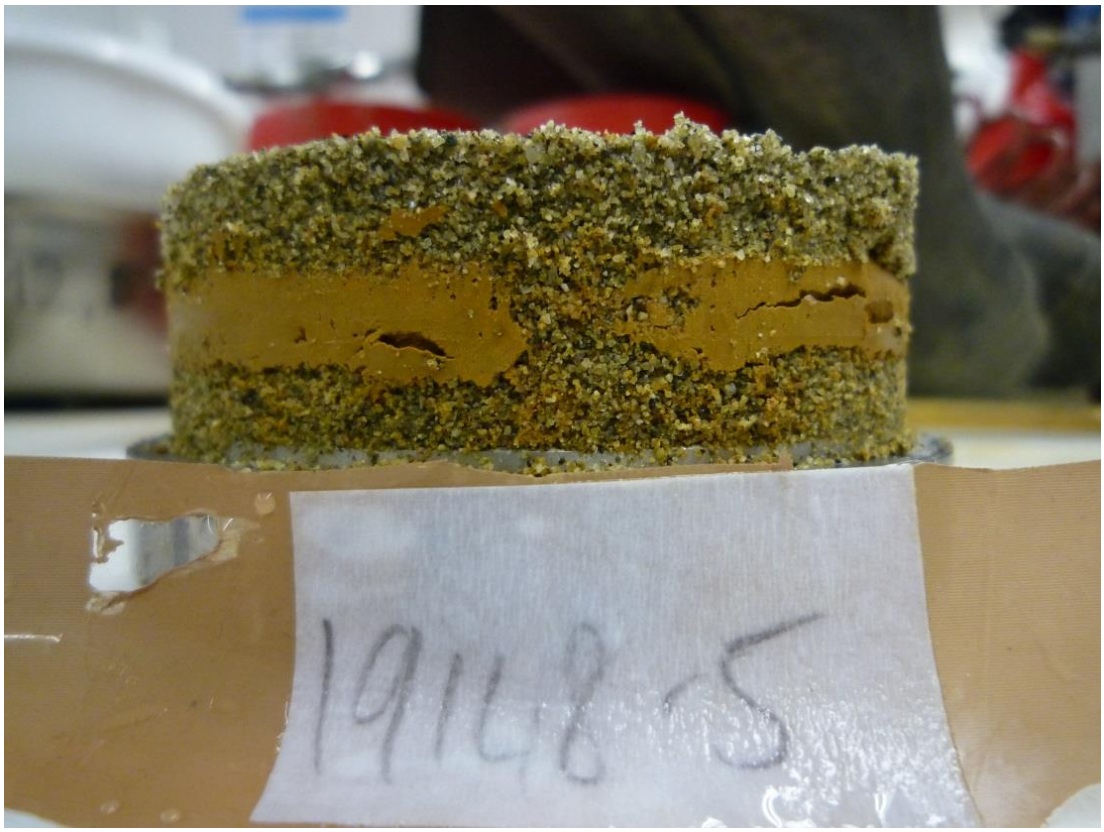

Fig. 26 Post-test state of sample 19148-5; side view.

The results obtained from the direct measurements on sample 19148-6 in the prolonged load steps are biased. The results of the measurements range in the order of 10^{-7} to 10^{-6} m/s. The post-test state of the sample shows a series of failures that have taken place in the specimen. The upper sand layer is compressed more in comparison to the lower one. Also it is visible, that the upper sand layer was not stable against intrusion of silt particles. The upper sand layer is disturbed and filled with silt particles, which was visible from all sides of the sample. In a part of the sample, silt and sand have mixed during the test (Fig. 27). The upper and middle layer in this zone build a mixture of sand and silt. The failure of the sample might also be influenced by a careless distribution and compaction of the material during the fabrication of the sample.

The obtained hydraulic conductivity might represent the permeability of the filter stones used in the oedometer cell. Since the silt layer broke, the *k*-value was supposed to reach the permeability range of sand (10^{-4} to 10^{-6} m/s), which was impossible because of the lower permeability of the filter stones. The comparison with the *k*-values determined from 19147-1 (*k*=1.01E-06 m/s for the loading stage and *k*=8.44E-07 m/s

for the reloading stage), where the permeability of the filter stones was measured, shows, that the same amount of results occurred for sample 19148-6.

Fig. 27 Post-test state of sample 19148-6, side view.

During the 160kPa load steps an average coefficient of permeability of 1.37E-10 m/s was computed for sample 19148-7. The *k*-value measured during the 320kPa load steps amounts to 7.52E-11 m/s.

Due to technical defects it was not possible to conduct a proper measurement on sample 19148-8 during the 320kPa load step. The estimated coefficient of permeability for the 320kPa load step amounts to 4.60E-10 m/s. Measurements taken during the 160kPa load step give a mean value of permeability of 4.92E-10 m/s. After the tests, both 19148-7 and 19148-8 were uniformly compressed and do not show any cracks or failures. Fig. 28 shows the post-test state of sample 19148-7.

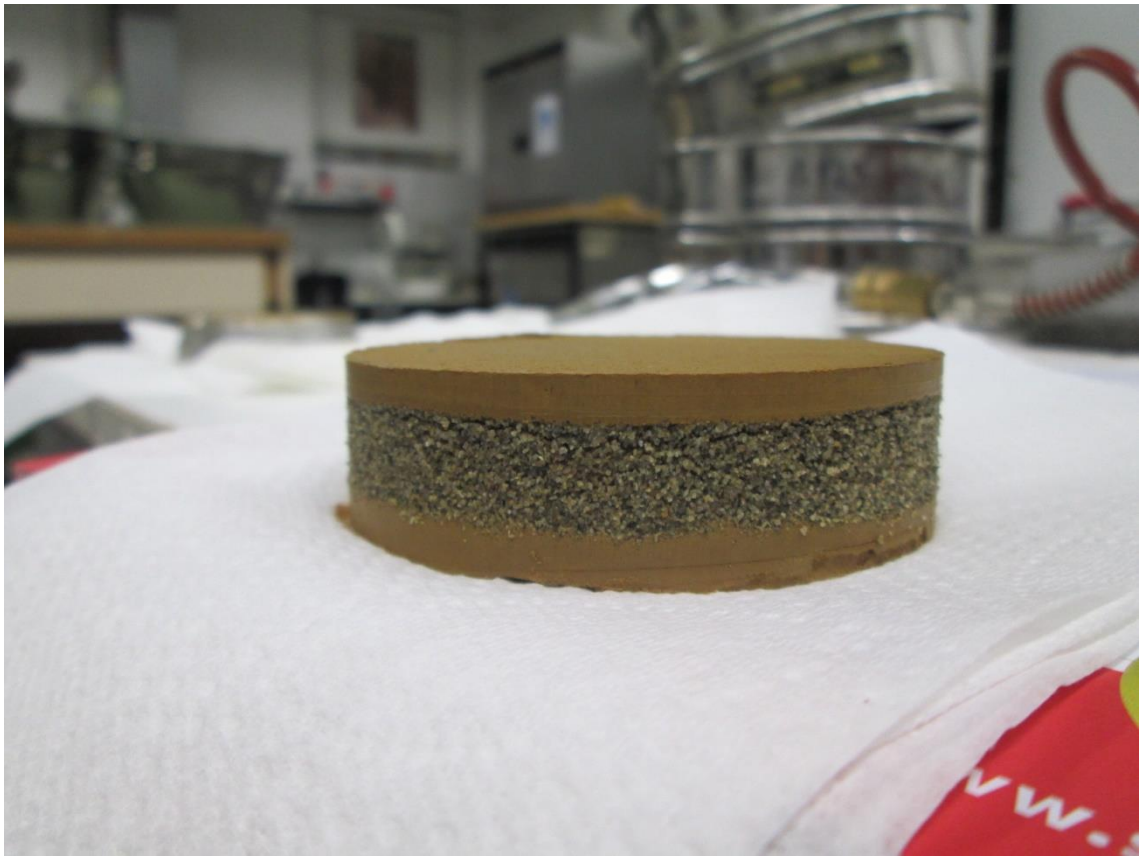

Fig. 28 Post-test state of sample 19148-7, side view.

Tab. 13 lists the values of permeability determined on layered samples in falling-head tests with the corresponding hydraulic gradient acting on the total height of the sample. Fig. 29 shows a plot of the mean permeability (Tab. 13) together with the lowest and highest values of permeability determined in a sample.

Tab. 13 Mean permeability values determined in layered samples by direct methods.

LAYERED SAMPLES				
		direct k [m/s]		
		falling-head test		
Sample type	Sample Nº	160 kPa	320 kPa	i
1	19148-1	-	1.16E-10*	32
2	19148-2	6.08E-10 (l)	3.36E-10 (l)	32
		4.37E-10 (r)	3.54E-10 (r)	
3	19148-3	2.07E-10 (l)	1.46E-10 (l)	31-32
2	19148-4	1.59E-10 (l)	9.18E-11 (l)	31-32
3	19148-6	1.08E-06 (l)	9.58E-07 (l)	32-33
2	19148-7	1.37E-10 (l)	7.52E-11 (l)	31-32
3	19148-8	4.92E-10 (l)	4.60E-10 (l)	35

* measured at 315 kPa
(l) loading stage
(r) reloading stage

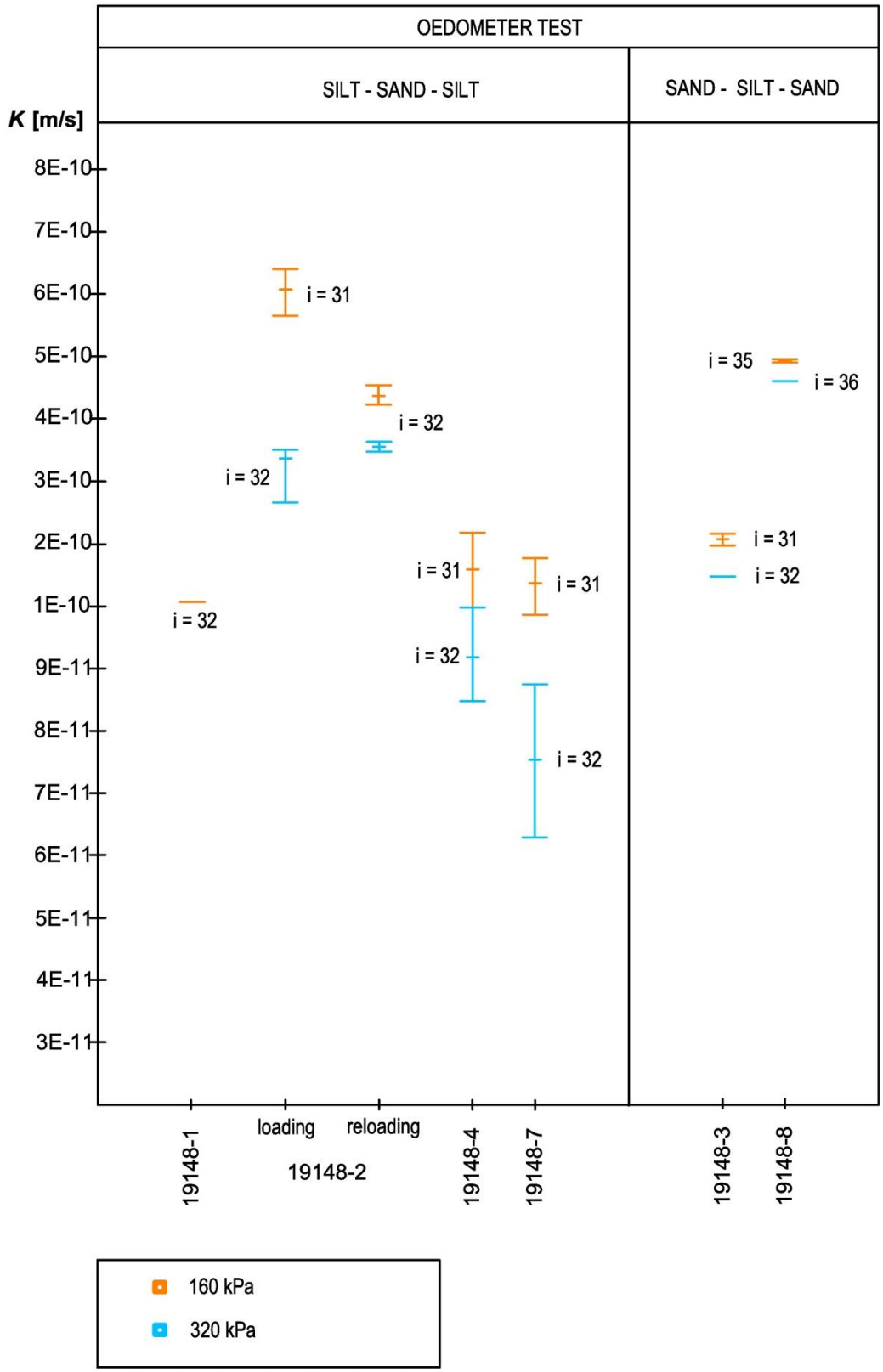

Fig. 29 Values of hydraulic conductivity determined in falling-head tests in layered samples: mean, minimum and maximum values for each sample

4.2 Triaxial permeability test

For measurements in the triaxial permeability cell the loose soil material (silt) was poured into a metal mould and compacted with a proctor. After unmounting from the mould the cylindric sample with a height of 11.93cm and a diameter of 9.87cm was coated with a rubber plastic, mounted to the triaxial permeability cell and tested according to the description in chapter 3.2. The samples were prepared to have the ideal water content of 13.4 wt% and a wet density of 2.06 g/cm^3.

The test on sample 19146-4 was run with a hydraulic gradient of 30 over a period of 40 days. The measurements during the first 14 days show a trend of decreasing permeability as the sample was still saturating. The measurements taken after the saturation phase yielded an average coefficient of permeability of 4.55E-10 m/s. After the test in the triaxial cell, the sample was used for oedometer tests (19146-42 and 19146-43).

Sample 19146-5T was tested with a hydraulic gradient of 30 over a period of 39 days. The measurements during the first 31 days do not show a clear trend. Experiences have shown, that the time span between two measurements should not be much more than a day. The optimum duration of a measurement was estimated to be 20 to 25 hours. The measurements taken after the unstable phase yielded an average coefficient of permeability of 4.58E-10 m/s.

19146-6 was tested with a hydraulic gradient of 30 over a period of 38 days. The measurements during the first 13 days show a trend of decreasing permeability as the sample was still saturating. The measurements taken after the saturation phase yielded an average coefficient of permeability of 5.08E-10 m/s.

4.3 Permeability cylinder

Three sand samples with a height of 12cm and a diameter of 10cm were tested in a permeability cylinder. The samples were prepared with a water content of 4.8 to 6.1 wt% and a wet density of 1.58 to 1.60 g/cm^3.

From 8 measurements taken from 19147-7 on one day with a hydraulic gradient of 2.9 - 3 an average hydraulic conductivity of 5.90E-05 m/s was obtained for the soil sample. On 19147-8, 6 measurements were taken on two days. The tests were run with a hydraulic gradient of 2.6. An average *k*-value of 1.87E-04 m/s was obtained for the soil

sample. The permeability of 19147-9 was measured in 5 test runs on one day with a hydraulic gradient of 2.7. The average *k*-value obtained from the test is 8.36E-05 m/s. From another 5 measurements taken on the same day with a hydraulic gradient of 2.5 the average *k*-value was determined to be 6.33E-05 m/s.

5 Discussion of test results

5.1 Direct methods

5.1.1 Falling-head tests

Tab. 14 lists the significant mean *k*-values determined in falling-head tests. Fig. 30, a plot of the data from direct measurements (Tab. 14), shows how permeability varies in dependence of the applied load and the reloading of the sample. The *k*-values determined in silt and layered samples show the same trend: Permeability decreases from the 160kPa to the 320kPa load step. Permeability during the 160kPa load step is lower in the reloading stage, while permeability during the 320kPa load step is lower in the loading stage. The lowest hydraulic conductivity is measured during the highest load step of the loading stage.

Sand samples show a different trend: The coefficient of permeability first increases with increasing load and drops at the end to a value lower than the permeability measured in the earliest observed load step (Fig. 30). A possible reason for the irregular trend in sand is, that other errors might have greater influence on measurements in sand than the reloading of the sample. Such errors might be systematic or random. Random errors occur through measurement mistakes (e.g. misreading of dials). The increasing sand permeability observed in direct measurements might be due to a systematic error like the formation of flow channels within the specimen. A trend of decreasing permeability is a systematic error, which might be due to the blockage of filter pores. It has been observed, that the time taken for a falling-head test can increase gradually with the repetition of the measurement. The effect has been observed during the permeability measurement of the filter stones on the sand samples 19147-1 and 19147-5. The average test duration in sample 19147-1 increases from 1.14 minutes for the first test run to 1.71 minutes for the thirteenth and last test run. This results in a decrease of the measured permeability from 8.96E-07 m/s (first run) to 5.94E-07 m/s (last run). The transportation of the materials finest fraction into the filter stones is believed to block the filter pores and gradually lower the measured permeability. It is recommended to use filter papers for all falling-head tests in order to prevent such errors.

Tab. 14 Mean coefficient of permeability *k* [m/s] determined in falling-head tests in silt, sand and layered samples

direct k [m/s]						
falling-head test						
	80 kPa	160 kPa		320 kPa		i
19146-8	-	8.10E-11	(l)	6.76E-11	(l)	32-33
		5.20E-11	(r)	5.97E-11	(r)	
19147-6	5.45E-05	5.95E-05	(l)	6.04E-05	(l)	30
	6.19E-05	6.23E-05	(r)	5.04E-05	(r)	
19148-1	-	-		1.16E-10*	(l)	32
19148-2		6.08E-10	(l)	3.36E-10	(l)	32
		4.37E-10	(r)	3.54E-10	(r)	
19148-3		2.07E-10	(l)	1.46E-10	(l)	31-32
19148-4		1.59E-10	(l)	9.18E-11	(l)	31-32
19148-7		1.37E-10	(l)	7.52E-11	(l)	31-32
19148-8		4.92E-10	(l)	4.60E-10	(l)	35

* measured at 315 kPa

(l) loading stage

(r) reloading stage

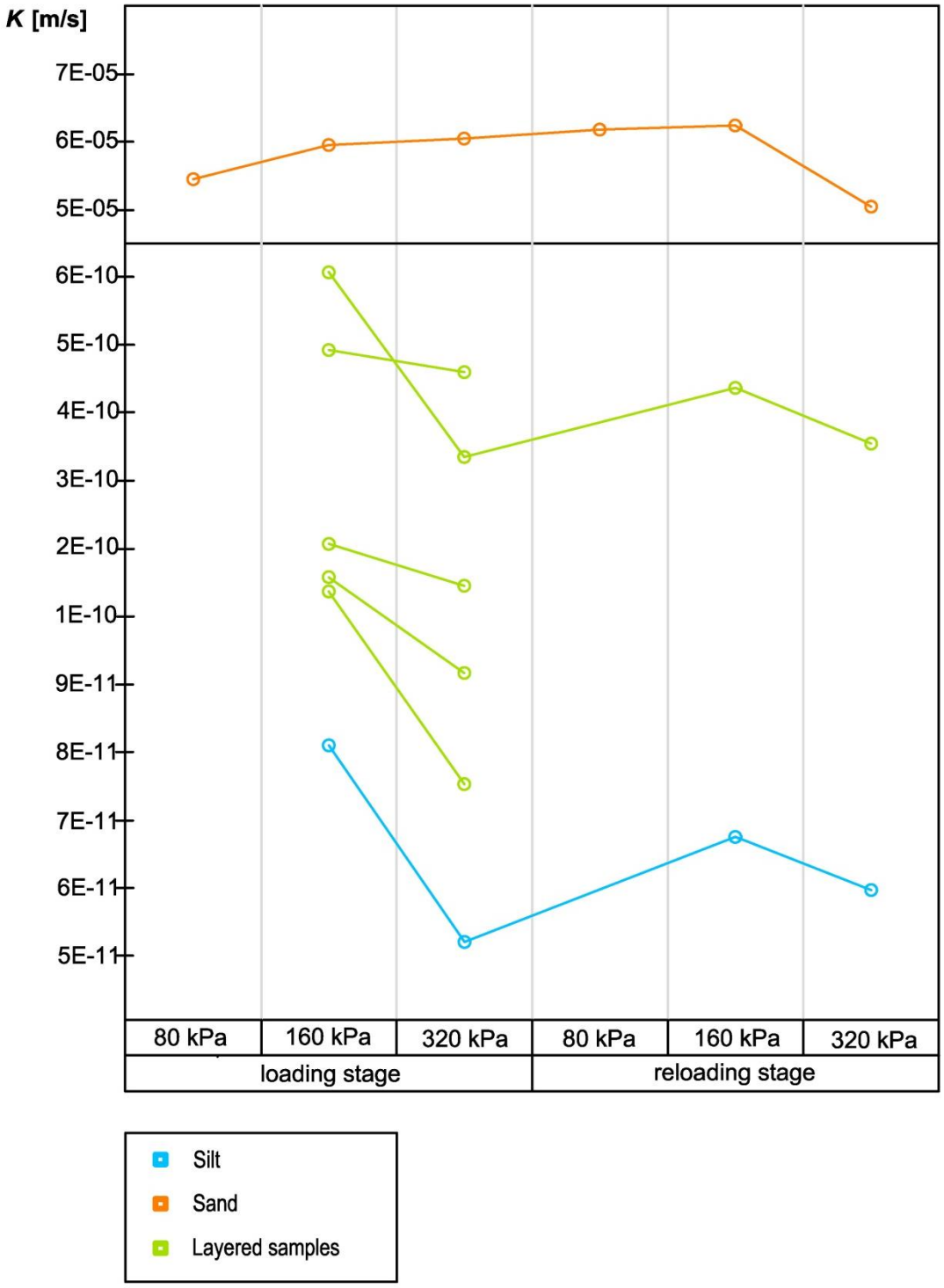

Fig. 30 Average permeability measured during different load steps in oedometer falling-head tests

5.1.2 Comparison of constant-head and falling-head tests

Tab. 15 lists the significant *k*-values of silt and sand determined in constant-head and falling-head tests. Hydraulic conductivity of silt, determined from triaxial constant-head permeability tests, ranges from 3.90E-10 m/s to 5.30E-10 m/s (Tab. 15). The results obtained through the oedometer falling-head test are at most lower with the power of ten. The values determined during the 160kPa and 320kPa load steps range between 4.70E-11 m/s and 8.69E-11 m/s (Tab. 15). The mean permeability of silt determined in the falling-head tests is 6.51E-11 m/s (Tab. 15Tab. 15). Fig. 31 shows a plot of the mean, the minimum and the maximum hydraulic conductivity determined for silt samples using both test types.

Fig. 32 shows the differences in sand permeability if determined in constant-head or falling-head arrangements. Values for sand samples determined directly in the oedometer falling-head test during the 80kPa, the 160kPa and the 320kPa load steps range from 5.04E-05 m/s to 6.23E-05 m/s (Tab. 9). The mean value for permeability in sand samples determined in these tests is 5.82E-05 m/s (Tab. 15). The hydraulic conductivity measured in the constant-head permeability cylinder arrangement is slightly higher – the results lie between 5.90E-05 m/s and 1.74E-04m/s (Tab. 15).

Tab. 15 Mean, minimum and maximum values of direclty measured permeability of representative samples with maximum and minimum values

Material	Test	Sample №	Mean k [m/s]	Max. k [m/s]	Min. k [m/s]
Silt	Constant-head	19146-4	4.55E-10	4.90E-10	3.90E-10
		19146-5T	4.58E-10	5.00E-10	4.10E-10
		19146-6	5.08E-10	5.30E-10	4.80E-10
	Falling-head	19146-8	6.51E-11	8.69E-11	4.70E-11
Sand	Falling-head	19147-6	5.82E-05	6.35E-05	5.00E-05
	Constant-head	19147-7	5.61E-05	5.70E-05	5.60E-05
		19147-8	1.87E-04	2.00E-04	1.70E-04
		19147-9	8.36E-05	8.70E-05	8.10E-05
			6.33E-05	6.40E-05	6.20E-05

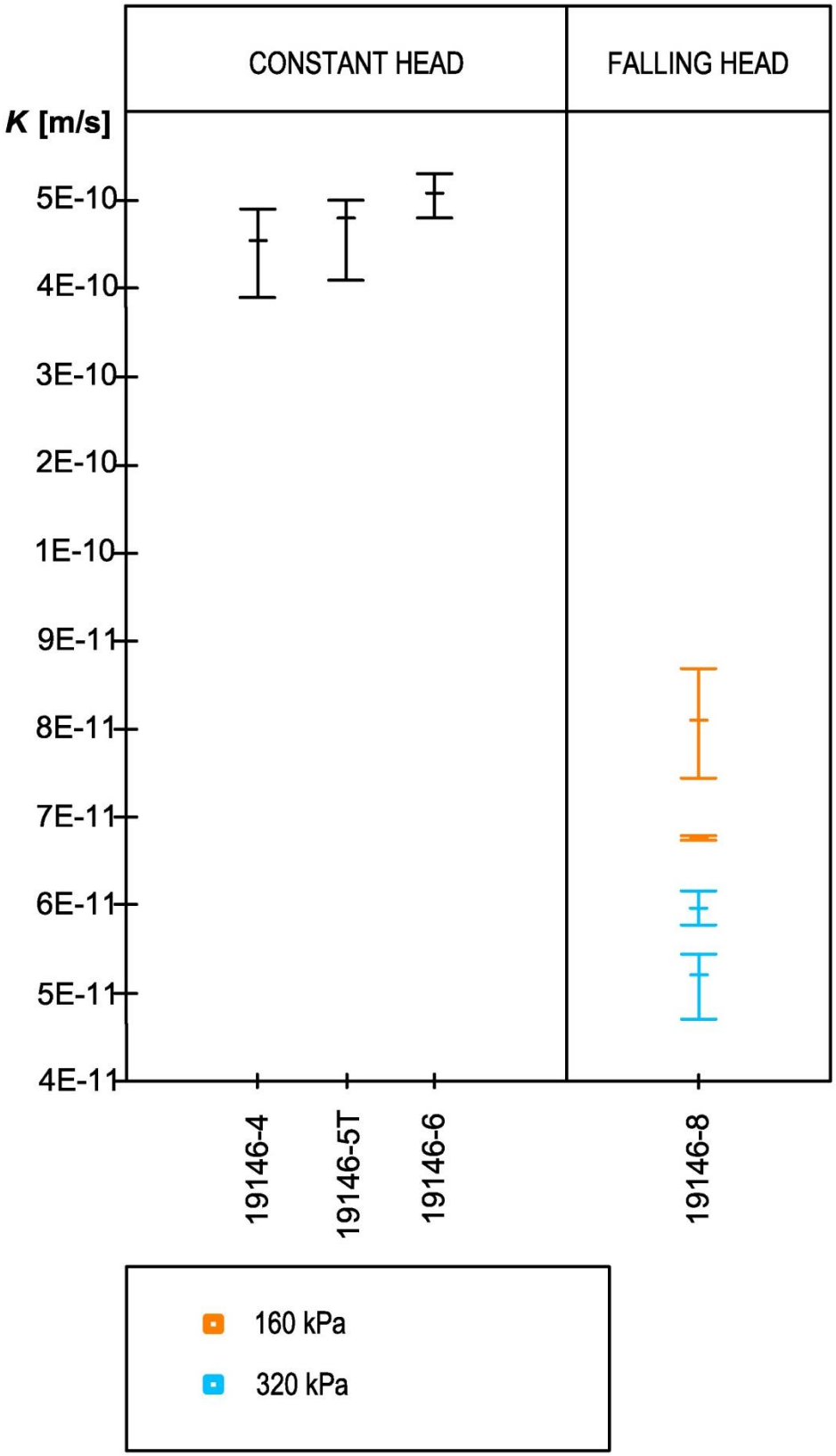

Fig. 31 Values of hydraulic conductivity determined in silt samples by direct methods (cmp. Tab. 15)

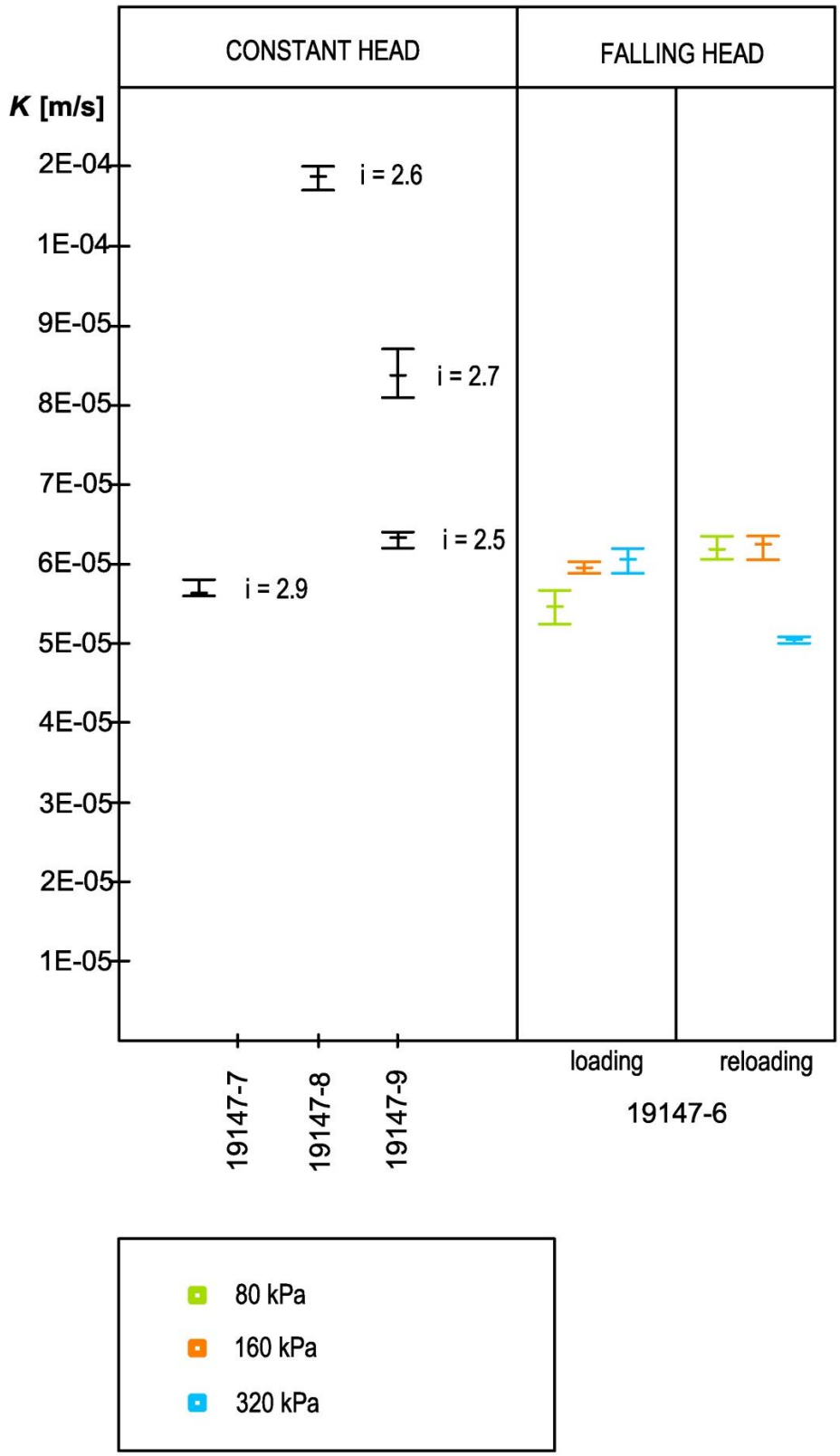

Fig. 32 Values of hydraulic conductivity determined in sand samples by direct methods (cmp. Tab. 15)

5.2 Graphical methods

5.2.1 Square-root-of-time method

The $\sqrt{time}$-settlement curves of silt samples deviate from the standard-curve in the initial section of the graph. The method has given *k*-values ranging from 1.70E-10 m/s to 9.43E-10 m/s, which is clearly above the coefficient of permeability determined in falling-head tests. Permeability in the 160kPa load steps is expected to be higher than in the 320kPa load steps. If using the square-root plot this is rather given than in a log-time plot.

5.2.2 Logarithm-of-time method

The values determined with the log-time method range from 5.09E-11 to 5.70E-10 m/s and cover approximately the range of results from direct measurements. In three of the log-time plot evaluations (19146-1, -42 and -43), higher coefficients of permeability were obtained for the 320kPa load step than for the 160kPa load step. For two samples (19146-42 and -43) the permeability during the 160kPa load step was by a factor of ten lower than during the 320kPa load step. The rest of the results obtained from Casagrande's method plot closer to *k*-values determined in the constant-head test and the values determined by Taylor's method. For this reason, the two exceptionally low results are considered to be incorrect.

Fig. 33 shows the extent of deviations due to the chosen method. Most of the results obtained from graphic evaluations (Tab. 7) are closer to hydraulic conductivity determined from triaxial permeability tests. In addition, the *k*-values in the field are believed to exceed values determined by any laboratory test (cmp. chapter 3.4.1), which indicates, that the higher coefficients of permeability determined from constant-head and Taylor's method might be the more realistic.

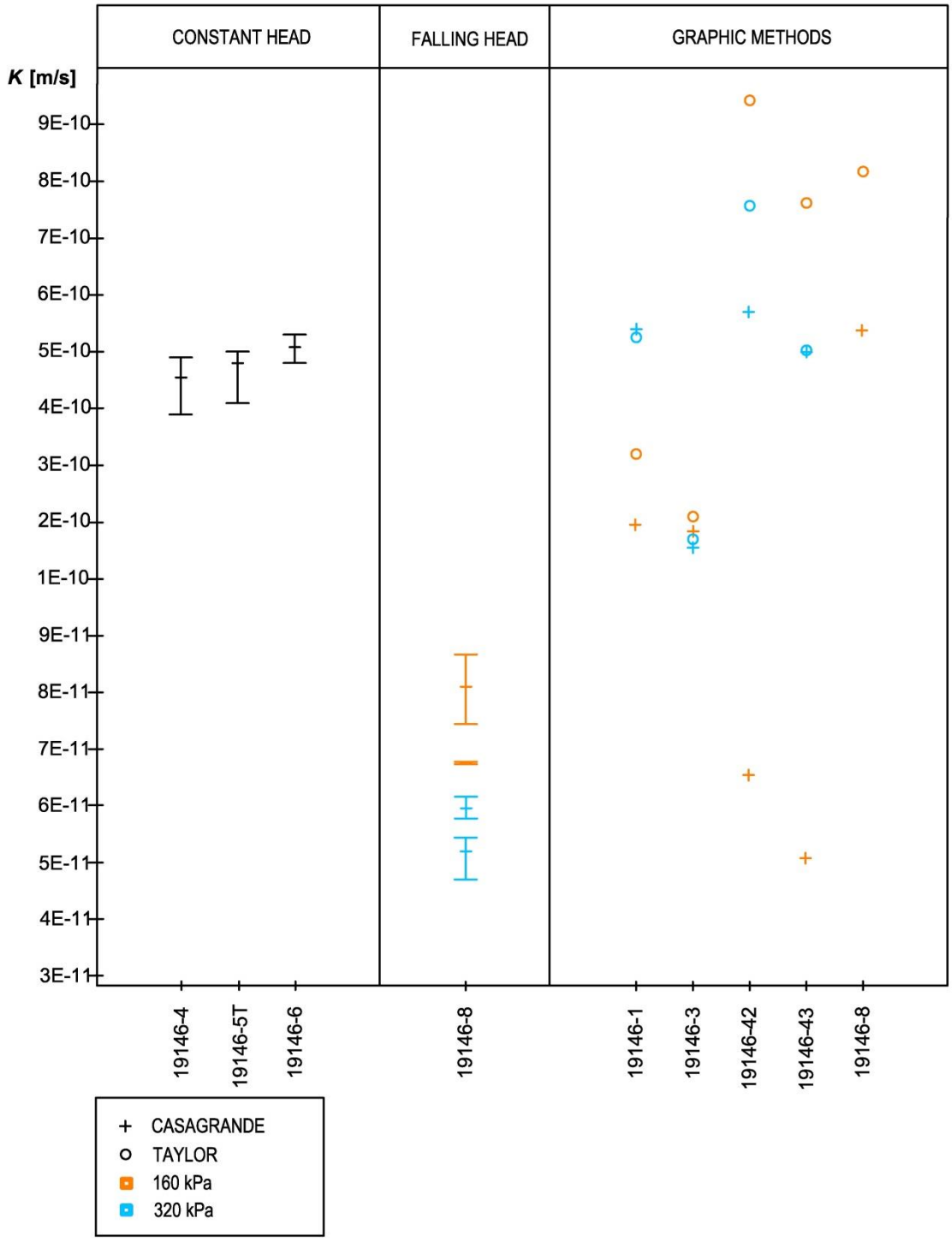

Fig. 33 Values of hydraulic conductivity determined in silt samples by direct and indirect methods

5.3 Mathematical method

Tab. 11 lists the permeability values calculated for layered samples of type 1, 2 and 3. The minimum, the maximum and the average hydraulic conductivity determined in silt and sand samples were used to calculate the minimum, the maximum and the mean permeability of layered samples. The mean calculated permeability for each sample type is plotted in Fig. 34 together with the average directly measured values of the samples 19148-1, -2, -3, -4, -7 and -8 (Tab. 13) during the 160kPa and 320kPa load steps of the loading stage.

The plot in Fig. 35 shows the mean permeability, regardless of the load steps, with the corresponding maximum and minimum values for each layered sample type. Maximum and minimum values have been calculated using the maximum/minimum permeability directly measured in silt and sand samples (Tab. 9). The measured and calculated data is listed in Tab. 16. The diagram points out, that the mean values of both the calculated and the measured permeability plot close together. The maximum difference between the mean calculated and measured values amounts to 8.90E-11 m/s.

The fact, that the calculated values are close to the measured permeability, can be interpreted in two ways. Either particle movement from the base to the filter material has not taken place in the tested material, or, the mathematical method is applicable regardless of filter stability. In order to know the limits of the methods applicability, further test with given filter stability need to be performed.

Tab. 16 Comparison of average calculated and measured values for layered samples of type 1, 2 and 3

	Determination	Mean	Max	Min
Type 1	Direct	1.16E-10	-	
	Calculated	1.03E-10	1.35E-10	7.29E-11
Type 2	Direct	2.22E-10	6.40E-10	6.29E-11
	Calculated	1.33E-10	1.74E-10	9.40E-11
Type 3	Direct	3.26E-10	4.94E-10	1.46E-10
	Calculated	2.66E-10	3.48E-10	1.88E-10

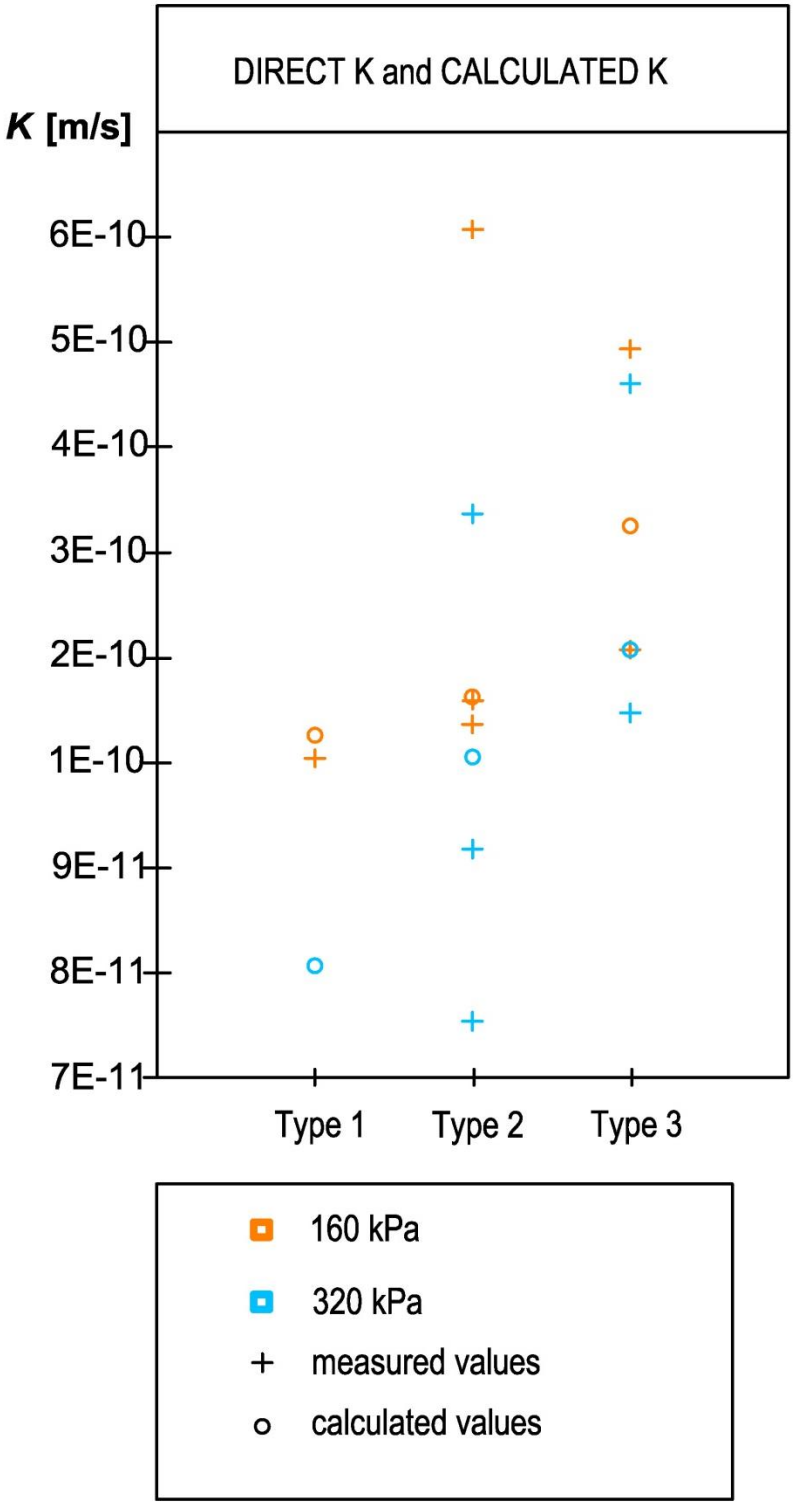

Fig. 34 Mean calculated permeability for each sample type and mean measured values of permeability for each sample

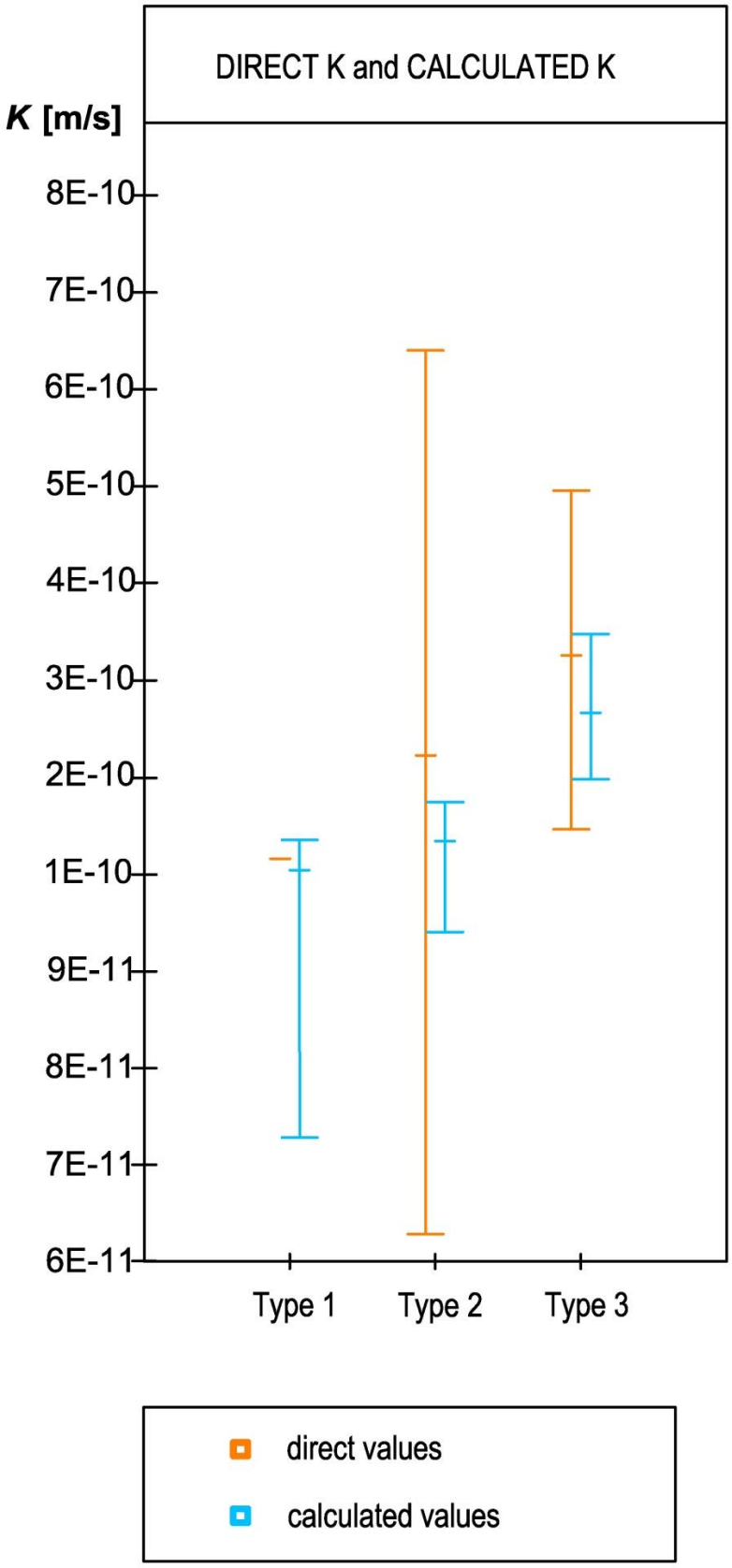

Fig. 35 Range of calculated and measured values for layered samples

6 Conclusion

Constant-head tests tend to give higher coefficients of permeability than falling-head tests. The effect is higher if testing fine-grained materials.

Falling-head tests should be conducted using filter paper covering the filter stones in order to prevent systematic biases due to the blockage of filter pores by the materials fine fraction. Before the test, layered samples should be checked for filter stability using the described criteria. The hydraulic gradient for the falling-head test should be chosen correspondingly. If the criteria are not applicable, filter stability can be ensured using filter paper between the layers. Permeability of silt and layered samples is lowest in the highest load step of the loading stage, while permeability in sand is lowest in the highest load step of the reloading stage.

Results from graphic methods vary depending on the used method. Permeability determined through a log-time plot can vary wide in dependence of the applied load and is not necessarily higher for lower load steps. Non-standard √time-settlement curves give values higher than the permeability determined in falling-head arrangements and partly exceed also the results from constant-head tests. The *k*-values obtained from Taylor's method are, with one exception, higher for lower load steps. All results from Taylor's method exceed the results from Casagrande's method. Taylor's method is believed to give the more satisfying results, since a clear relationship between permeability in lower and higher load steps was visible. Additionally, the occurrence of two exceptionally low values of permeability determined through the log-time plot indicate, that the √time-plot should be preferred. Also the consideration, that the highest coefficient of permeability determined by any laboratory method should be the closest to real field values (Tewatia & Venkatachalam, 1997), aspects in the favour of preferring constant-head tests and the square-root-of-time plot.

The comparison with measured permeability shows, that the mathematic approach for permeability determination in layered samples gives plausible values. Still, restrictions of the applicability cannot be excluded. Further studies incorporating the filter stability should be conducted.

7 Summary

Due to the heterogeneity and complexity of naturally deposited layered soils and the geotechnical significance of permeability in such deposits, a series of laboratory tests were conducted concerning permeability in layered soils. Artificial samples made up of horizontal layers of silt and sand were fabricated and tested in falling-head tests. Pure silt and sand were tested in constant-head and falling-head arrangements. Graphic methods for C_v-determination in cohesive soils were applied to the time-settlement curves of silt in order to determine k. A mathematical solution for permeability determination in layered deposits was applied and compared with measured values.

The implementation and comparison of diverse laboratory tests have shown, that permeability in fine-grained materials can differ with more than the power of ten in dependence of the chosen test. Constant-head arrangements generally showed higher results for permeability than falling-head tests. This effect was higher if fine-grained materials were tested. The square-root-of-time curve fitting method gives the highest values and is considered to be more accurate than the log-time method. The occurrence of exceptional values and incorrect relationships between permeability under low and high load respectively, aspect in the favour of preferring the √time-plot to the log-time plot for graphical determination of C_v and k. Concerning the direct measurements, constant-head tests are considered to give the more accurate results: The majority of the graphically determined values range around the constant-head test results.

8 Appendix

8.1 Graphic C_v-determination

8.1.1 19146-1

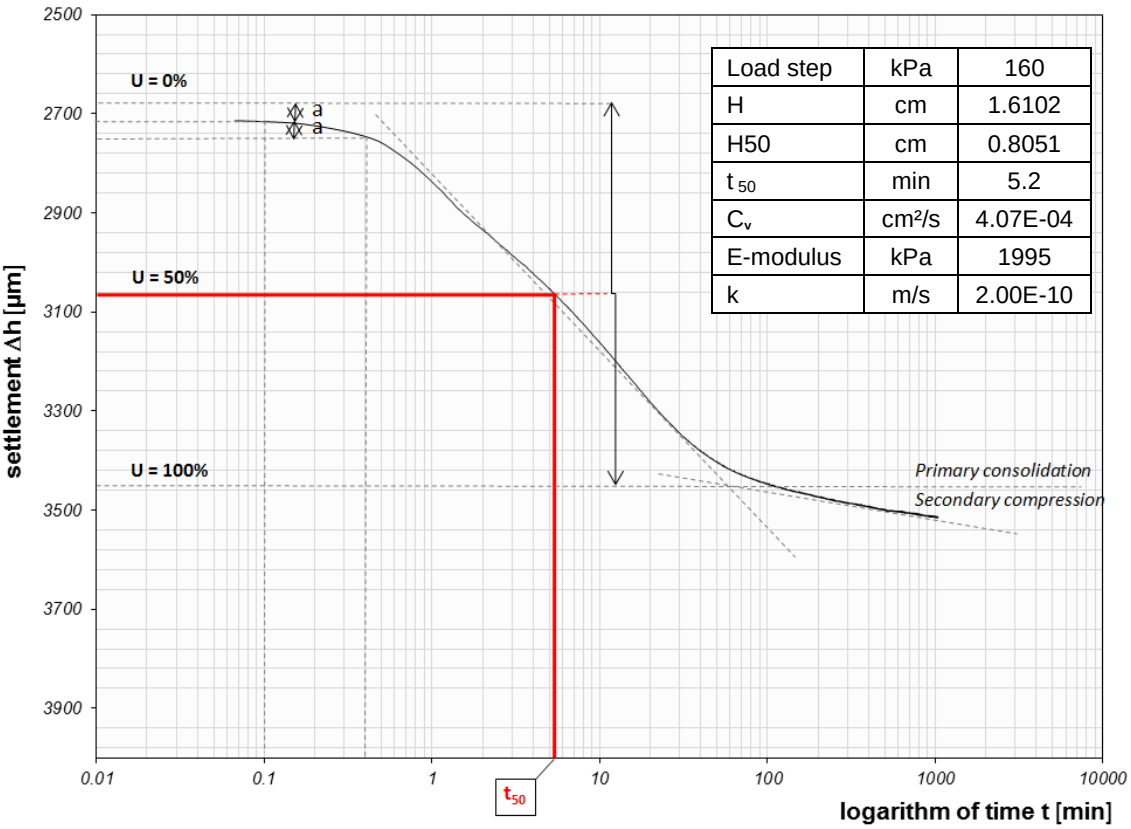

Fig. 36 Sample 19146-1: Log-time plot of the 160kPa load step

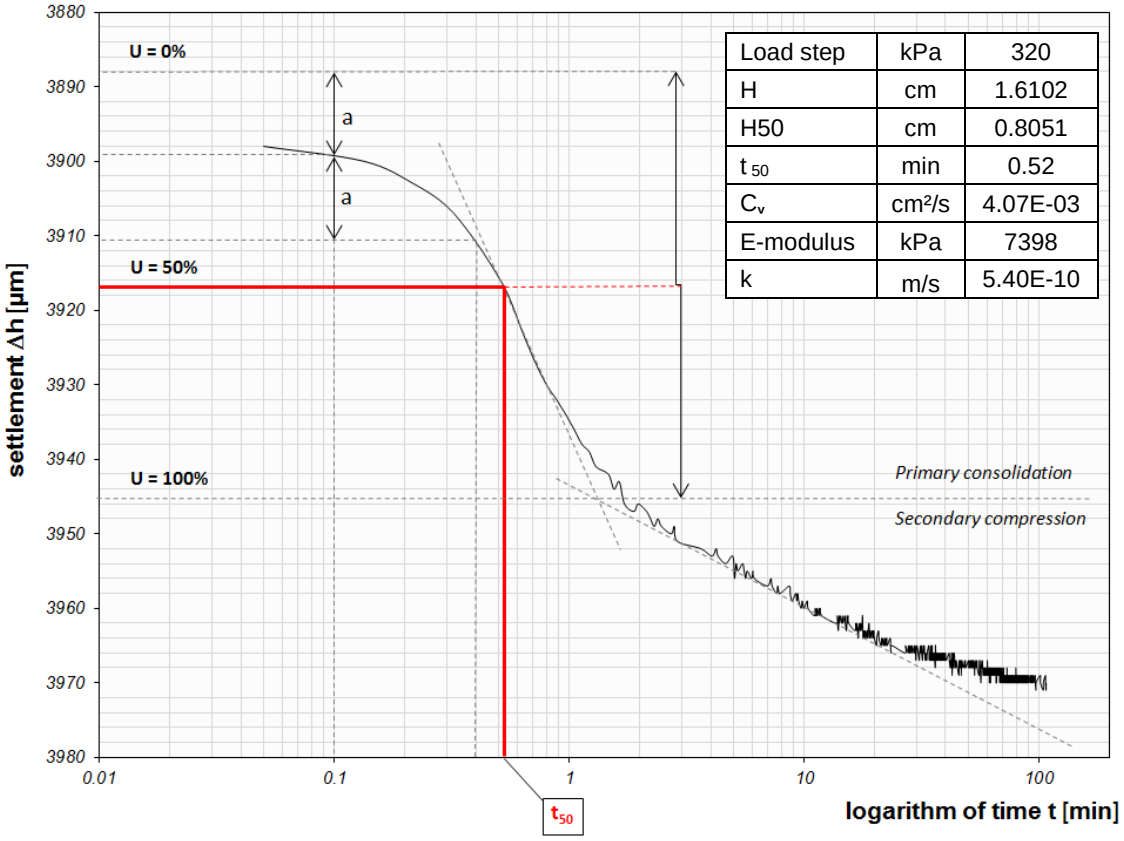

Fig. 37 Sample 19146-1: Log-time plot of the 320kPa load step

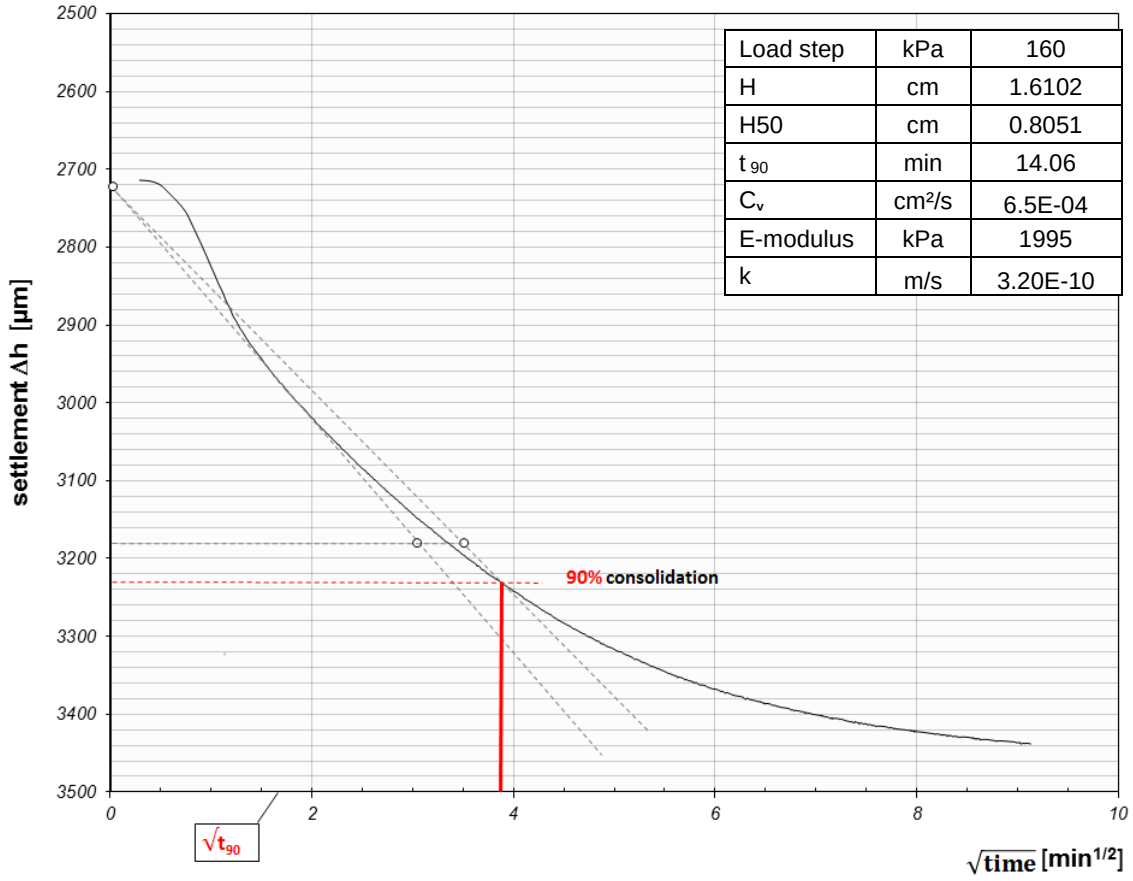

Fig. 38 Sample 19146-1: √time plot of the 160kPa load step

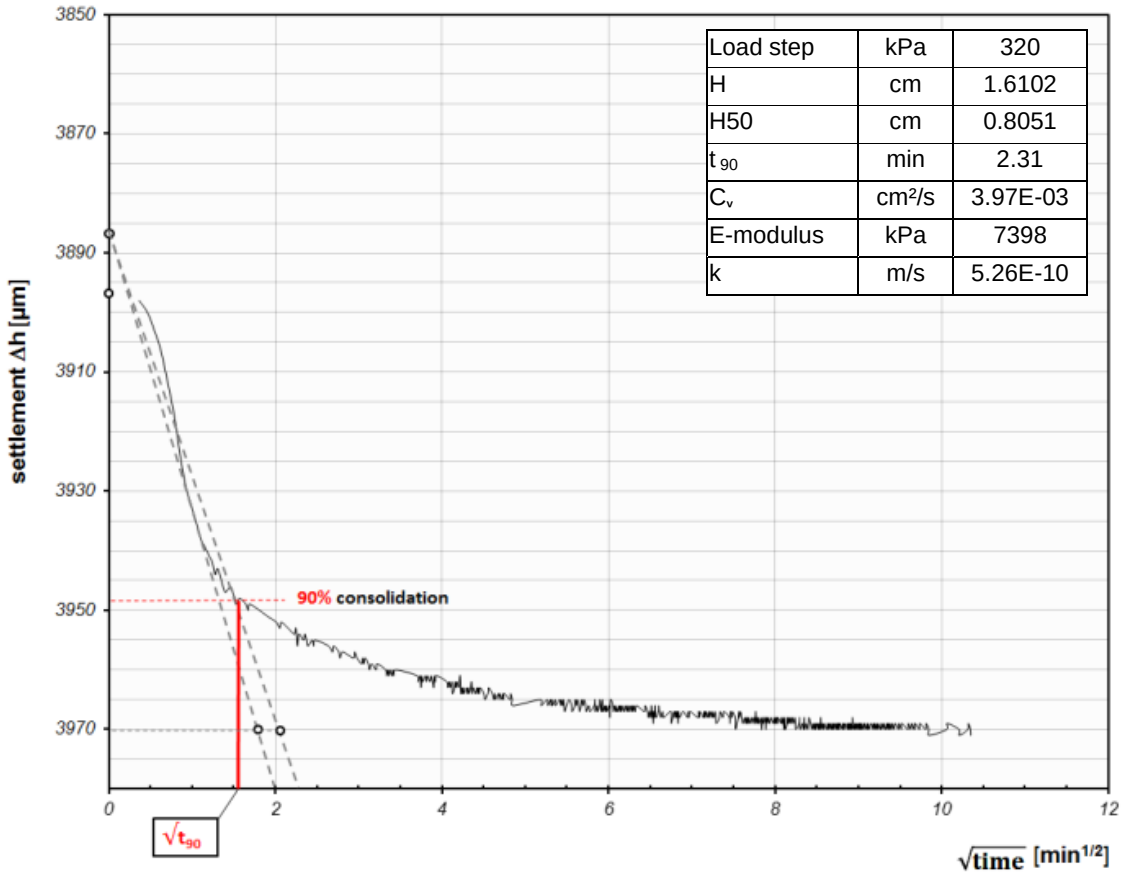

Load step	kPa	320
H	cm	1.6102
H50	cm	0.8051
t_{90}	min	2.31
C_v	cm²/s	3.97E-03
E-modulus	kPa	7398
k	m/s	5.26E-10

Fig. 39 Sample 19146-1: √time plot of the 320kPa load step

8.1.2 19146-3

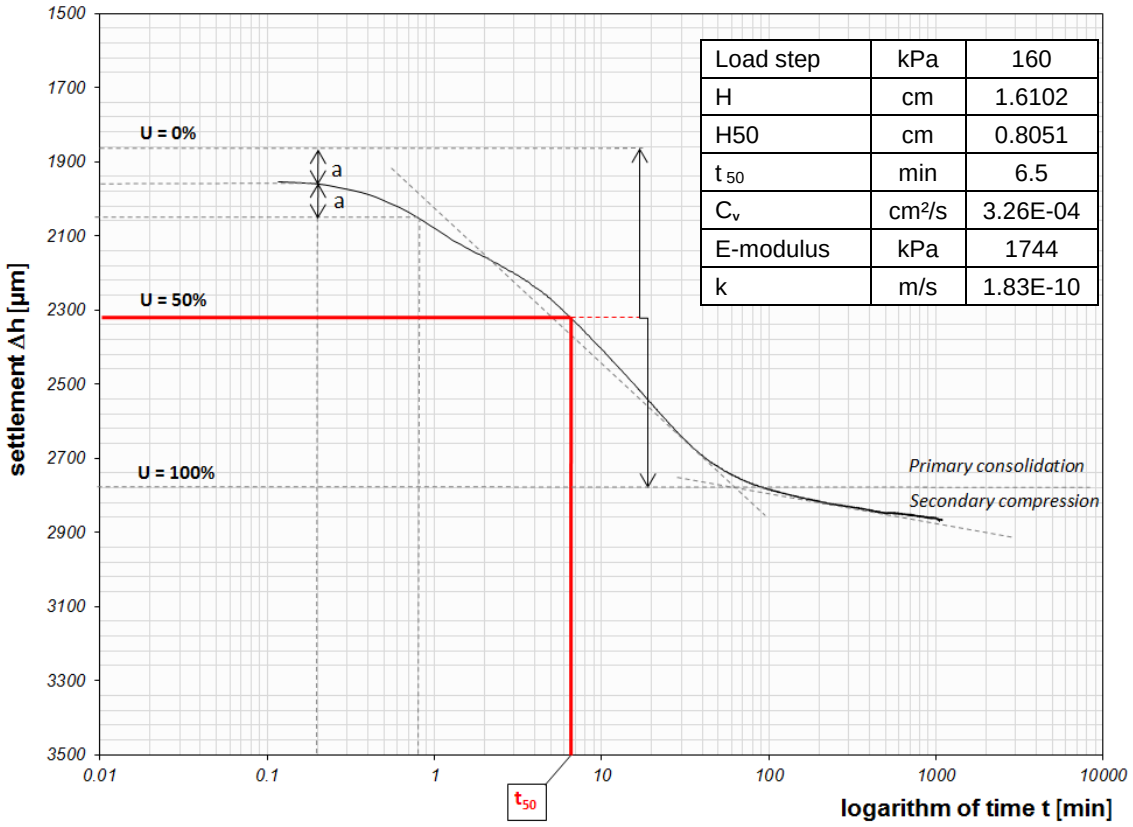

Fig. 40 Sample 19146-3: Log-time plot of the 160kPa load step

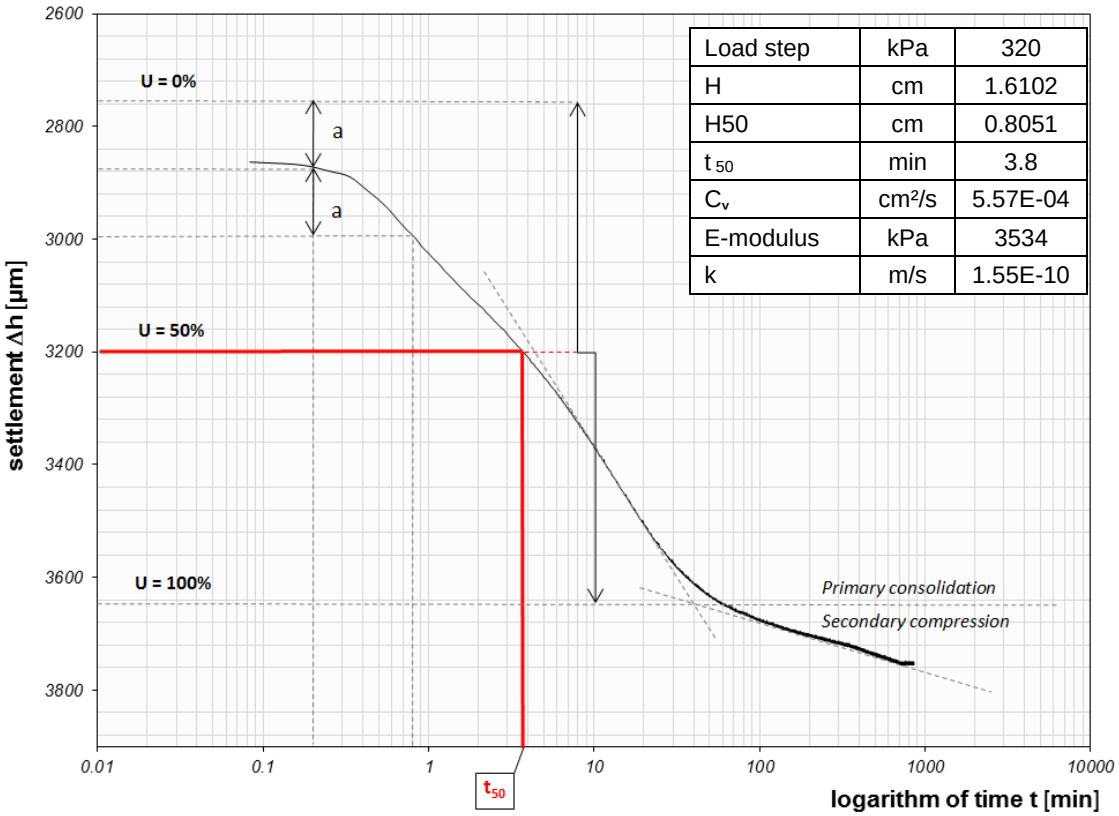

Fig. 41 Sample 19146-3: Log-time plot of the 320kPa load step

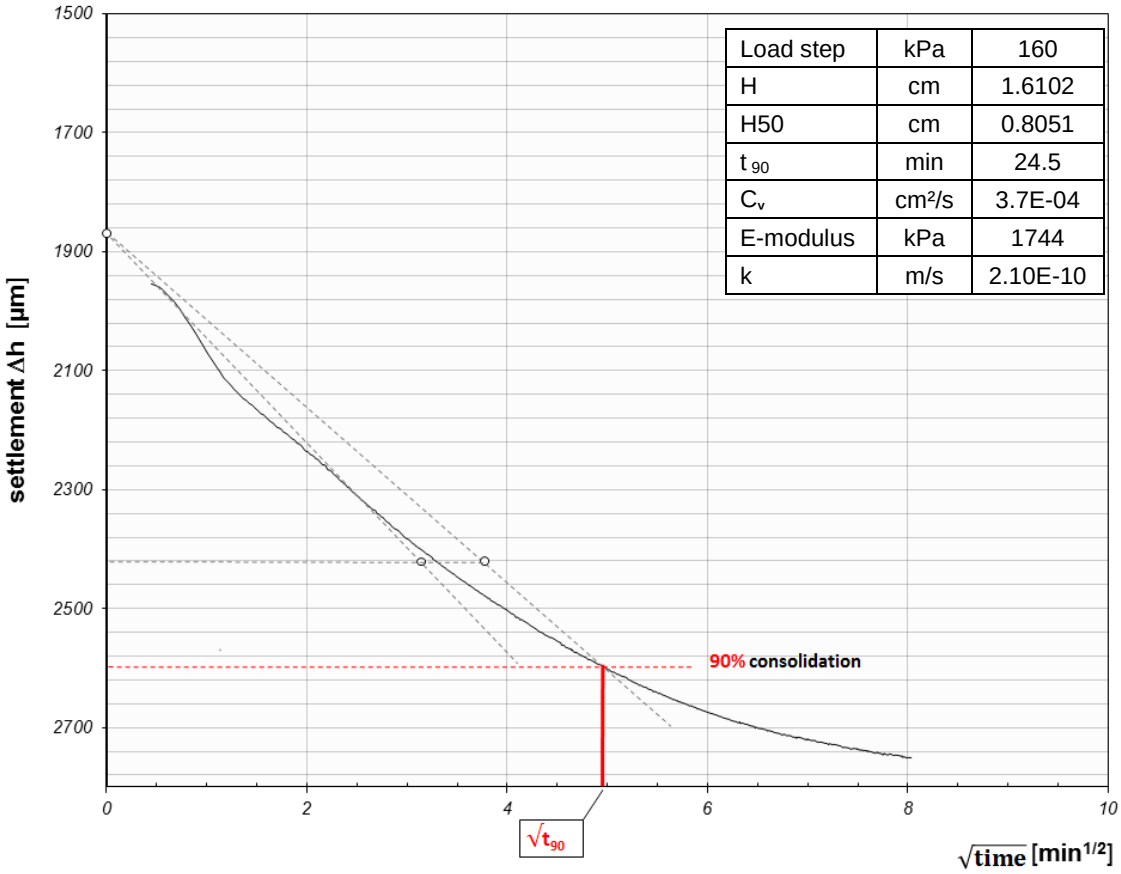

Fig. 42 Sample 19146-3: √time plot of the 160kPa load step

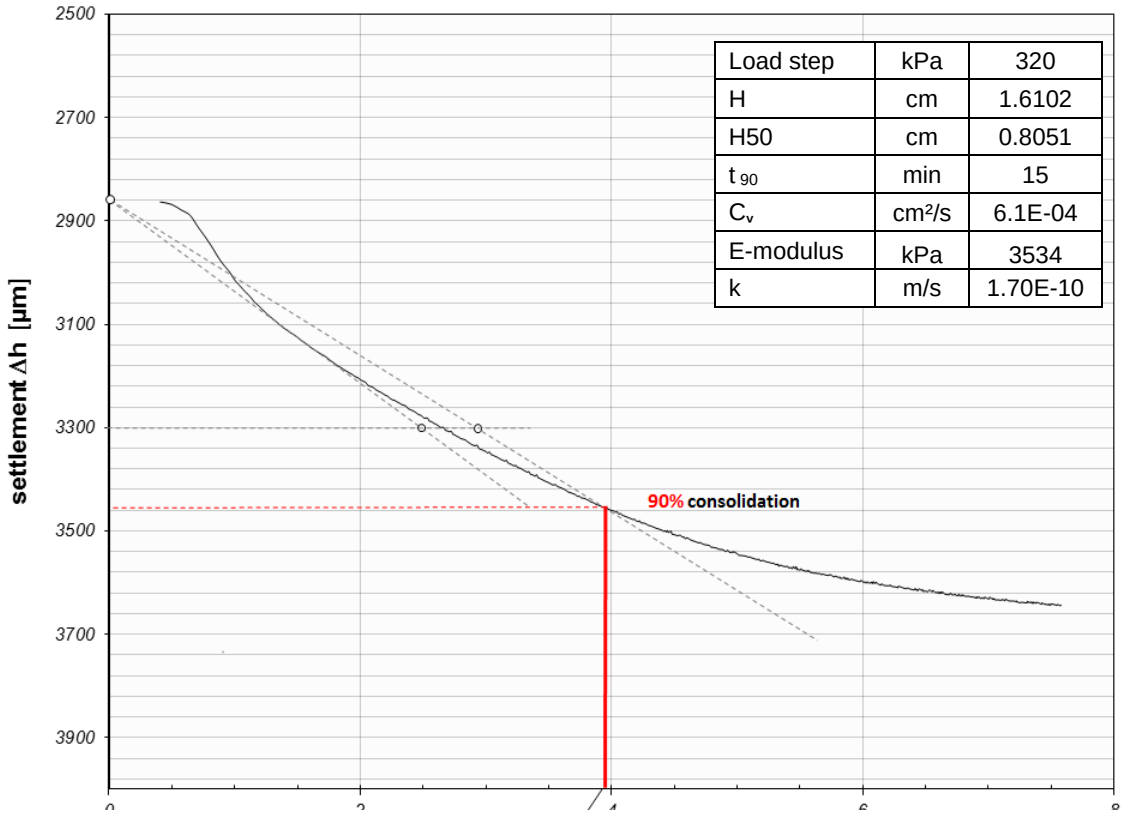

Fig. 43 Sample 19146-3: vtime plot of the 320kPa load step

8.1.3 19146-42

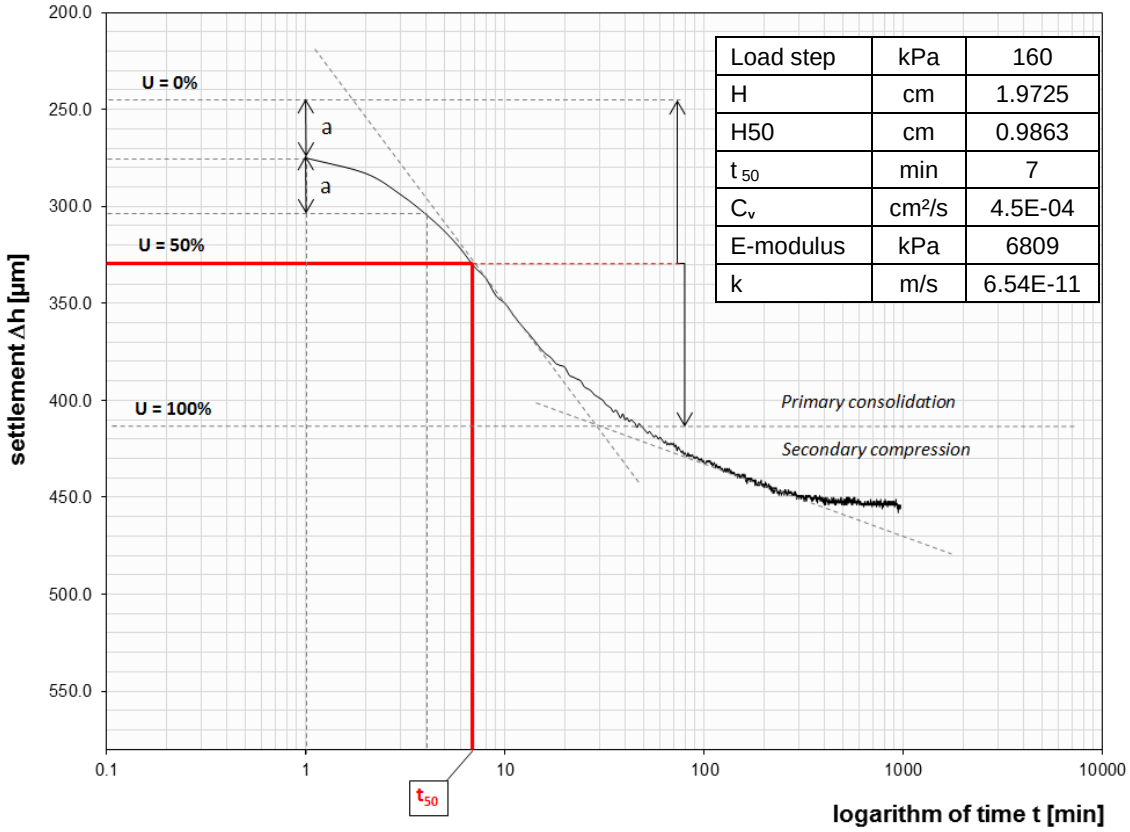

Fig. 44 Sample 19146-42: log-timeplot of the 160kPa load step

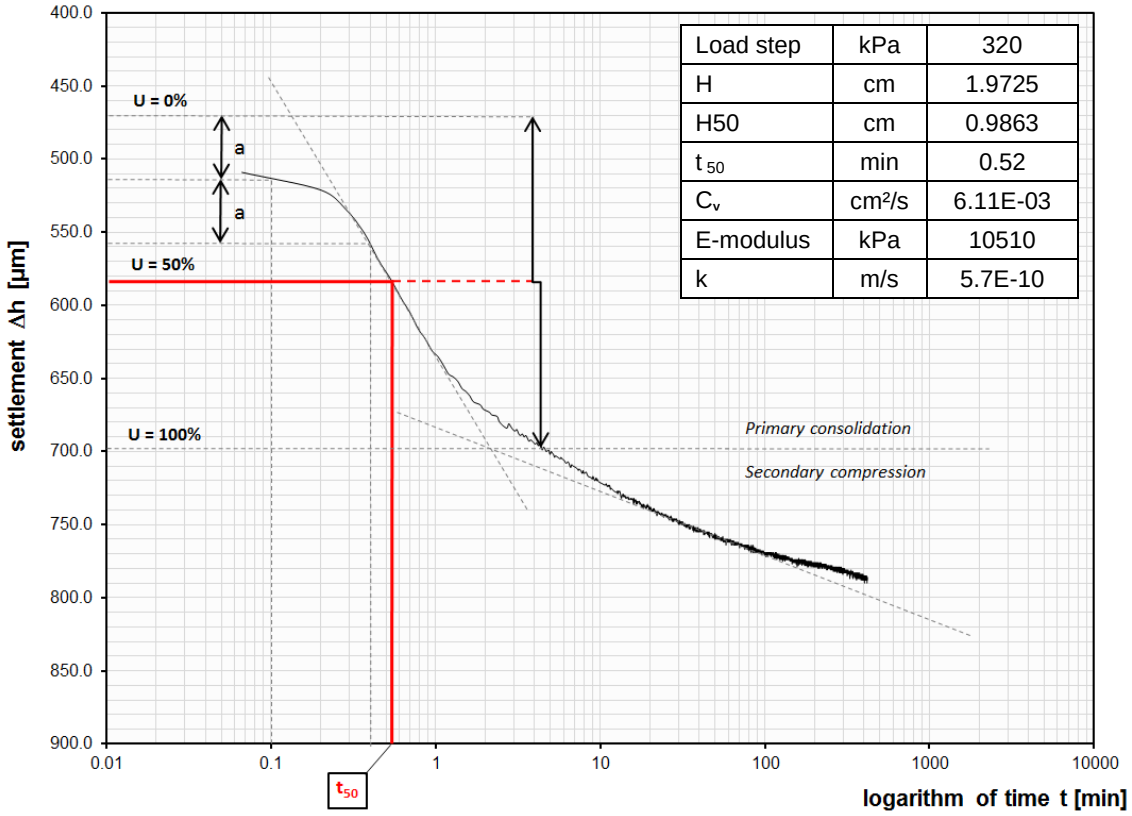

Fig. 45 Sample 19146-42: log-timeplot of the 320kPa load step

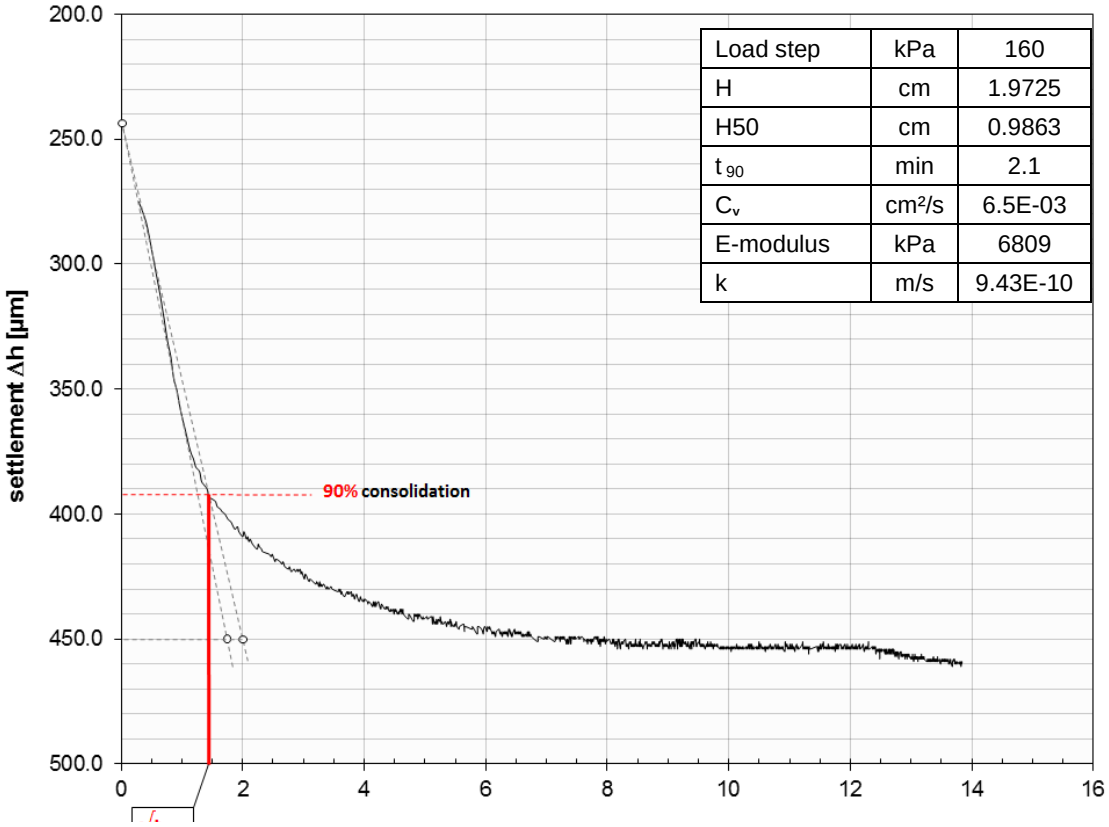

Fig. 46 Sample 19146-42: √time plot of the 160kPa load step

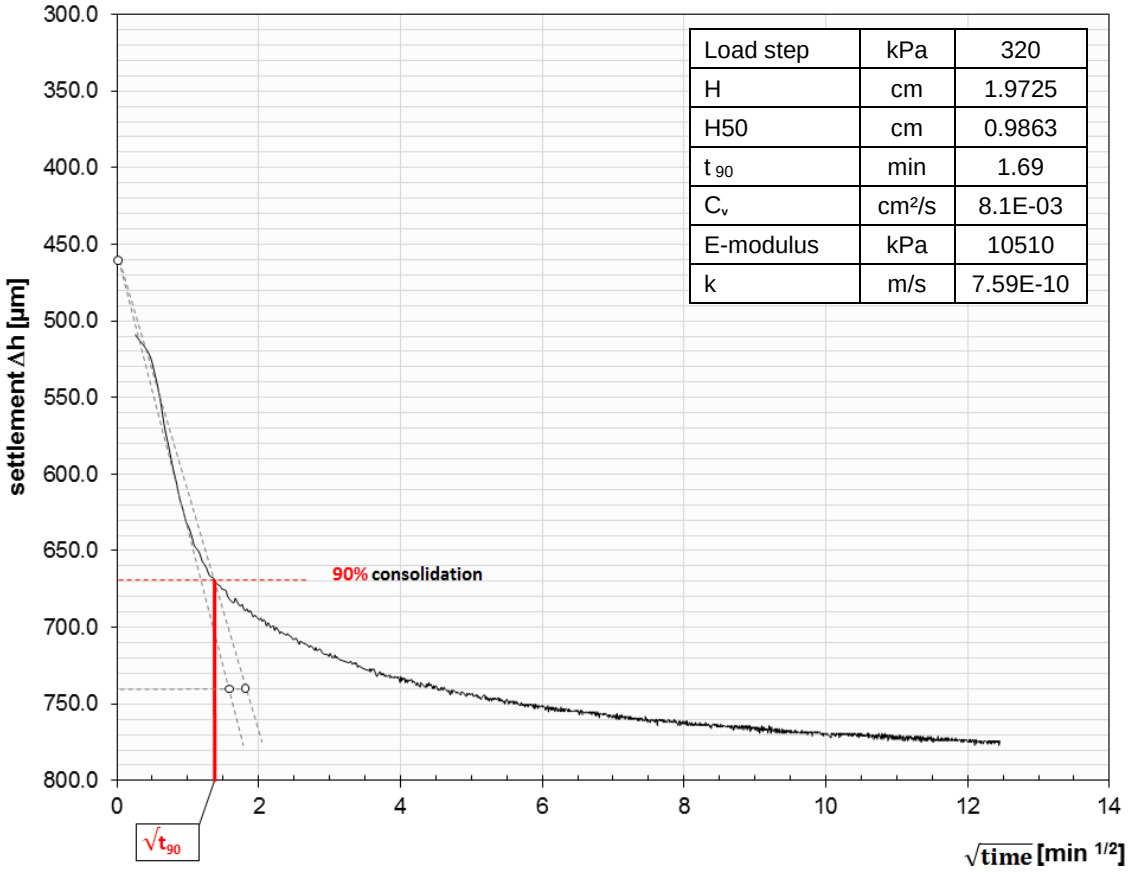

Fig. 47 Sample 19146-42: √time plot of the 320kPa load step

8.1.4 19146-43

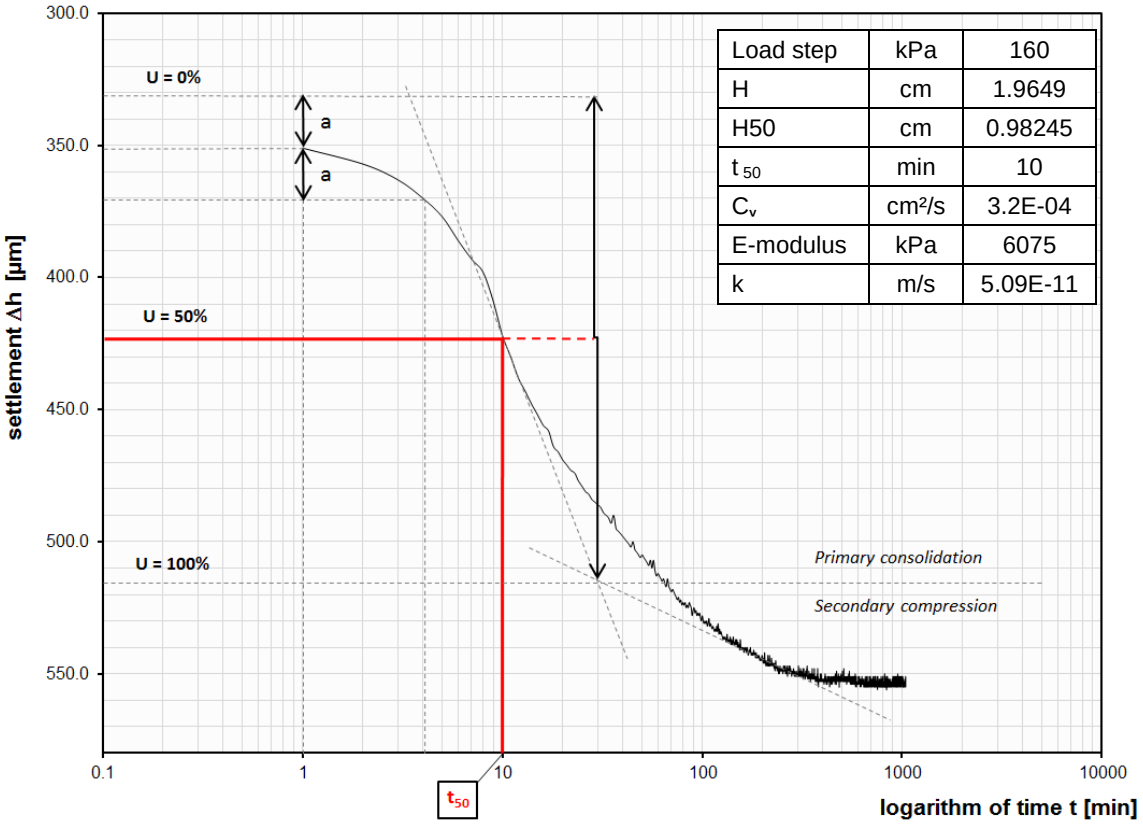

Fig. 48 Sample 19146-43: log-timeplot of the 160kPa load step

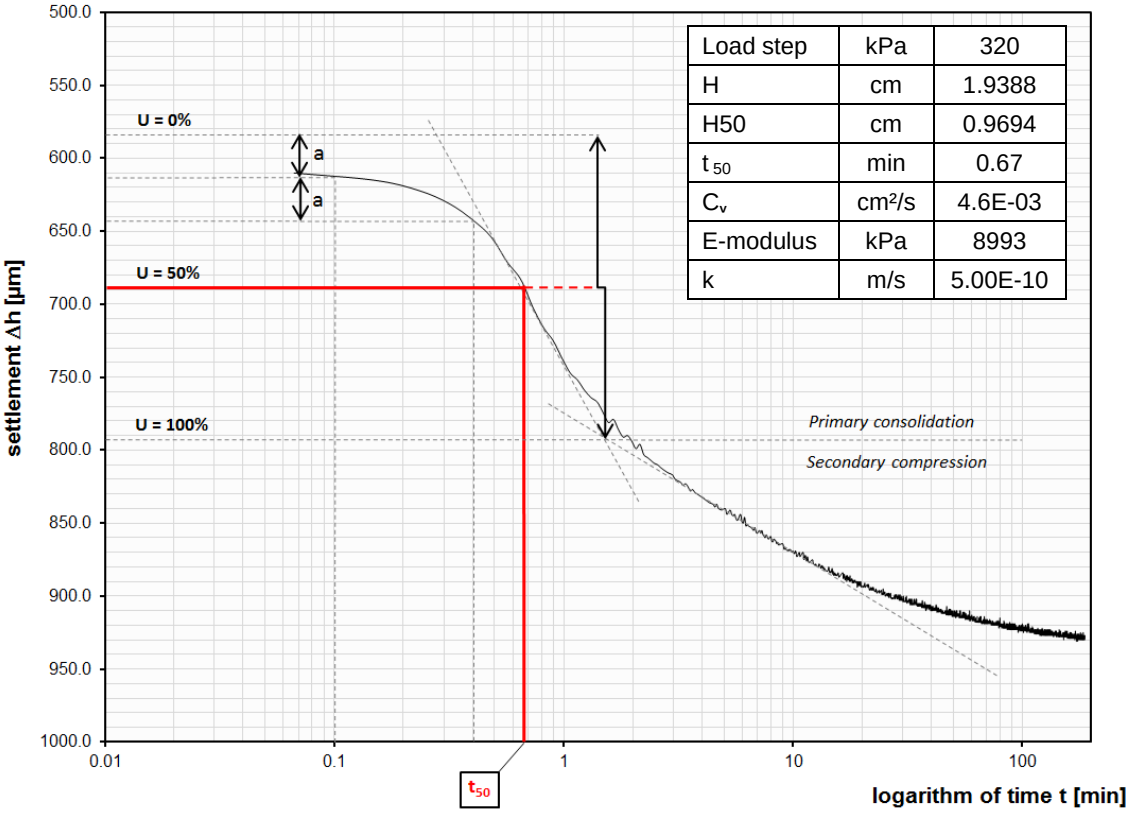

Fig. 49 Sample 19146-43: log-timeplot of the 320kPa load step

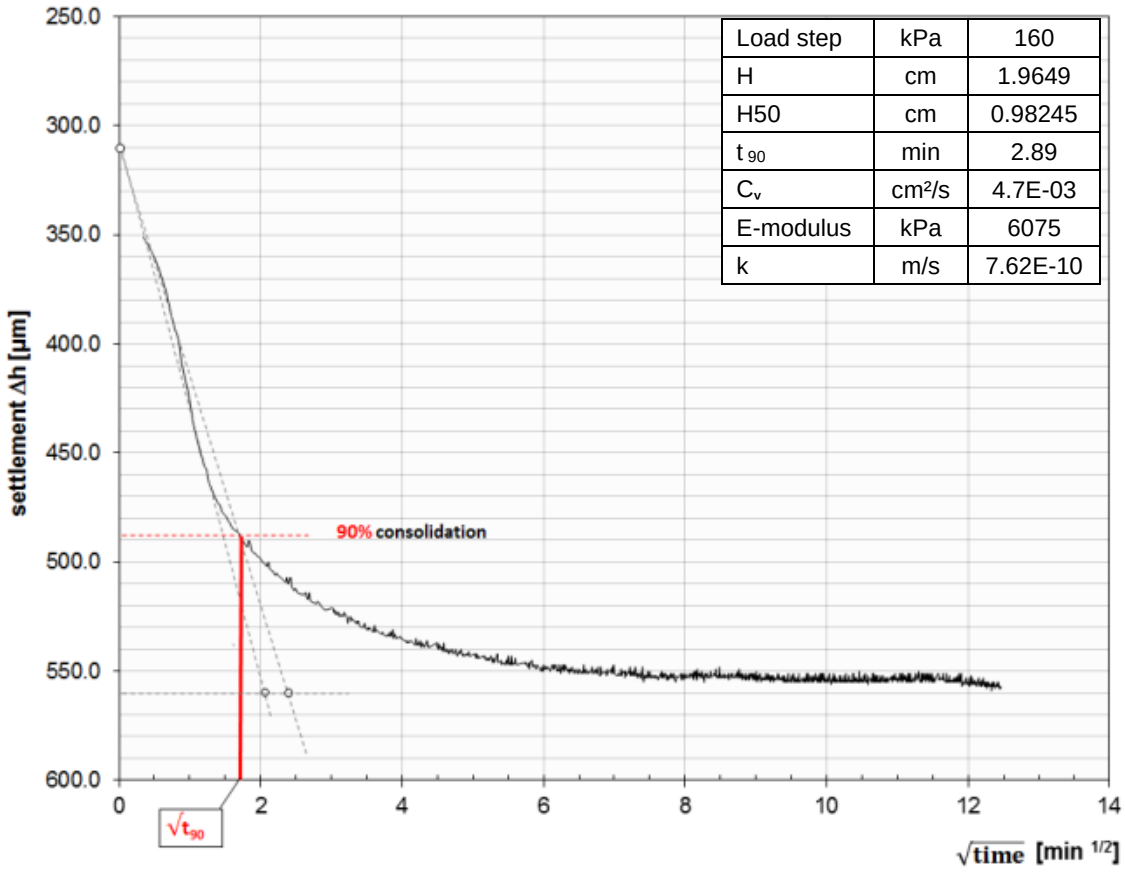

Fig. 50 Sample 19146-43: √time plot of the 160kPa load step

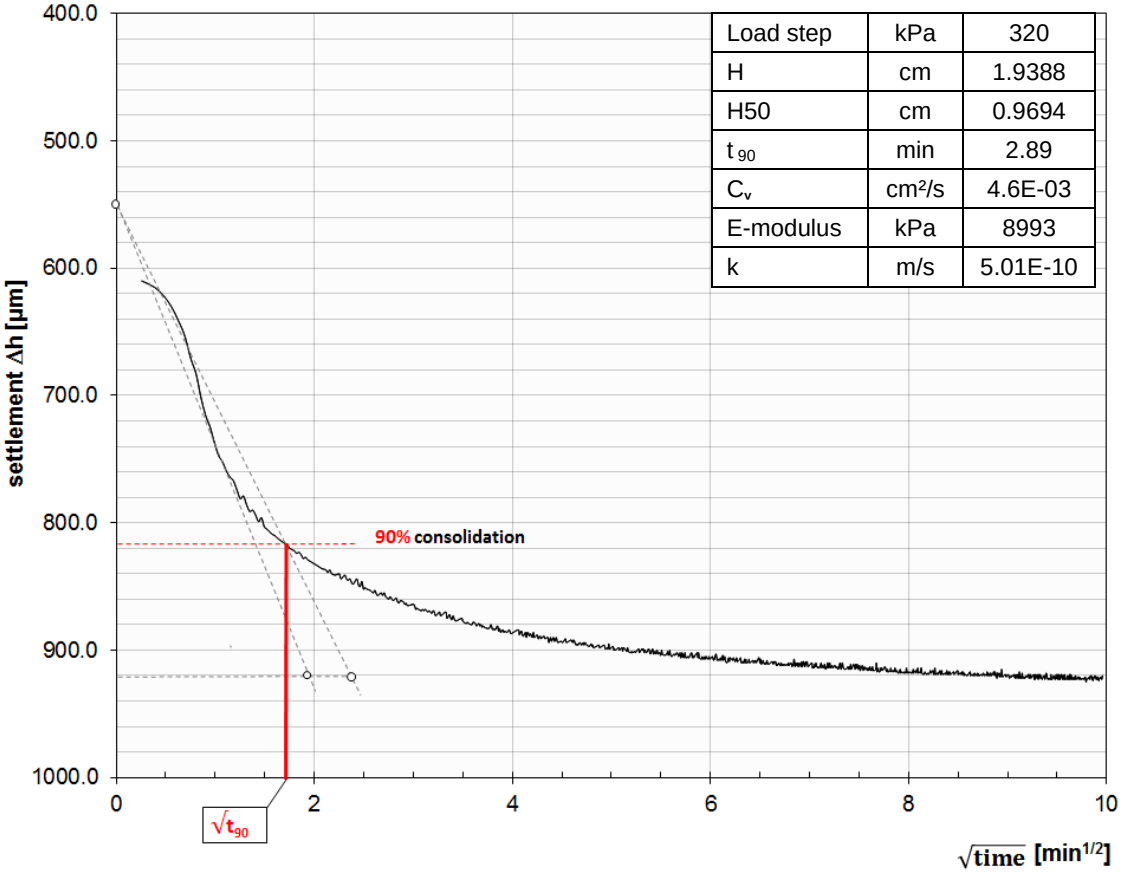
Load step kPa 320
H cm 1.9388
H50 cm 0.9694
t 90 min 2.89
Cv cm²/s 4.6E-03
E-modulus kPa 8993
k m/s 5.01E-10
400.0
500.0
600.0
700.0
800.0
900.0
1000.0
settlement Δh [µm]
90% consolidation
√t90
0
2
4
6
8
10
√time [min1/2]

8.1.5 19146-8

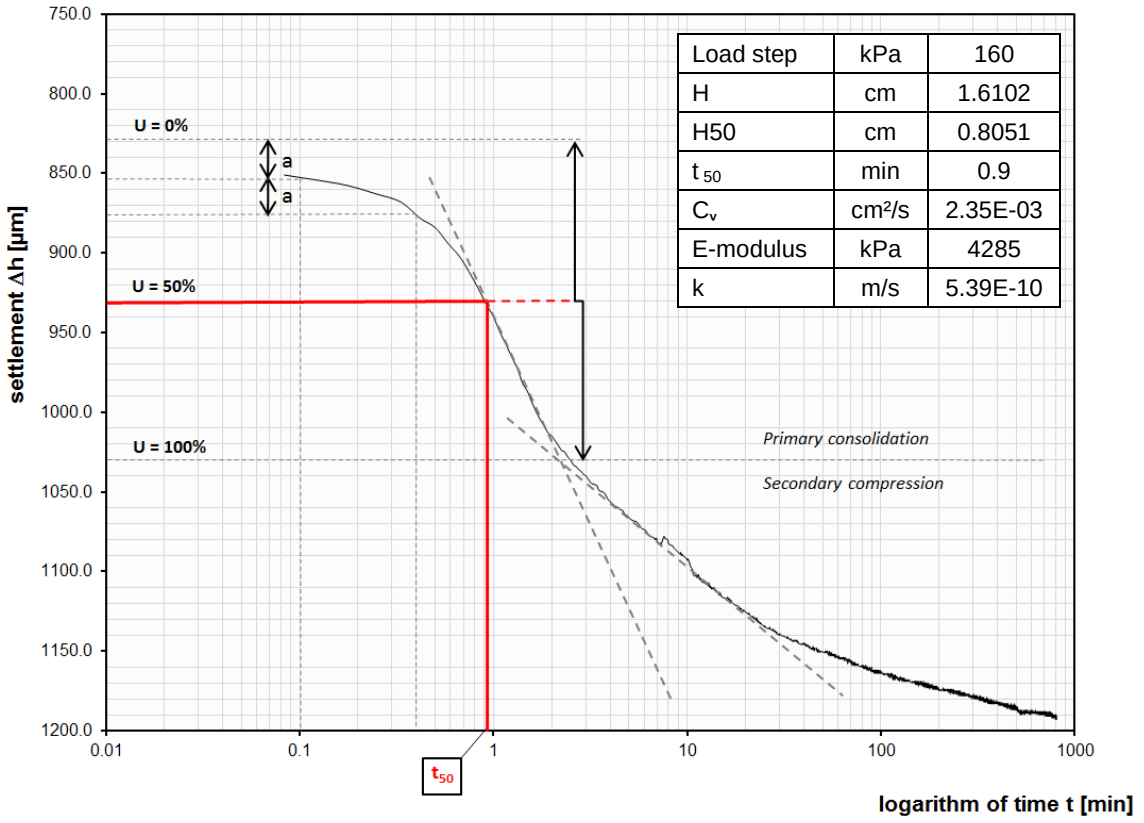

Fig. 51 Sample 19146-8: log-timeplot of the 160kPa load step

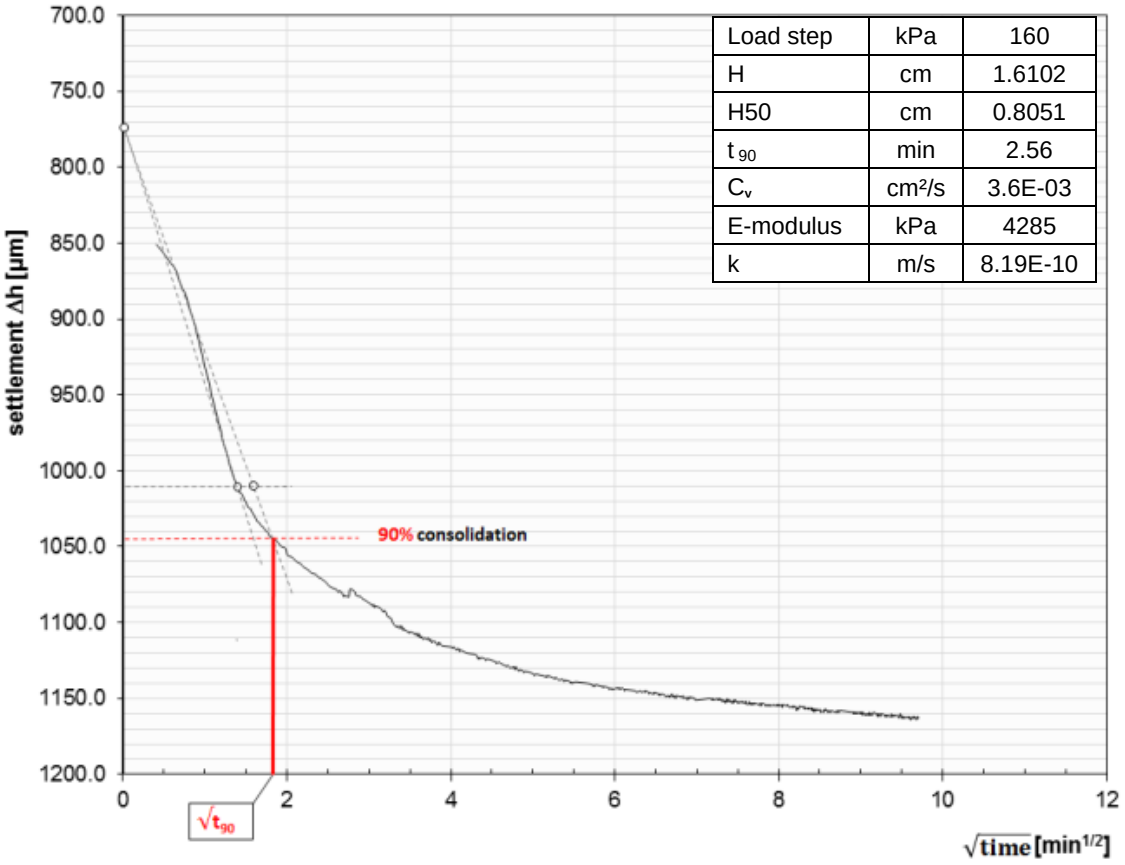

Fig. 52 Sample 19146-8: √time plot of the 160kPa load step

9 Bibliography

Adam et al.; published by Boley C. (2012)
"Handbuch Geotechnik: Grundlagen – Anwendungen – Praxiserfahrungen"

Berner, U. (2015)
„Gründungen in weichen Böden – Erfahrungen aus dem Bodenseeraum", 12. Biberacher Geotechnikseminar, Akademie der Hochschule Biberach

Das, B.M. (2002)
"Principles of Geotechnical Engineering"

Das, B.M. (2012)
"Soil Mechanics Laboratory Manual"

DIN ISO/TS 17892-11

DIN 18 130 Part 1

Gebreselassie, B.; Kempfert, H.-G. (2004)
"Excavation in Deep Soft Lacustrine Soil Deposit", 5th International Conference on Case Histories in Geotechnical Engineering, New York, pap.Nr.5.59

Head, K.H. (1982)
"Manual of Soil Laboratory Testing, Volume 2: Permeability, Shear Strength and Compressibility Tests"

Hoffmann, E. (2015)
"Evolution der Erde und des Lebens: Von der Urzelle zum Homo sapiens, 2015

Martelloni, G.; Segoni, S.; Fanti, R.; Catani, F. (2011)
"Rainfall thresholds for the forecasting of landslide occurence at regional scale", Landslides (2012), 9:485-495

Müller G. (1996)
"Naturwissenschaften", Volume 53, Issue 10, pp 237-247

OENORM B4422-1

OENORM B4420

Olson R. E. (1986)
"State of the Art: Consolidation Testing", Consolidation of Soils, Yong and Townsend, p.7-70

Poisel, R.; Hoffmann, R.; Preh, A.; Schiffer, M. (2012)
"Gschliefgraben mudslide (Austria): Hazard evaluation and risk mitigation", Natural Hazards, Vol. 61, Issue 1

Poscher, G. (1994)
"Fazies und Genese der pleistozänen Terrassensedimente im Tiroler Inntal und seinen Seitentälern – Teil 1: der Achenseedamm", Jahresbuch der Geologischen Bundesanstalt, Band 137, Heft 1, p. 171-186

Poscher, G. (1993)

"Neuergebnisse der Quartärforschung in Tirol", Geologie des Oberinntaler Raumes – Schwerpunkt Blatt 144 Landeck, Arbeitstagung Geol.B.-A., p.7-27

Saucke, U. (2004)
"Bewertung der Erosionsanfälligkeit strukturierter körniger Sedimente", Veröffentlichungen des Instituts für Bodenmechanik und Felsmechanik der Universität Fridericiana in Karlsruhe, Heft 162

Saucke, U.; Brauns, J., (1999)
„Die Bedeutung strukturierter Sedimente im Hinblick auf Strömungsvorgänge und hydraulische Untergrundstabilität", Morphodynamik der Elbe, p.86-89

Saucke, U. (2006)
"Nachweis der Sicherheit gegen innere Erosion für körnige Erdstoffe", Geotechnik 29, Nr.1

Shahriar, M.A.; Sivakugan, N.; Urquhart, A.; Tapiolas, M.; Das B.M. (2013)
"A Study on the Influence of Ground Water Level on Foundation Settlement in Cohesionless Soil", Proceedings of the 18th International Conference on Soil Mechanics and Geotechnical Engineering, Paris

Soumaya, B. (2005)
"Setzungsverhalten von Flachgründungen in normal-konsolidierten bindigen Böden", Schriftenreihe Geotechnik Universitaet Kassel, Heft 16

Striegler, W.; Werner D. (1969)
"Dammbau in Theorie und Praxis"

Tewatia S.K.; Venkatachalam K. (1997)
"Improved $\sqrt{t}$ Method to Evaluate Consolidation Test Results", Technical Note, Geotechnical Testing Journal, Vol.20, No.1, p.121-125

Turner, A.K.; Schuster, R.L. (1996)
"Landslides – Investigation and Mitigation", Special Report 247, Transportation Research Board, National Research Council

Van Asch, Th.W.J.; Buma, J.; Van Beek, L.P.H. (1999)
"A view on some hydrological triggering systems in landslides", Geomorphology 30, p. 25-32

Von Soos, P.; Engel J.; published by Witt, K. J. (2008)
"Grundbau-Taschenbuch: Teil 1: Geotechnische Grundlagen"